이학박사학위논문

Synaptic and behavioral function of neuropsychiatric disorder-related genes, *Cereblon* and *Lrrtm3*

신경정신질환 관련 유전자 ***Cereblon*** 및 ***Lrrtm3***의

시냅스 및 행동학적 기능 연구

2016년 8월

서울대학교 대학원

자연과학대학 협동과정 뇌과학 전공

최 태 용

Abstract

Synaptic and behavioral function of neuropsychiatric disorder-related genes, *Cereblon* and *Lrrtm3*

Choi Tae-Yong

Interdisciplinary Program in Neuroscience

The Graduate School

Seoul National University

The brain, the most complex organ in our body, generates our every behaviors and it is composed of numerous neurons. Neurons are connected and communicated each other, and this junctional space between two cells is called the synapse. There are many proteins in a neuron and around a synapse and these proteins are important for several functions in the brain such as a neuronal or synaptic development, maintaining these structures, or

communication of the nervous system. If only one of them has a problem, this system abnormally works and it finally causes various brain diseases. Diseases induced by synaptic dysfunction are called the synaptopathy. To conquer synaptopathy, it is necessary to understand the original function of the genes or the proteins, that the mutation of them is found in human neuropsychiatric disorder patients, in a neuron or a synapse, and how the mutated products change normal function. These understandings not only can contribute to understand how the brain works but also will help to establish strategies for treatment of the neuropsychiatric disorders.

Synaptic cell-adhesion molecules (CAMs) are necessary for connecting pre- and post-synaptic neurons at the synapse like a glue for normal neuronal or synaptic development and function. Leucine-rich repeat transmembrane proteins (LRRTMs) are recently identified synaptic cell-adhesion molecules and also contribute to the development and the function of excitatory synapse. The correlation between the mutation of these genes and some neuropsychiatric disorders are also reported. The LRRTM family is compose of four members, LRRTM1 to LRRTM4, but the molecular and cellular roles of LRRTM3 are not studied yet compared with others. On the other hand, there were some genetic studies and clinical case reports about the association between the mutation of *LRRTM3* and Alzheimer's disease (AD) or autism-spectrum disorders (ASDs). In chapter I, based on these background I studied the neuronal and synaptic function of LRRTM3 by using *Lrrtm3* knockout (KO) mice.

Intellectual disability (ID) is another common neuropsychiatric disorder, and recent studies have addressed this disorder as a synaptopathy. The mutation of gene *cereblon* (*CRBN*) was found from mild intellectual disability patients, and some additional studies were reported to reveal the correlation between the intellectual disability or developmental

delay and the mutation of *CRBN*. CRBN that binds with other proteins to form $CRL4^{CRBN}$ E3 ubiquitin ligase complex acts as the substrate receptor by binding with target proteins such as α subunit of large-conductance calcium-activated potassium (BK) channel or α subunit of AMP kinase (AMPK). However, how CRBN regulates the neuronal function and how *CRBN* mutation causes cognitive deficits are still unknown. In chapter II, I studied the neuronal, synaptic and behavioral role of CRBN by using *Crbn* KO mice.

These researches to reveal the neuronal, synaptic or behavioral roles of neuropsychiatric disorder-related genes not only are fundamental to understand these diseases but also will contribute to seek therapeutic plans.

Keywords : Synapse, Synaptic plasticity, Synaptopathy, Neuropsychiatric disorder, Cereblon (CRBN), LRRTM3

Student Number : 2013-30928

Contents

List of Figures

General Introduction

Chapter I.

Chapter II.

List of Tables

Chapter I.

Chapter II.

Abbreviations

AD	Alzheimer's disease
AMPA	a-amino-3-hydroxy-5-methyl-4-isoxazolepropionic acid
ANOVA	Analysis of variance
ASDs	Autism-spectrum disorders
BK channel	Large-conductance, Ca^{2+}-activated K^{+} channel
CA	Cornus ammonius
CAMs	Cell-adhesion molecules
Cm	Membrane capacitance
CRBN	Cereblon
CUL4A	Cullin-4A
DDB1	DNA-binding protein 1
DG	Dentate gyrus
EPSC	Excitatory postsynaptic current
GABA	γ-aminobutyric acid
ID	Intellectual disability
IMiDs	Immunomodulatory drugs
IPSC	Inhibitory postsynaptic current
KO	Knockout

LRR	Leucine-rich repeat
LRRTMs	Leucine-rich repeat transmembrane proteins
LTP	Long-term potentiation
LTD	Long-term depression
NLGNs	Neuroligins
NMDA	N-methyl-D-aspartic acid
NRXNs	Neurexins
PDZ	PSD95/Dlg/ZO-1
PP	Perforant path
PPR	Paired-pulse ratio
Pr	Release probability
PSD95	Postsynaptic density protein 95
R_{in}	Input resistance
RMP	Resting membrane potential
ROC1	Regulator of cullins 1
SC	Schaffer-collateral
SEM	Standard error of mean
SHANKs	SH3 and multiple ankyrin repeat domains proteins

General Introduction

Our behavior is generated by the working of the nervous system, and this system is composed of many neuronal cells; for instance, there are about 100 billion neurons in the human brain. These cells are connected and communicated each other, and this junctional space between two neurons is called the synapse. A single neuron connects with others via about a thousand synapses. Therefore, the brain is the most complex organ with various neuronal synaptic networks.

There are numerous proteins in a neuron and around a synapse, and these proteins are important for several functions in the nervous system such as a neuronal or synaptic development, maintaining these structures, or communicating each other via generating action potential and synaptic transmission. If only one protein is mutated, the function of the neuron or the synapse does not work normally and it finally causes various brain diseases. For example, the mutation of SHANK family proteins, the postsynaptic scaffolding protein to form signaling complex in the excitatory synapses (Berkel et al., 2010; Durand et al., 2007; Leblond et al., 2012; Peça et al., 2011; Schmeisser et al., 2012; Won et al., 2012; Yi et al., 2016), or of Neurexins (NRXNs) or Neuroligins (NLGNs), that are well-known synaptic cell-adhesion molecules expressed on pre- or postsynaptic membrane to assist synaptogenesis and various synaptic function (Etherton et al., 2009; Jamains et al., 2003; Kim et al., 2008; Sudhof, 2008; Tabuchi et al., 2007), is found in many autism-spectrum disorder (ASD) and other neuropsychiatric disorder patients. Like this, brain diseases caused by synaptic dysfunction are called synaptopathy. To overcome synaptopathy, it is necessary to understand the original function of the genes or the proteins that the mutation of them is found in human patients, in a neuron or a synapse, and how the mutated products change normal function in various levels with i*n vitro* (e.g. by using

molecular, biochemical or cellular approaches), *ex vivo* (e.g. by using slice electrophysiological approach) and *in vivo* (e.g. by using behavioral approach) studies. These understandings can extend not only the knowledge of the basic function of the brain but also the detailed mechanism of neuropsychiatric disorders. And it will help to establish strategies for treatment of these diseases.

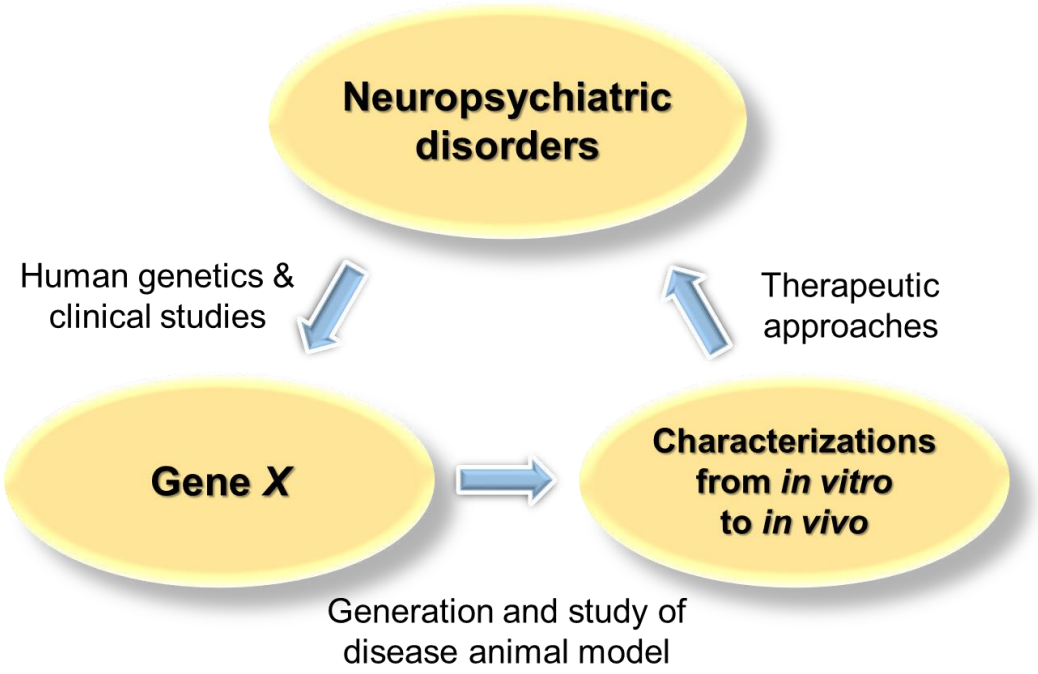

Figure 1. Simplified general approaches of neuropsychiatric disorders.

Synaptic Cell-Adhesion Molecule : LRRTM3

Many kinds of cell-adhesion molecules are expressed on the cell membranes and these proteins are involved in various cellular function such as the movement of the cell to another specific location or the attachment of the cell with another one. In the neurons, synaptic cell-adhesion molecules are essential for the link between pre- and post-synaptic

neurons to meet each other to form the synapse – it acts like a glue - for normal neuronal or synaptic development and communication. NRXNs, aforementioned presynaptic cell-adhesion molecule binds with NLGNs, were firstly discovered in 1990 as a receptor of α-latrotoxin, a component of the venom from black widow spider. When α-latrotoxin binds to NRXNs on presynaptic terminal, it evokes huge amounts of neurotransmitter release. NRXNs have the extracellular domain similar with laminin A, slit, and agrin that have the function of axon guidance and synaptogenesis (Ushkaryov et al., 1990). Thus many researchers predicted that NRXNs are also important for synapse development and function. NRXNs' postsynaptic binding partner, NLGN-1, was firstly identified in 1995 (Ichtchenko et al., 1995), and other NLGN members were also found (Budreck & Scheiffele, 2007; Laumonnier et al., 2004; Varoqueaux et al., 2004). Binding of NRXNs and NLGNs induces to meet presynaptic and postsynaptic neurons at synapses, and mediates synapse development and transforming information through synapses. If one of these proteins is mutated, synaptic development and/or function is abnormal in the brain, and it causes severe brain diseases such as autism-spectrum disorders (ASDs), schizophrenia and learning disability (Sudhof, 2008).

NRXNs bind not only with NLGNs but also with other types of postsynaptic adhesion proteins such as leucine-rich repeat transmembrane proteins (LRRTMs). LRRTM family proteins have shared domain structures that is composed of ten leucine-rich repeat (LRR) domains, a single transmembrane segment, and a different cytoplasmic region that ends with a type I PDZ-binding motif that mediates binding to the excitatory postsynaptic scaffolding protein PSD95 (de Wit & Ghosh, 2014; Ko & Kim, 2007; Ko, 2012). The LRRTM family is compose of four members, LRRTM1 to LRRTM4, and is selectively expressed in neurons with a differential distribution in the brain; for instance, LRRTM1 and LRRTM2 are widely expressed, but LRRTM3 and LRRTM4 are expressed only in dentate gyrus (DG) in the hippocampus (de Wit et al., 2013; Laurén et al., 2003; Um et al.,

2016). LRRTMs contribute to the development and function of excitatory synapse via the interaction with NRXNs or other presynaptic adhesion molecules, and the correlation between the mutation of these genes and neuropsychiatric disorders are reported. For example, LRRTM1 induces the development of excitatory synapses via interacting with its presynaptic partner NRXNs, and the mutation of this gene is related to schizophrenia and handedness. LRRTM4, another example, is important for normal excitatory synapse development and function in hippocampal DG areas, and the mutation of this gene is related to ASDs (de Wit et al., 2009; de Wit et al., 2013; Ko et al., 2009; Linhoff et al., 2009; Siddiqui et al., 2010; Siddiqui et al., 2013; Um et al., 2016). There were some human genetic and clinical about the association between the mutation of *LRRTM3* and Alzheimer's disease or ASDs (Majercak et al., 2006; Michaelson et al., 2012; Pinto et al., 2010; Sousa et al., 2010; Wang et al., 2014), but the molecular and cellular roles of LRRTM3 are not studied yet compared with other LRRTMs. In chapter I, I thus studied the neuronal and synaptic function of LRRTM3 by using *Lrrtm3* knockout (KO) mice.

Intracellular Signaling Molecule : CRBN

Intellectual disability is another common neuropsychiatric disorder, and this disease is caused by various genetic or environmental factors. Recently, researchers have tried to address intellectual disability as a synaptopathy. Synaptopathy is induced not only by the mutation of genes encoding synaptic cell-adhesion molecules aforementioned that link between presynaptic and postsynaptic neurons to induce synaptogenesis and synaptic communications, but also by troubles in various intracellular signaling molecules. Ubiquitination is one of important mechanism of posttranslational modification and protein degradation, and many proteins are involved in this event (Mabb & Ehlers, 2010; Yi &

Ehlers, 2005). Cereblon (CRBN) is recently reported protein to form $CRL4^{CRBN}$ E3 ubiquitin ligase complex that is composed of other proteins, DNA-binding protein 1 (DDB1), cullin-4A (CUL4A), and regulator of cullins 1 (ROC1) (Fischer et al., 2014; Ito et al., 2010; Xu et al., 2013). In this complex, CRBN acts as the substrate receptor by binding with target proteins such as α subunit of large-conductance Ca^{2+}-activated K^+ (BK) channel or α subunit of AMP kinase (AMPK) (Jo et al., 2005; Lee et al., 2011). The mutation of gene *cereblon* (*CRBN*) was firstly found from mild intellectual disability patients, and some additional studies were reported to reveal the correlation between the intellectual disability or developmental delay and the mutation of *CRBN* (Dijkhuizen et al., 2006; Papuc et al., 2015). However, how CRBN regulates the neuronal function and how *CRBN* mutation causes cognitive problem are still unknown. In chapter II, I studied the neuronal, synaptic and behavioral role of CRBN by using *Crbn* KO mice.

A drug thalidomide is another important issue of CRBN biology. It was firstly marketed late 1950s and was prescribed for pregnant women for inhibiting nausea and morning sickness, but the use of this drug was prohibited after a few years later because it induced infants with phocomelia (malformation of the limbs) and other severe developmental or neuropsychiatric disorders. Action mechanisms of this drug was recently unveiled. Thalidomide binds with CRBN and inhibits $CRL4^{CRBN}$ E3 ubiquitin ligase function (Ito et al., 2010). Because of this mechanism, thalidomide and its derivatives lenalinomide and pomalidomide, called immunomodulatory drugs (IMiDs), are recently used for the treatment of multiple myeloma. However, there were some clinical reports that multiple myeloma patients who were prescribed these drugs showed cognitive impairment (Patel et al., 2015; Rollin-Sillaire et al., 2013). It suggests that thalidomide acts as CRBN inhibitor and the memory defects induced by IMiDs in human multiple myeloma patients is induced by similar mechanism in *CRBN* mutated human intellectual disability patients. Thus, I tested this possibility using biochemical, electrophysiological and behavioral approaches.

Purposes

Key purposes of this thesis are to reveal the neuronal, synaptic and behavioral function of two neuropsychiatric disorder-related genes, *cereblon* and *Lrrtm3*. To achieve this goal, the researches listed below are addressed in subsequent two/three chapters.

- To characterize the role of LRRTM3 on synaptic function using *Lrrtm3* KO mice.
- To elucidate the synaptic and behavioral function of CRBN using *Crbn* KO mice.
- To investigate the effect of thalidomide on synaptic and behavioral function.
- To find the rescue strategy of *Crbn* deficiency-induced cognitive impairment.

These researches to reveal the neuronal, synaptic or behavioral roles of neuropsychiatric disorder-related genes not only are fundamental to understand these diseases but also will contribute to find therapeutic approaches.

References

1. Berkel, S., Marshall, C.R., Weiss, B., Howe, J., Roeth, R., Moog, U., Endris, V., Roberts, W., Szatmari, P., Pinto, D., Bonin, M., Riess, A., Engels, H., Sprengel, R., Scherer, S.W., Rappold, G.A. (2010) Mutations in the SHANK2 synaptic scaffolding gene in autism spectrum disorder and mental retardation. Nat Genet. 42(6):489-91.
2. Budreck, E.C., Scheiffele, P. (2007) Neuroligin-3 is a neuronal adhesion protein at GABAergic and glutamatergic synapses. Eur J Neurosci. 26(7):1738-48.
3. de Wit, J., Ghosh, A. (2014) Control of neural circuit formation by leucine-rich repeat proteins. Trends Neurosci. 37(10):539-50.
4. de Wit, J., O'Sullivan, M.L., Savas, J.N., Condomitti, G., Caccese, M.C., Vennekens, K.M., Yates, J.R. 3rd., Ghosh, A. (2013) Unbiased discovery of glypican as a receptor for LRRTM4 in regulating excitatory synapse development. Neuron. 79(4):696-711.
5. de Wit, J., Sylwestrak, E., O'Sullivan, M.L., Otto, S., Tiglio, K., Savas, J.N., Yates, J.R. 3rd., Comoletti, D., Taylor, P., Ghosh, A. (2009) LRRTM2 interacts with Neurexin1 and regulates excitatory synapse formation. Neuron. 64(6):799-806.
6. Durand, C.M., Betancur, C., Boeckers, T.M., Bockmann, J., Chaste, P., Fauchereau, F., Nygren, G., Rastam, M., Gillberg, I.C., Anckarsäter, H., Sponheim, E., Goubran-Botros, H., Delorme, R., Chabane, N., Mouren-Simeoni, M.C., de Mas, P., Bieth, E., Rogé, B., Héron, D., Burglen, L., et al., (2007) Mutations in the gene encoding the synaptic scaffolding protein SHANK3 are associated with autism spectrum disorders. Nat Genet. 39(1):25-7.
7. Dijkhuizen, T., van Essen, T., van der Vlies, P., Verheij, J.B., Sikkema-Raddatz, B., van der Veen, A.Y., Gerssen-Schoorl, K.B., Buys, C.H., Kok, K. (2006) FISH and array-CGH analysis of a complex chromosome 3 aberration suggests that loss of CNTN4 and CRBN contributes to mental retardation in 3pter deletions. Am J Med Genet A. 140(22):2482-7.
8. Etherton, M.R., Blaiss, C.A., Powell, C.M., Südhof, T.C. (2009) Mouse neurexin-

1alpha deletion causes correlated electrophysiological and behavioral changes consistent with cognitive impairments. Proc Natl Acad Sci U S A. 106(42):17998-8003.

9. Fischer, E.S., Böhm, K., Lydeard, J.R., Yang, H., Stadler, M.B., Cavadini, S., Nagel, J., Serluca, F., Acker, V., Lingaraju, G.M., Tichkule, R.B., Schebesta, M., Forrester, W.C., Schirle, M., Hassiepen, U., Ottl, J., Hild, M., Beckwith, R.E., Harper, J.W., Jenkins, J.L., Thomä, N.H. (2014) Structure of the DDB1-CRBN E3 ubiquitin ligase in complex with thalidomide. Nature. 512(7512):49-53.
10. Higgins, J.J., Pucilowska, J., Lombardi, R.Q., Rooney, J.P. (2004) A mutation in a novel ATP-dependent Lon protease gene in a kindred with mild mental retardation. Neurology. 63(10):1927-31.
11. Ichtchenko, K., Hata, Y., Nguyen, T., Ullrich, B., Missler, M., Moomaw, C., Südhof, T.C. (1995) Neuroligin 1: a splice site-specific ligand for beta-neurexins. Cell. 81(3):435-43.
12. Ito, T., Ando, H., Suzuki, T., Ogura, T., Hotta, K., Imamura, Y., Yamaguchi, Y., Handa, H. (2010) Identification of a primary target of thalidomide teratogenicity. Science. 327(5971):1345-50.
13. Jamain, S., Quach, H., Betancur, C., Råstam, M., Colineaux, C., Gillberg, I.C., Soderstrom, H., Giros, B., Leboyer, M., Gillberg, C., Bourgeron, T.; Paris Autism Research International Sibpair Study. (2003) Mutations of the X-linked genes encoding neuroligins NLGN3 and NLGN4 are associated with autism. Nat Genet. 34(1):27-9.
14. Jo, S., Lee, K.H., Song, S., Jung, Y.K., Park, C.S. (2005) Identification and functional characterization of cereblon as a binding protein for large-conductance calcium-activated potassium channel in rat brain. J Neurochem. 94(5):1212-24.
15. Kim, H.G., Kishikawa, S., Higgins, A.W., Seong, I.S., Donovan, D.J., Shen, Y., Lally, E., Weiss, L.A., Najm, J., Kutsche, K., Descartes, M., Holt, L., Braddock, S., Troxell, R., Kaplan, L., Volkmar, F., Klin, A., Tsatsanis, K., Harris, D.J., Noens, I., et al.,

(2008) Disruption of neurexin 1 associated with autism spectrum disorder. Am J Hum Genet. 82(1):199-207.

16. Ko, J. (2012) The leucine-rich repeat superfamily of synaptic adhesion molecules: LRRTMs and Slitrks. Mol Cells. 34(4):335-40.
17. Ko, J., Fuccillo, M.V., Malenka, R.C., Südhof, T.C. (2009) LRRTM2 functions as a neurexin ligand in promoting excitatory synapse formation. Neuron. 64(6):791-8.
18. Ko, J., Kim, E. (2007) Leucine-rich repeat proteins of synapses. J Neurosci Res. 85(13):2824-32.
19. Laumonnier, F., Bonnet-Brilhault, F., Gomot, M., Blanc, R., David, A., Moizard, M.P., Raynaud, M., Ronce, N., Lemonnier, E., Calvas, P., Laudier, B., Chelly, J., Fryns, J.P., Ropers, H.H., Hamel, B.C., Andres, C., Barthélémy, C., Moraine, C., Briault, S. (2004) X-linked mental retardation and autism are associated with a mutation in the NLGN4 gene, a member of the neuroligin family. Am J Hum Genet. 74(3):552-7.
20. Laurén, J., Airaksinen, M.S., Saarma, M., Timmusk, T. (2003) A novel gene family encoding leucine-rich repeat transmembrane proteins differentially expressed in the nervous system. Genomics. 81(4):411-21.
21. Leblond, C.S., Heinrich, J., Delorme, R., Proepper, C., Betancur, C., Huguet, G., Konyukh, M., Chaste, P., Ey, E., Rastam, M., Anckarsäter, H., Nygren, G., Gillberg, I.C., Melke, J., Toro, R., Regnault, B., Fauchereau, F., Mercati, O., Lemière, N., Skuse, D., et al., (2012) Genetic and functional analyses of SHANK2 mutations suggest a multiple hit model of autism spectrum disorders. PLoS Genet. 8(2):e1002521.
22. Lee, K.M., Jo, S., Kim, H., Lee, J., Park, C.S. (2011) Functional modulation of AMP-activated protein kinase by cereblon. Biochim Biophys Acta. 1813(3):448-55.
23. Linhoff, M.W., Laurén, J., Cassidy, R.M., Dobie, F.A., Takahashi, H., Nygaard, H.B., Airaksinen, M.S., Strittmatter, S.M., Craig, A.M. (2009) An unbiased expression screen for synaptogenic proteins identifies the LRRTM protein family as synaptic organizers. Neuron. 61(5):734-49.
24. Mabb, A.M., Ehlers, M.D. (2010) Ubiquitination in postsynaptic function and

plasticity. Annu Rev Cell Dev Biol. 26:179-210.

25. Majercak, J., Ray, W.J., Espeseth, A., Simon, A., Shi, X.P., Wolffe, C., Getty, K., Marine, S., Stec, E., Ferrer, M., Strulovici, B., Bartz, S., Gates, A., Xu, M., Huang, Q., Ma, L., Shughrue, P., Burchard, J., Colussi, D., Pietrak, B., et al., (2006) LRRTM3 promotes processing of amyloid-precursor protein by BACE1 and is a positional candidate gene for late-onset Alzheimer's disease. Proc Natl Acad Sci U S A. 103(47):17967-72.
26. Michaelson, J.J., Shi, Y., Gujral, M., Zheng, H., Malhotra, D., Jin, X., Jian, M., Liu, G., Greer, D., Bhandari, A., Wu, W., Corominas, R., Peoples, A., Koren, A., Gore, A., Kang, S., Lin, G.N., Estabillo, J., Gadomski, T., Singh, B., et al., (2012) Whole-genome sequencing in autism identifies hot spots for de novo germline mutation. Cell. 151(7):1431-42.
27. Papuc, S.M., Hackmann, K., Andrieux, J., Vincent-Delorme, C., Budişteanu, M., Arghir, A., Schrock, E., Ţuţulan-Cuniţă, A.C., Di Donato, N. (2015) Microduplications of 3p26.3p26.2 containing CRBN gene in patients with intellectual disability and behavior abnormalities. Eur J Med Genet. 58(5):319-23.
28. Patel, U.H., Mir, M.A., Sivik, J.K., Raheja, D., Pandey, M.K., Talamo, G. (2015) Central neurotoxicity of immunomodulatory drugs in multiple myeloma. Hematol Rep. 7(1):5704.
29. Peça, J., Feliciano, C., Ting, J.T., Wang, W., Wells, M.F., Venkatraman, T.N., Lascola, C.D., Fu, Z., Feng, G. (2011) Shank3 mutant mice display autistic-like behaviours and striatal dysfunction. Nature. 472(7344):437-42.
30. Pinto, D., Pagnamenta, A.T., Klei, L., Anney, R., Merico, D., Regan, R., Conroy, J., Magalhaes, T.R., Correia, C., Abrahams, B.S., Almeida, J., Bacchelli, E., Bader, G.D., Bailey, A.J., Baird, G., Battaglia, A., Berney, T., Bolshakova, N., Bölte, S., Bolton, P.F. et al., (2010) Functional impact of global rare copy number variation in autism spectrum disorders. Nature. 466(7304):368-72.
31. Rollin-Sillaire, A., Delbeuck, X., Pollet, M., Mackowiak, M.A., Lenfant, P., Noel,

M.P., Facon, T., Leleu, X., Pasquier, F., Le Rhun, E. (2013) Memory loss during lenalidomide treatment: a report on two cases. BMC Pharmacol Toxicol. 14:41.

32. Schmeisser, M.J., Ey, E., Wegener, S., Bockmann, J., Stempel, A.V., Kuebler, A., Janssen, A.L., Udvardi, P.T., Shiban, E., Spilker, C., Balschun, D., Skryabin, B.V., Dieck, St., Smalla, K.H., Montag, D., Leblond, C.S., Faure, P., Torquet, N., Le Sourd, A.M., Toro, R., et al., (2012) Autistic-like behaviours and hyperactivity in mice lacking ProSAP1/Shank2. Nature. 486(7402):256-60.
33. Siddiqui, T.J., Pancaroglu, R., Kang, Y., Rooyakkers, A., Craig, A.M. (2010) LRRTMs and neuroligins bind neurexins with a differential code to cooperate in glutamate synapse development. J Neurosci. 30(22):7495-506.
34. Siddiqui, T.J., Tari, P.K., Connor, S.A., Zhang, P., Dobie, F.A., She, K., Kawabe, H., Wang, Y.T., Brose, N., Craig, A.M. (2013) An LRRTM4-HSPG complex mediates excitatory synapse development on dentate gyrus granule cells. Neuron. 79(4):680-95.
35. Sousa, I., Clark, T.G., Holt, R., Pagnamenta, A.T., Mulder, E.J., Minderaa, R.B., Bailey, A.J., Battaglia, A., Klauck, S.M., Poustka, F., Monaco, A.P.; International Molecular Genetic Study of Autism Consortium (IMGSAC). (2010) Polymorphisms in leucine-rich repeat genes are associated with autism spectrum disorder susceptibility in populations of European ancestry. Mol Autism. 1(1):7.
36. Südhof, T.C. (2008) Neuroligins and neurexins link synaptic function to cognitive disease. Nature. 455(7215):903-11.
37. Tabuchi, K., Blundell, J., Etherton, M.R., Hammer, R.E., Liu, X., Powell, C.M., Südhof, T.C. (2007) A neuroligin-3 mutation implicated in autism increases inhibitory synaptic transmission in mice. Science. 318(5847):71-6.
38. Um, J.W., Choi, T.Y., Kang, H., Cho, Y.S., Choii, G., Uvarov, P., Park, D., Jeong, D., Jeon, S., Lee, D., Kim, H., Lee, S.H., Bae, Y.C., Choi, S.Y., Airaksinen, M.S., Ko, J. (2016) LRRTM3 Regulates Excitatory Synapse Development through Alternative Splicing and Neurexin Binding. Cell Rep. 14(4):808-22.
39. Ushkaryov, Y.A., Petrenko, A.G., Geppert, M., Südhof, T.C. (1990) Neurexins:

synaptic cell surface proteins related to the alpha-latrotoxin receptor and laminin. Science. 257(5066):50-6.

40. Varoqueaux, F., Jamain, S., Brose, N. (2004) Neuroligin 2 is exclusively localized to inhibitory synapses. Eur J Cell Biol. 83(9):449-56.
41. Wang, J., Yu, J.T., Jiang, T., Tan, M.S., Wang, H.F., Tan, L., Hu, N., Sun, L., Zhang, W., Tan, L. (2014) Association of LRRTM3 polymorphisms with late-onset Alzheimer's disease in Han Chinese. Exp Gerontol. 52:18-22.
42. Won, H., Lee, H.R., Gee, H.Y., Mah, W., Kim, J.I., Lee, J., Ha, S., Chung, C., Jung, E.S., Cho, Y.S., Park, S.G., Lee, J.S., Lee, K., Kim, D., Bae, Y.C., Kaang, B.K., Lee, M.G., Kim, E. (2012) Autistic-like social behaviour in Shank2-mutant mice improved by restoring NMDA receptor function. Nature. 486(7402):261-5.
43. Xu, G., Jiang, X., Jaffrey, S.R. (2013) A mental retardation-linked nonsense mutation in cereblon is rescued by proteasome inhibition. J Biol Chem. 288(41):29573-85.
44. Yi, F., Danko, T., Botelho, S.C., Patzke, C., Pak, C., Wernig, M., Südhof, T.C. (2016) Autism-associated SHANK3 haploinsufficiency causes Ih channelopathy in human neurons. Science. 352(6286):aaf2669.
45. Yi, J.J., Ehlers, M.D. (2005) Ubiquitin and protein turnover in synapse function. Neuron. 47(5):629-32.

Chapter I.

LRRTM3, a postsynaptic cell-adhesion molecule related to autism-spectrum disorders (ASDs), regulates excitatory synaptic function.

Abstract

The four members of the LRRTM family (LRRTM1-4) are postsynaptic cell-adhesion molecules (CAMs) fundamental for the development and the function of excitatory synapses, and these proteins are implicated in various neuropsychiatric disorders. Here, I studied the detailed synaptic function of LRRTM3 in hippocampal performant path (PP)-DG synapses, highly enriched regions of this protein, using *Lrrtm3* knockout (KO) mice. *Lrrtm3* KO mice showed alterations in excitatory synaptic transmission and neuronal intrinsic properties in hippocampal dentate gyrus (DG) granule cells, but not in CA1 pyramidal neurons. However, long-term potentiation (LTP) is intact in PP-DG synapses of *Lrrtm3* KO mice. Collectively, these results indicate that LRRTM3 is a key regulator of excitatory synaptic transmission, but not plasticity, in PP-DG synapses in the hippocampus.

Introduction

Synapses are organized by specific proteins called synaptic cell-adhesion molecules (CAMs) that act like a glue mediating various synaptic function such as synapse assembly, maturation, specification, and plasticity (Betancur et al., 2009; Dalva et al., 2007; de Wit & Ghosh, 2016). Many studies have found many kinds of synaptic cell-adhesion molecules and discovered their roles under different synaptogenesis contexts and physiological function. Well-known examples are neurexins (NRXNs), presynaptic cell-adhesion molecules that bind with neuroligins (NLGNs) or other kinds of postsynaptic cell-adhesion molecules to induce synapse development and function (Budreck & Scheiffele, 2007; Siddiqui et al., 2010; Südhof, 2008; Varoqueaux et al., 2004). Leucine-rich repeat (LRR)-containing transmembrane proteins (LRRTMs), another interacting partner of NRXNs, in particular, have emerged as being important for various synaptic roles. Notably, LRRTMs as well as NGLs (netrin-G ligands), SALMs (synaptic adhesion-like molecules), Slitrks (Slit and Trk-like family), and FLRTs (fibronectin LRR transmembrane proteins) were shown to be essential for various aspects of synapse development and function (de Wit et al., 2011; de Wit & Ghosh, 2014; Ko & Kim, 2007; Ko, 2012).

There are four LRRTM family, LRRTM1 to LRRTM4, which are only found in vertebrates (Laurén et al., 2003). These proteins share similar domain structures which is composed of ten LRR domains and a single transmembrane region but a different cytoplasmic area that ends with a type I PDZ-binding motif that interacts with PSD95, a major excitatory postsynaptic scaffolding protein (Laurén et al., 2003; Linhoff et al., 2009; Siddiqui et al., 2013). Previously, it was discovered that all LRRTMs induce presynaptic differentiation in heterogous synapse-formation assay,

although LRRTM3 displays lower synaptogenic activity relative to other LRRTM family members (de Wit et al., 2009; Ko et al., 2009; Linhoff et al., 2009; Siddiqui et al., 2010).

Postsynaptic LRRTMs binds with not only NRXNs, but also different types of presynaptic ligands. For instance, LRRTM1 and LRRTM2 bind to a subset of presynaptic NRXN splice variants (Ko et al., 2009; Siddiqui et al., 2010), but LRRTM4 binds with heparin sulfate proteoglycans and protein tyrosine phosphatases σ (HSPGs/PTPσ) (de Wit & Ghosh, 2014; de Wit et al., 2013; Ko et al., 2015; Siddiqui et al., 2013). LRRTM family proteins show spatially different expression patterns in the brain. For example, LRRTM1 and LRRTM2 are expressed in all areas, whereas LRRTM3 and LRRTM4 are highly enriched in the dentate gyrus (DG), in the hippocampus (Laurén et al., 2003; Linhoff et al., 2009; Siddiqui et al., 2013; Um et al., 2016).

A sort of LRRTMs have a regulatory role of excitatory synaptic transmission through AMPA (a-amino-3-hydroxy-5-methyl-4-isoxazolepropionic) receptor trafficking. For example, double knockdown (DKD) of LRRTM1 and LRRTM2 in the hippocampal CA1 areas decreases AMPA receptor-mediated synaptic transmission and long-term potentiation (LTP) in Schaffer-collateral (SC)-CA1 synapses (Soler-Llavina et al., 2011; Soler-Llavina et al., 2013). LRRTM4 also form physical complexes with GluA2 subunit of AMPA receptors and is required for cLTP-induced synaptic surface trafficking of GluA1 subunits (Shanks et al., 2012; Siddiqui et al., 2013).

Studying the role of LRRTM proteins in vivo using their knockout (KO) mice or by shRNA-mediated knockdown (KD) of their genes have unveiled functional and behavioral defects. *Lrrtm1* KO mice show enhancement of vGluT1 expression level and altered distribution of synaptic vesicles, and changed synaptic morphology

(Linhoff et al., 2009; Takashima et al., 2011). These mice also have cognitive problems with schizophrenia-like and claustrophobia-like behaviors (Takashima et al., 2011; Voikar et al., 2013). *Lrrtm4* KO mice also exhibited decreased excitatory synapse density and synaptic transmission in hippocampal DG granule cells, but not in CA1 pyramidal neurons (Siddiqui et al., 2013). *Lrrtm4* KD in cortical areas also inhibited synaptic development and reduced excitatory synaptic transmission (de Wit et al., 2013). Not surprisingly, the mutation of *LRRTM* genes are associated with various neuropsychiatric disorders in human (de Wit & Ghosh, 2014). Ironically, there were some human genetic or clinical reports related to the correlation between the mutation of *LRRTM3* gene and ASDs (Michaelson et al., 2012; Sousa et al., 2010) or late-onset Alzheimer's disease (LOAD) (Majercak et al., 2006; Lincoln et al., 2013), but the molecular and physiological roles of LRRTM3 are not studied yet.

In this study, I studied the synaptic function of LRRTM3 in the hippocampus using *Lrrtm3* KO mice, especially comparing the synaptic transmission between in perforant path (PP)-DG synapses, where LRRTM3 is highly expressed in, and in SC-CA1 synapses that lack this protein. I also researched how LRRTM3 modulates neuronal function such as excitability and other intrinsic neuronal properties such as membrane capacitance (Cm) and resting membrane potential (RMP). Finally, I will compare synaptic phenotypes observed in *Lrrtm3* KO mice and in other classes of *Lrrtm* KO mice – especially *Lrrtm4* KO mice (Siddiqui et al., 2013) which was intensively studied in PP-DG synapses - to clarify individual characteristics of LRRTM3.

Materials and Methods

Animals

All mice were housed in an animal facility with a specific pathogen-free barrier under controlled environmental conditions (temperature, 22 ± 1℃; humidity, 55%; and a 12h/12h light/dark cycle, lights on at 07:00). Mice were allowed access to food and water *ad libitum*. Wild-type (WT) and *Lrrtm3* KO mice of the C57BL/6 background were used (Laakso et al., 2012). All experiments were approved by the Institutional Animal Care and Use Committee (IACUC) at Seoul National University.

Slice preparation

Using 2- to 6-week-old (both sexes) WT and *Lrrtm3* KO mice, 300 μm of transverse hippocampal slices were prepared as described previously (Choi et al., 2015; Seo et al., 2014). After decapitation, brains were rapidly removed and placed in ice-cold, oxygenated (95% O_2 and 5% CO_2) dissection buffer (see table 1). Slices were transferred to a holding chamber in an incubator containing oxygenated (95% O_2 and 5% CO_2) artificial cerebrospinal fluid (ACSF) (see table 1) at 28–30°C for at least 30 minutes before recording.

Whole-cell patch-clamp recordings

After recovery, slices were transferred to a submerged-type recording chamber where they were continuously perfused with external solution gassed with 95% O_2 / 5% CO_2 at a flow rate of 2 ml/min. Slices were equilibrated for at least 5 min prior to the recordings and all of the experiments were performed at 23-25°C excluding

LTP experiments (27-28°C). All recordings were performed in hippocampal DG granule cells identified by their size and morphology. Recordings were obtained using a Multiclamp 700B amplifier (Molecular Devices) under visual control with differential interference contrast illumination in an upright microscope (BX51WI; Olympus). Patch pipettes (4-6 MΩ) were filled with various internal solutions for experimental purposes (see table 2). Evoked synaptic responses were elicited by electrical stimulation (0.2-ms current pulses) using a concentric bipolar electrode at lateral perforant path (LPP) placed at least 300 μm in front of the recorded postsynaptic granule cell. External solution A for some eEPSC experiments (see table 3) were recorded using a modified external solution containing elevated divalent cations (4 mM Ca^{2+} and Mg^{2+}) to reduce network excitability and prevent polysynaptic responses upon stimulation (Clem & Huganir, 2010). External solution B containing decreased K^{+} ions for reducing resting membrane potential to decrease the possibility of more neuronal firing is used other eEPSC experiments (see table 3). For induction of LTP, high-frequency stimulation (HFS, consisting of 8 trains of 8 stimuli at 200 Hz, with intertrain interval of 2 s) with depolarization at 0 mV was applied to LPP-DG synapses (Wang et al., 1997; Jo et al., 2014). Only cells with an access resistance <20 MΩ and an input resistance >100 MΩ were studied. The cells were discarded if the input or the access resistance changed more than 20%. Data were acquired and analyzed using pClamp 10.6 (Molecular Devices). Signals were filtered at 2 kHz and digitized at 10 kHz with Digidata 1440A (Axon Instruments).

Statistical analysis

Data analyses and graphical display were performed with SigmaPlot (Version 11.0, Systat Software, Germany). All displayed values represent the mean ± standard error of mean (SEM). Significant differences between groups were determined using Student′s t-test.

Table 1. Composition of dissection buffer, ACSF and modified external solutions.

(in mM)	Dissection buffer	Normal ACSF	Modified ACSF-1	Modified ACSF-2
NaCl		124	124	125
KCl	5	5	5	5
NaH_2PO_4	1.23	1.23	1.23	1.23
$NaHCO_3$	26	26	26	26
Glucose	10	10	10	10
Sucrose	212.7			
$MgCl_2$	10	1.5	1.5	1.5
$CaCl_2$	0.5	2.5	2.5	2.5
Picrotoxin			0.1	
Tetrodotoxin (TTX)			0.001	0.001
DL-AP5			0.05	0.05
CNQX				0.02
Applications	Slice preparation	Slice recovery, measuring neuronal intrinsic properties (Fig. 1), sEPSC recordings (Fig. 2)	mEPSC recordings (Fig. 3)	mIPSC recordings (Fig. 4)

Table 2. Composition of internal solutions using in this study.

(in M)	Cs-based Internal Solution-1	Cs-based Internal Solution-2	K-based Internal Solution
Cs-$MeSO_4$	130		
CsCl		130	
K-gluconate			135
EGTA	0.5	1.1	
TEA-Cl	5		
NaCl	8	10	8
$MgCl_2$		2	
$CaCl_2$		0.1	
HEPES	10	10	10
QX-314	1		
ATP-Mg	4	2	2
GTP-Na	0.4		0.2
Phosphocreatine-Na_2	10		
Spermine	0.1		
Commom requirements	pH 7.4		
	280-290 mOsm		
Applications	mEPSC and eEPSC recordings (Fig. 3, 5, 6, and 7)	mIPSC recordings (Fig. 4)	Measuring neuronal intrinsic properties (Fig. 1 and 2)

Table 3. Composition of External Solution A and B.

(in mM)	External Solution A	External Solution B
NaCl	125	125
KCl	5	**2.5**
NaH_2PO_4	1.23	1.23
$NaHCO_3$	26	26
Glucose	10	10
$MgCl_2$	**4**	1.5
$CaCl_2$	**4**	2.5
Picrotoxin	0.1	0.1
Reasons	**Increasing divalent cations** reduces network activity.	**Reducing $[K^+]_e$** decreases the resting membrane potential and the possibility of the neuronal firing.
Applications	eEPSC recordings (Fig. 5a, 6a, 6c, and 7a)	eEPSC recordings (Fig. 5b, 6b, and 7b)

Results

Lrrtn3 KO mice show decreased excitability in the hippocampal DG granule cells.

Many researches to investigate the role of synaptic cell-adhesion molecules (CAMs) have focused on various synaptic phenotypes such as synaptogenesis, synaptic transmission and plasticity of these proteins. However, it is unclear and many previous researches did not focus on whether synaptic cell-adhesion molecules modulate neuronal intrinsic properties. I simply predicted that these proteins are important for not only synapse development and function but also for neuronal intrinsic properties like neuronal excitability, because of the Hebb's hypothesis – neurons that fire together wire together, and neurons that fire out of sync lose their link (Hebb, 1949). To test my prediction, I recorded the neuronal excitability by injecting various step depolarizing currents under current-clamp mode. Firing rates were decreased in DG granule cells in where LRRTM3 proteins are highly expressed from *Lrrtm3* KO mice (Figure 1a). However, firing rates in CA1 pyramidal neurons, hippocampal areas of no or less expression of LRRTM3, are similar between WT and *Lrrtm3* KO mice (Figure 1b). I also checked neuronal intrinsic properties such as membrane capacitance (Cm), input resistance (R_{in}) and resting membrane potential (RMP) in hippocampal DG granule cells and CA1 pyramidal neurons from WT and *Lrrtm3* KO mice. Interestingly, RMP in DG granule cells from *Lrrtm3* KO mice was higher than it of WT neurons, but Cm and R_{in} were not significantly different between two groups (Figure 1c). All neuronal intrinsic properties were similar in CA1 pyramidal neurons from WT and *Lrrtm3* KO mice. These results indicate that LRRTM3 protein is not only important for excitatory synapse development and function but also for neuronal excitability and other neuronal intrinsic properties.

Excitatory synaptic transmission is altered in Lrrtm3 KO PP-DG synapses.

It was recently revealed that LRRTM3 mediates excitatory synapse development in vitro (Um et al., 2016). Therefore, the next question is whether LRRTM3 proteins are important for excitatory synaptic function such as excitatory synaptic transmission and plasticity. To address this question, I first tested spontaneous excitatory postsynaptic currents (sEPSCs) in hippocampal DG granule cells and CA1 pyramidal neurons from WT and *Lrrtm3* KO mice. The amplitude of sEPSCs in DG granule cells from *Lrrtm3* KO mice was decreased, but the frequency was not different between two groups (Figure 2a). However, the amplitude and the frequency of sEPSCs are similar in CA1 pyramidal neurons of WT and *Lrrtm3* KO mice (Figure 2b). Next, I tested miniature EPSCs (mEPSCs), that measure with blocker of voltage-gated Na^+ channel (tetrodotoxin, TTX) to exclude neuronal activities, in hippocampal DG granule cells and CA1 pyramidal neurons. The amplitude of mEPSC was decreased similarly observed in sEPSC experiments, but the frequency of mEPSC was increased in DG granule cells from *Lrrtm3* KO mice (Figure 3a). The amplitude and the frequency of mEPSCs are similar in CA1 pyramidal neurons of WT and *Lrrtm3* KO mice (Figure 3b).

Next, I measured input-output (I-O) relationship by evoked excitatory synaptic transmission from perforant path (PP) to DG granule cells (PP-DG synapses). I commonly have used ACSF containing 5 mM KCl, but high extracellular K^+ concentration increases resting membrane potential and it sometimes causes polysynaptic responses and unexpected evoked excitatory postsynaptic currents (eEPSCs) with large Na^+ currents. Therefore, I added more divalent cations (4 mM $CaCl_2$ and $MgCl_2$) to reduce network excitability and then tested eEPSC experiments. Under this experimental condition (External Solution A, see Materials and Methods), there were no statistical difference between WT and *Lrrtm3* KO mice (Figure 4a). However, I-O responses of eEPSCs were significantly decreased

in *Lrrtm3* KO mice under different experimental conditions (External Solution B, See Materials and Methods) (Figure 4b). Taken together, excitatory basal synaptic transmission in hippocampal DG granule cells are decreased in *Lrrtm3* KO mice.

LRRTM3 proteins are not expressed in inhibitory synapses and thus are not involved in inhibitory synapse development (Um et al., 2016). It suggests that this protein does not affect inhibitory synaptic function, but it is not revealed yet. To verify this point, I recorded miniature inhibitory postsynaptic currents (mIPSCs) in hippocampal DG granule cells from WT and *Lrrtm3* KO mice. As a results, the amplitude and the frequency are not statistically different between WT and Lrrtm3 KO mice (Figure 5). It means that LRRTM3 does not affect inhibitory synaptic transmission.

Lrrtm3 KO mice show increased presynaptic release probability in PP-DG synapses.

When the number of synapses are reduced, the frequency of mEPSCs is usually decreased too. However, *Lrrtm3* KO mice have decreased synapse number (Um et al., 2016), but showed increased frequency of mEPSCs (Figure 3a). How can I explain this contradictory results? I hypothesized that *Lrrtm3* KO mice have increased presynaptic release probability (Pr) to compensate postsynaptic (decreased amplitudes of sEPSCs and mEPSCs and I-O relationships) and neuronal defects (decreased excitability). To verify this hypothesis, I first tested paired-pulse ratio (PPR), an indicator of Pr. As a results, *Lrrtm3* KO mice showed reduced PPR; lower PPR means higher Pr (Figure 6a and 6b). I also confirmed the increased Pr in excitatory synapses with altered short-term plasticity induced by repetitive stimulation composed of 20 pulses at 20 Hz (Figure 6c). These results suggest that

Lrrtm3 KO mice have increased excitatory presynaptic release probability in PP-DG synapses.

Lrrtm3 KO mice have intact Long-term potentiation (LTP) in PP-DG synapses.

Lastly, I tested whether LRRTM3 proteins affect synaptic plasticity. AMPA/NMDA ratio is one of functional plasticity measured by AMPA receptor-mediated EPSCs recorded at -70 mV divided by NMDA receptor-mediated responses as current amplitudes at 100 ms after the stimulation holding at +40 mV. Figure 7a shows that As a result, AMPA/NMDA ratio was slightly reduced, but not statistically different, in PP-DG synapses from *Lrrtm3* KO mice (Figure 7a). Long-term potentiation induced by high-frequency stimulation (HFS) that is composed of 8 trains of 8 stimuli at 200 Hz (intertrain interval of 2 s) with depolarization at 0 mV applied to LPP-DG synapses was similar between WT and *Lrrtm3* KO mice (Figure 7b).

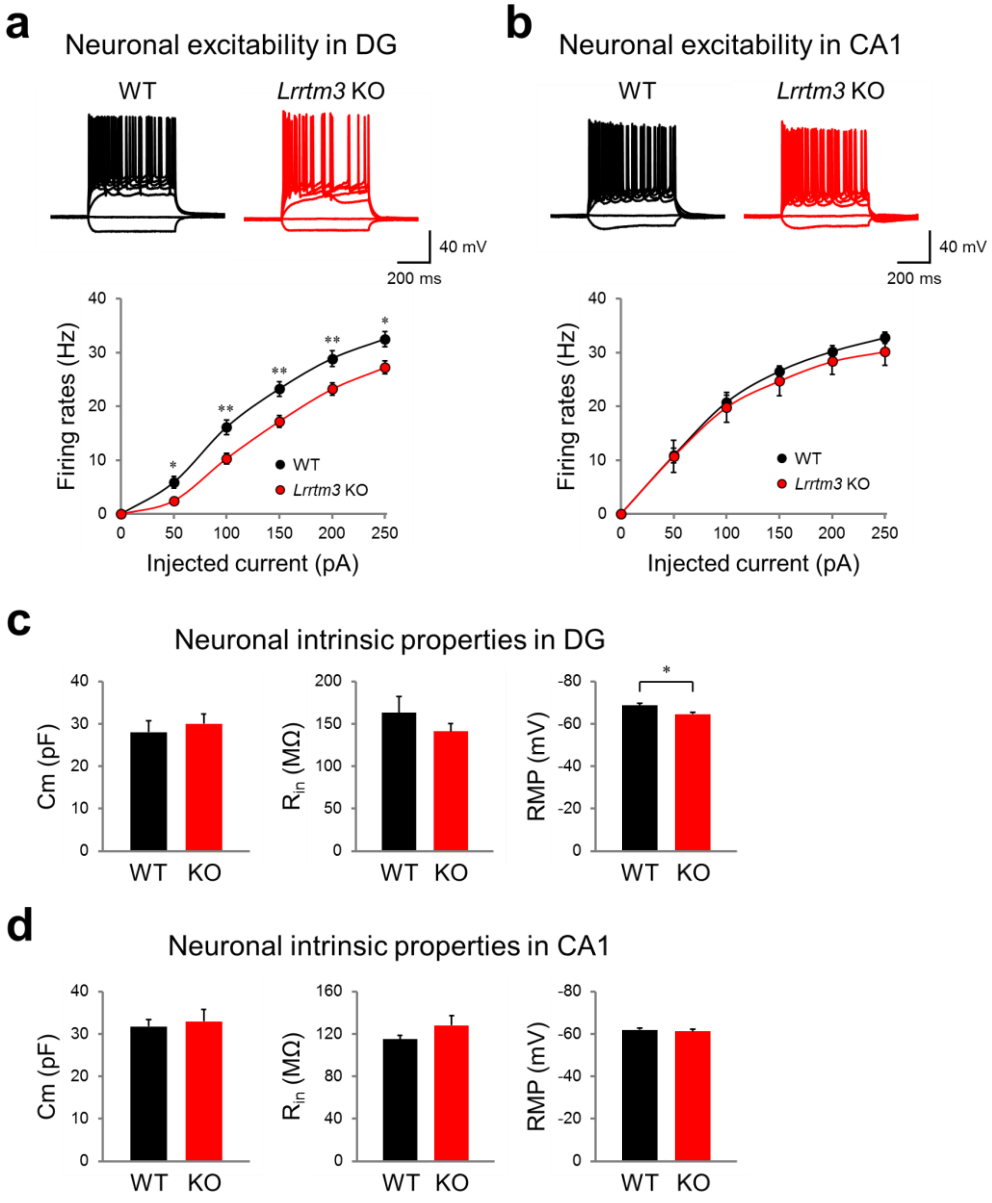
a
Neuronal excitability in DG
WT
Lrrtm3 KO
40 mV
200 ms
Firing rates (Hz)
Injected current (pA)
WT
Lrrtm3 KO
b
Neuronal excitability in CA1
WT
Lrrtm3 KO
40 mV
200 ms
Firing rates (Hz)
Injected current (pA)
WT
Lrrtm3 KO
c
Neuronal intrinsic properties in DG
Cm (pF)
R_in (MΩ)
RMP (mV)
WT KO
d
Neuronal intrinsic properties in CA1
Cm (pF)
R_in (MΩ)
RMP (mV)
WT KO

Figure 1. Intrinsic properties are altered in the hippocampal DG granule cells, but not in CA1 pyramidal neurons, from *Lrrtm3* KO mice.

(a and b) Representative traces (top) and summary graphs (bottom) of neuronal excitability measured as firing rates in response to step depolarizing currents (500 ms duration) under current-clamp mode in DG granule cells (a) or CA1 pyramidal neurons (b) from WT (left, black) or *Lrrtm3* KO mice (right, red) (top).

(c and d) Hippocampal DG granule cells (c, right), but not CA1 pyramidal neurons (d, right), from *Lrrtm3* KO mice exhibit a more positive resting membrane potential (RMP) than WT. Membrane capacitance (Cm) (c and d, left) and input resistance (Rin) (c and d, middle) of both regions are not statistically different. Individual points (a and b) or bar graphs (c and d) represent means ± SEM (*$p < 0.05$ and **$p < 0.01$, Student's t-test; WT_{DG}, n = 16 cells from 3 mice; KO_{DG}, n = 13, 3; WT_{CA1}, n = 18, 8; and KO_{CA1}, n = 11, 5).

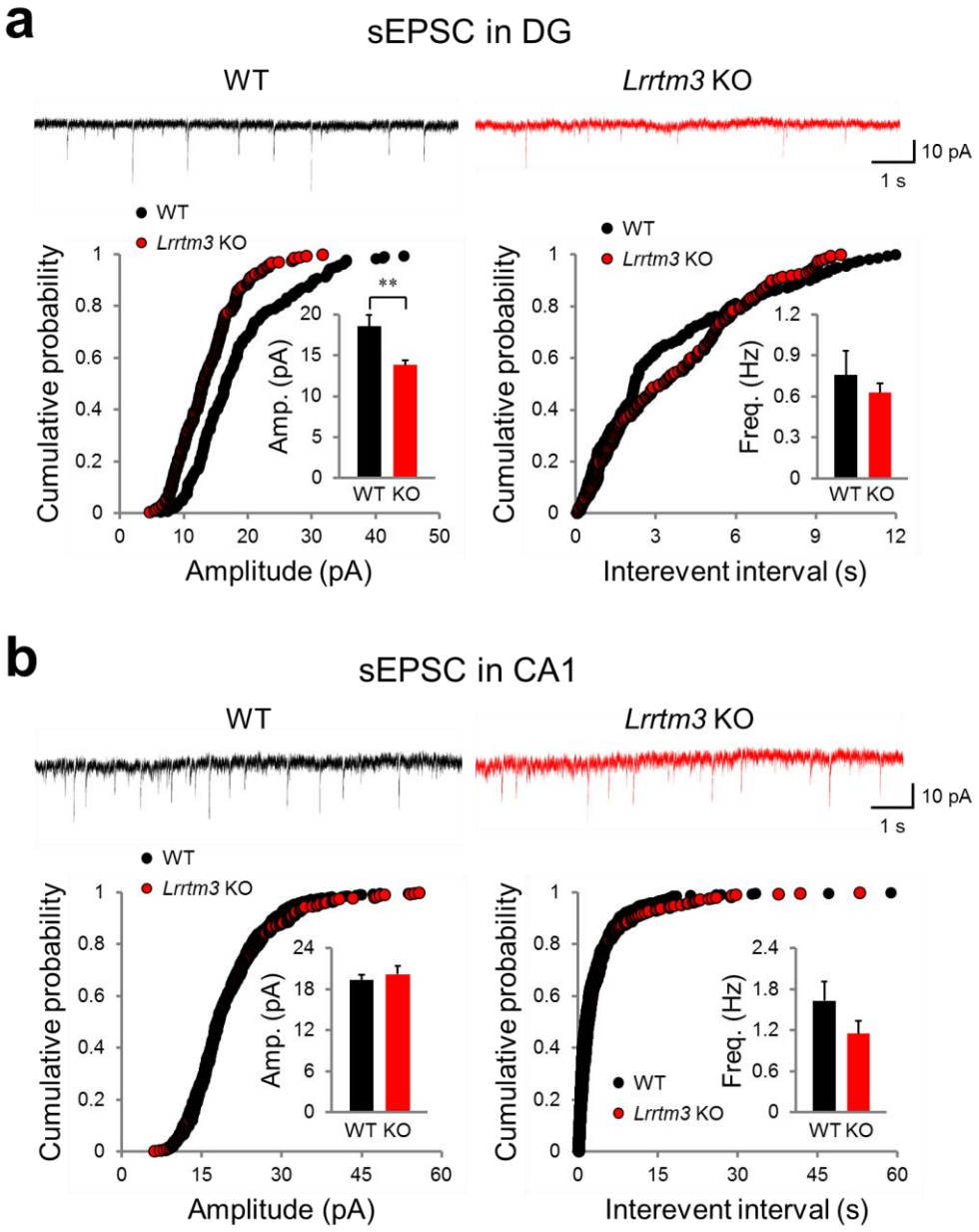
a
sEPSC in DG
WT
Lrrtm3 KO
10 pA
1 s
WT
Lrrtm3 KO
Cumulative probability
Amplitude (pA)
Amp. (pA)
**
WT KO
Interevent interval (s)
Freq. (Hz)
b
sEPSC in CA1

Figure 2. Spontaneous EPSCs (sEPSCs) are reduced in hippocampal DG granule cells, but not in CA1 pyramidal neurons, from *Lrrtm3* KO mice.

(a) Amplitudes but not frequencies of sEPSCs are reduced in *Lrrtm3* KO DG granule cells. Representative traces of sEPSCs from WT (left, black) or *Lrrtm3* KO DG granule cells (red, right) (top). Cumulative plots of amplitudes (left) and frequencies (right) (bottom). The inset compares the average or frequency of sEPSCs. Bar graphs represent means ± SEM (** $p < 0.01$, Student's t-test; WT, n = 12 cells from 4 mice; and KO, n = 9, 2).

(b) Amplitudes and frequencies of sEPSCs are similar between WT and *Lrrtm3* KO CA1 pyramidal neurons. Representative traces of sEPSCs from WT (left, black) or *Lrrtm3* KO pyramidal neurons (red, right) (top). Cumulative plots of amplitudes (left) and frequencies (right) (bottom). The inset compares the average or frequency of sEPSCs. Bar graphs represent means ± SEM (WT, n = 12 cells from 5 mice; and KO, n = 7, 3).

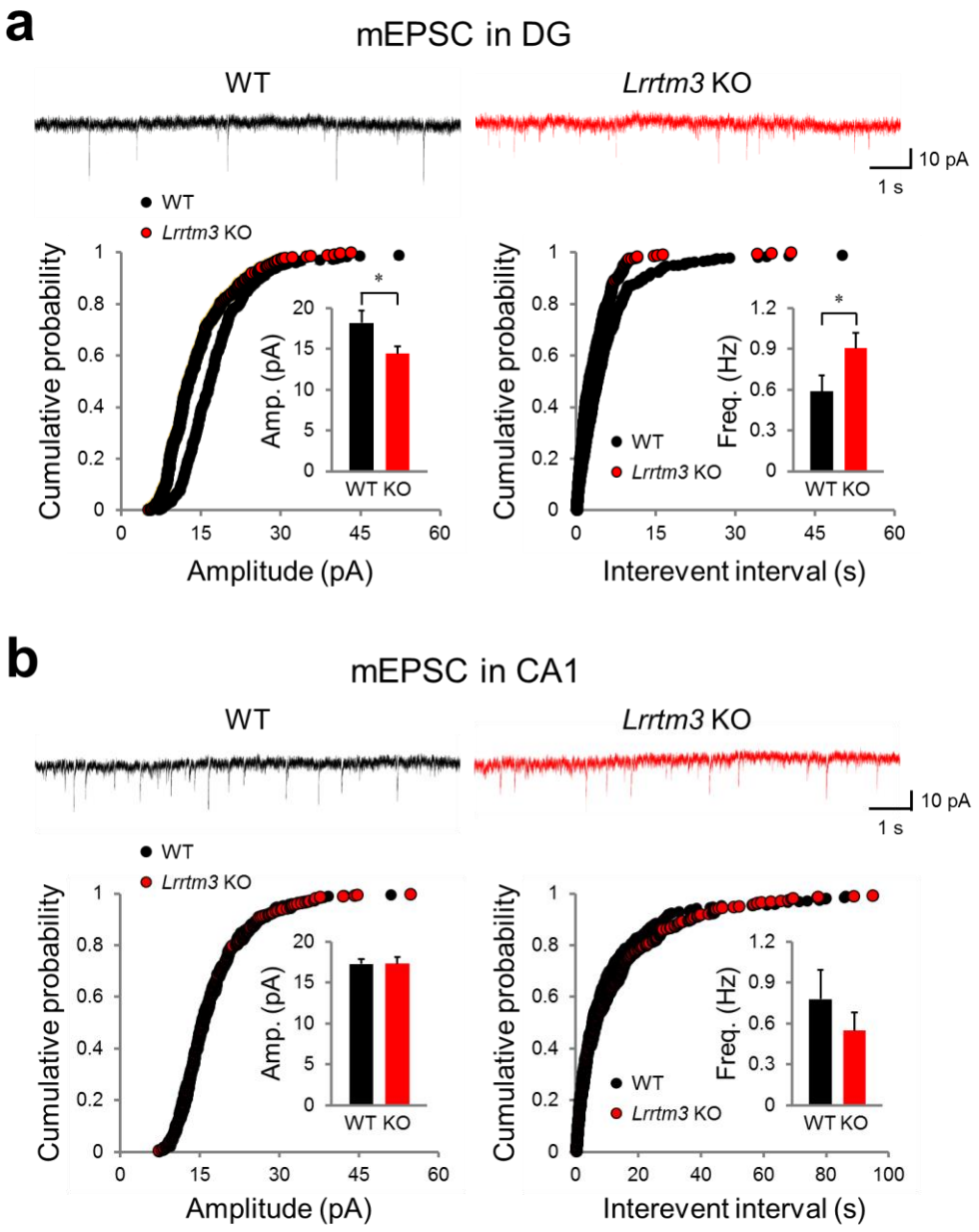
a
mEPSC in DG
WT
Lrrtm3 KO
10 pA
1 s
WT
Lrrtm3 KO
Cumulative probability
Amplitude (pA)
Amp. (pA)
WT KO
Interevent interval (s)
Freq. (Hz)
b
mEPSC in CA1

Figure 3. Miniature EPSCs (mEPSCs) are altered in hippocampal DG granule cells, but not in CA1 pyramidal neurons, from *Lrrtm3* KO mice.

(a) Amplitudes of mEPSCs are decreased, but frequencies of mEPSCs are increased in *Lrrtm3* KO DG granule cells. Representative traces of mEPSCs from WT (left, black) or *Lrrtm3* KO DG granule cells (red, right) (top). Cumulative plots of amplitudes (left) and frequencies (right) (bottom). The inset compares the average or frequency of mEPSCs. Bar graphs represent means ± SEM (* $p < 0.05$, Student's t-test; WT, n = 15 cells from 5 mice; and KO, n = 14, 3).

(b) Amplitudes and frequencies of mEPSCs are similar between WT and *Lrrtm3* CA1 pyramidal neurons. Representative traces of mEPSCs from WT (left, black) or Lrrtm3 KO CA1 pyramidal neuronas (red, right) (top). Cumulative plots of amplitudes (left) and frequencies (right) (bottom). The inset compares the average or frequency of mEPSCs. Bar graphs represent means ± SEM (WT, n = 15 cells from 4 mice; and KO, n = 17, 3).

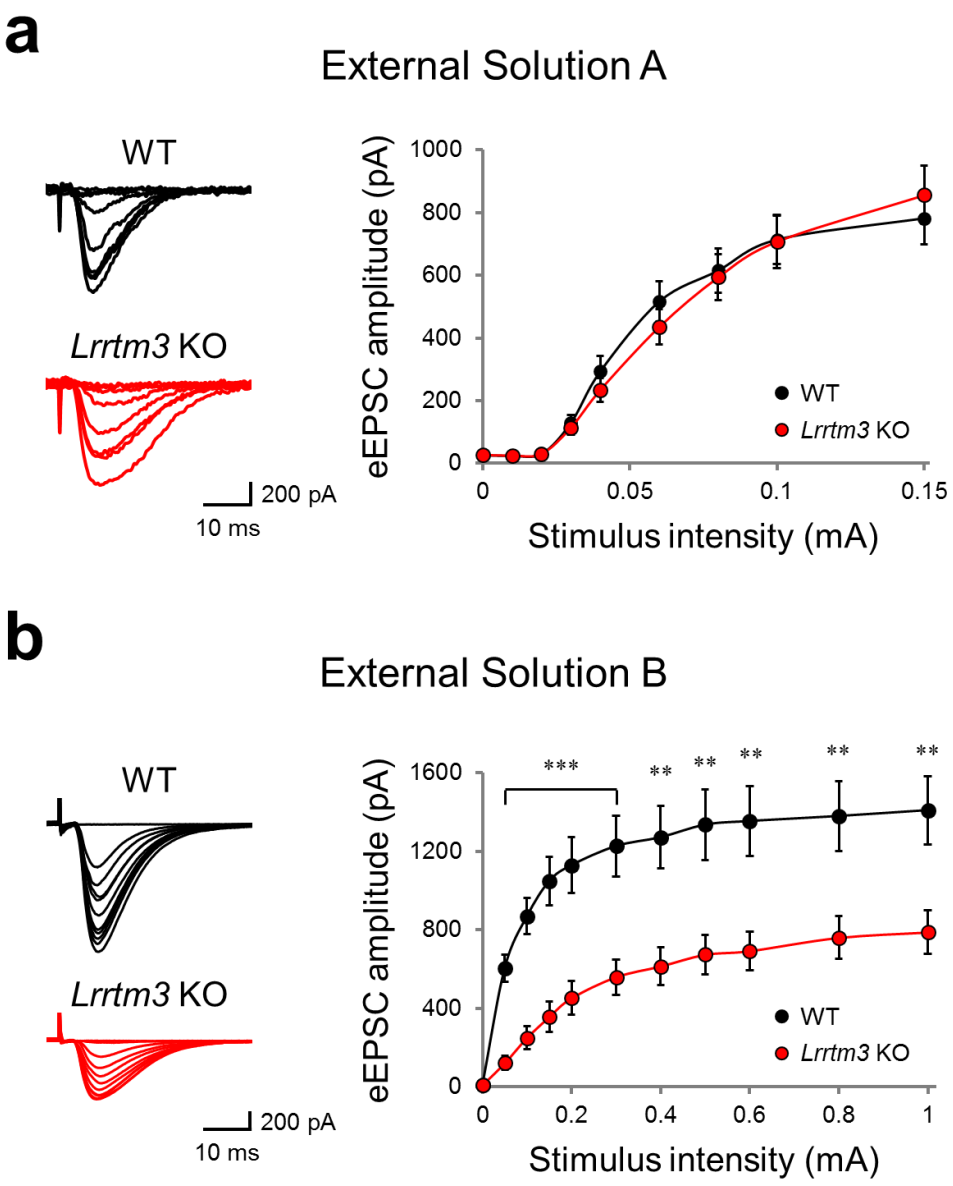
a
External Solution A
WT
Lrrtm3 KO
200 pA
10 ms
eEPSC amplitude (pA)
1000
800
600
400
200
0
0
0.05
0.1
0.15
Stimulus intensity (mA)
WT
Lrrtm3 KO
b
External Solution B
WT
Lrrtm3 KO
200 pA
10 ms
eEPSC amplitude (pA)
1600
1200
800
400
0
***
**
**
**
**
**
0
0.2
0.4
0.6
0.8
1
Stimulus intensity (mA)
WT
Lrrtm3 KO

Figure 4. *Lrrtm3* KO mice show decreased evoked excitatory synaptic transmission in PP-DG synapses.

(a and b) Evoked excitatory synaptic transmission is decreased under the electrophysiological experiment using external solution B (b), but similar using external solution A (a) (see *Materials and Methods*) in *Lrrtm3* KO mice. Representative traces (left) and summary graph (right) of evoked EPSCs (eEPSCs) recorded in PP-DG synapses from WT (top, blacK) or *Lrrtm3* KO brain slices (bottom, red). The synaptic input-output relationship is obtained by plotting the amplitudes of eEPSCs against stimulus intensities. Individual points represent means ± SEM (**$p < 0.01$ and ***$p < 0.001$, Student's t-test; WT, n = 20 slices from 4 mice; and KO, n = 17, 3 for Figure 5a; WT, n = 11, 2; and KO, n = 13, 2 for Figure 5b).

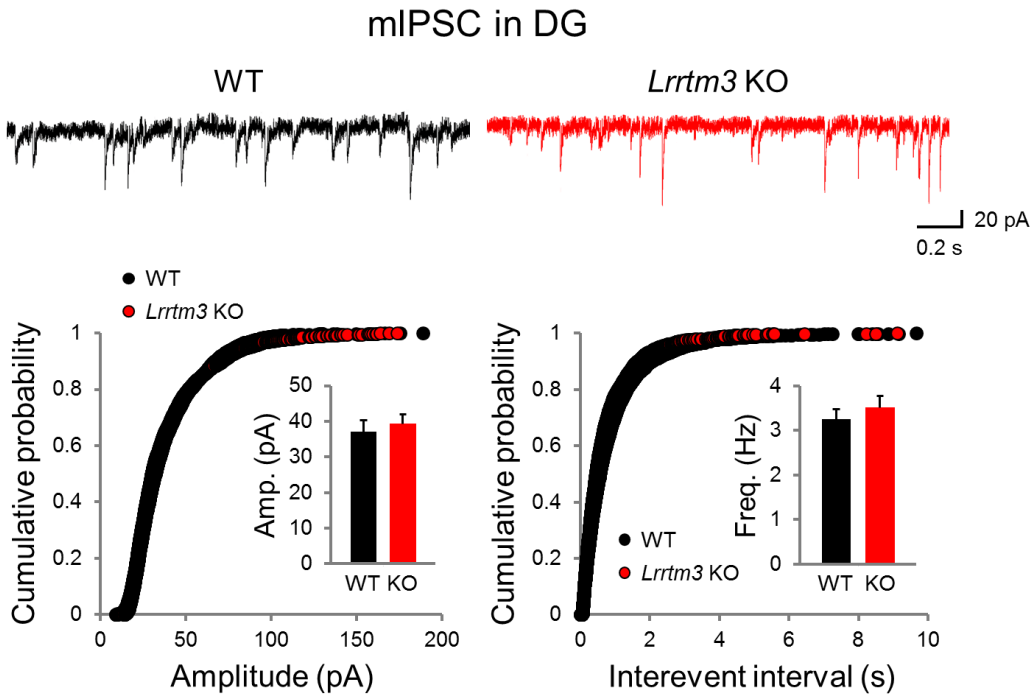

Figure 5. Inhibitory basal synaptic transmission is not altered in *Lrrtm3* KO mice.

Amplitudes and frequencies of mIPSCs are not significantly different in hippocampal DG granule cells from WT and *Lrrtm3* KO mice. Representative traces of mIPSCs from WT (left, black) or *Lrrtm3* KO DG granule cells (red, right) (top). Cumulative plots of amplitudes (left) and frequencies (right) (bottom). The inset compares the average or frequency of mIPSCs. Bar graphs represent means ± SEM (WT, n = 17 cells from 3 mice; and KO, n = 13, 2).

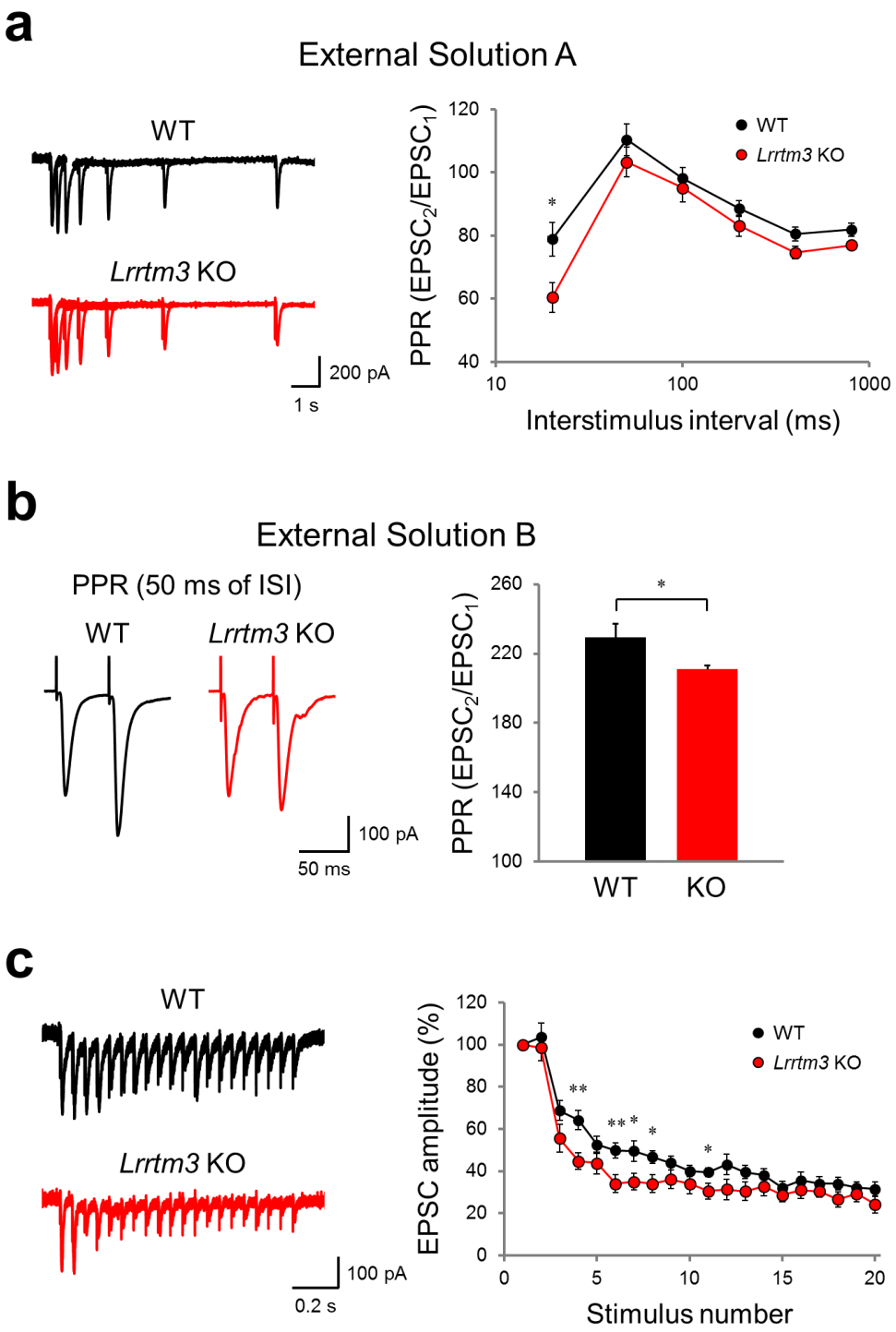
a
External Solution A
WT
Lrrtm3 KO
200 pA
1 s
PPR (EPSC2/EPSC1)
120
100
80
60
40
10
100
1000
Interstimulus interval (ms)
WT
Lrrtm3 KO
*
b
External Solution B
PPR (50 ms of ISI)
WT
Lrrtm3 KO
100 pA
50 ms
PPR (EPSC2/EPSC1)
260
220
180
140
100
WT
KO
*
c
WT
Lrrtm3 KO
100 pA
0.2 s
EPSC amplitude (%)
120
100
80
60
40
20
0
0
5
10
15
20
Stimulus number
WT
Lrrtm3 KO
**
**
*
*
*

Figure 6. *Lrrtm3* KO mice show increased excitatory presynaptic release probability in PP-DG synapses.

(a and b) Paired-pulse ratio (PPR) is decreased in PP-DG synapses from *Lrrtm3* KO mice under two different experimental conditions. (a) The ratio of paired-pulse responses (second eEPSC amplitude/first eEPSC amplitude) are plotted against interstimulus intervals (ISIs, ms). The electrophysiological experiment is conducting with external solution A (see *Materials and Methods*). Representative traces (left) and summary graph (right) of PPR. Individual points represent means ± SEM (*$p < 0.05$, Student's t-test; WT, n = 24 slices from 4 mice; and KO, n = 22, 4).

(b) PPR induced by 50 ms of interstimulus interval (ISI) between WT (black) and *Lrrtm3* KO mice (red). The electrophysiological experiment is conducting with external solution B (see *Materials and Methods*). Representative traces (left) and summary graph (right) of PPR. Bar graphs represent means ± SEM (*$p < 0.05$, Student's t-test; WT, n = 12, 2; and KO, n = 17, 2).

(c) Short-term synaptic plasticity (STP) is altered in PP-DG synapses from *Lrrtm3* KO mice. eEPSCs in response to 20 pulses at 20 Hz stimulation are recorded at DG granule cells in hippocampal slices and Relative amplitude of EPSCs are plotted as a function of stimulus number in WT (top, black) or *Lrrtm3* KO mice (bottom, red). Representative traces (left) and summary graph (right) of STP. Individual points represent means ± SEM (*$p < 0.05$ and **$p < 0.01$, Student's t-test; WT, n = 11 slices from 4 mice; and KO, n = 10, 4).

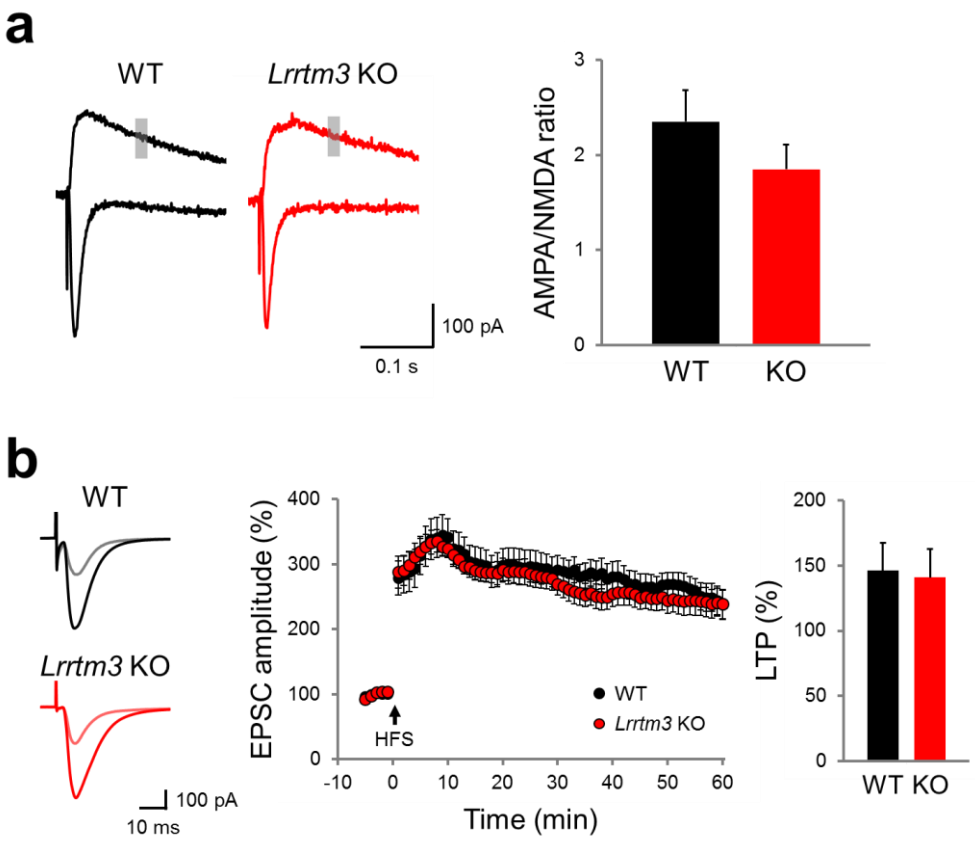
a
WT
Lrrtm3 KO
100 pA
0.1 s
AMPA/NMDA ratio
3
2
1
0
WT
KO
b
WT
Lrrtm3 KO
100 pA
10 ms
EPSC amplitude (%)
400
300
200
100
0
HFS
WT
Lrrtm3 KO
-10
0
10
20
30
40
50
60
Time (min)
LTP (%)
200
150
100
50
0
WT KO

Figure 7. *Lrrtm3* KO mice have normal long-term synaptic plasticity.

(a) AMPA/NMDA ratio is not statistically different in PP-DG synapses from WT and *Lrrtm3* KO mice. Representative traces (left) and summary graph (right) of evoked AMPA and NMDA receptor-mediated EPSCs recorded in the same cells from WT (black) and *Lrrtm3* KO mice (red). AMPA and NMDA receptor-mediated EPSCs are measured by their different time courses; AMPAR-mediated responses are recorded at the peak amplitude at a holding potential of -70 mV, and NMDAR-mediated responses are measured as current amplitude at 100 ms after the stimulation (gray rectangular areas) at holding potential of +40 mV. Bar graphs represent means ± SEM (WT, n = 29, 4; and KO, n = 23, 4).

(b) Lack of LRRTM3 does not affect the expression of long-term potentiation (LTP) in hippocampal PP-DG synapses. Representative traces of eEPSCs 1min before (gray and pink) and 1 h after (black and red) tetanic stimulation (left). Summary time courses (middle) and quantification of the LTP magnitude (right) for WT (black) and Lrrtm3 KO mice (red). Individual points (middle) or bar graphs (right) represent means ± SEM (WT, n = 12 cells from 5 mice; and KO, n = 15, 5).

Discussion

Summary of this study

In this study, I found four key observations related to physiological function of LRRTM3. First, synaptic interactions through LRRTM3 mediate not only excitatory synapse development (Um et al., 2016), but also neuronal intrinsic properties such as excitability (Figure 1). Second, this protein affects excitatory, but not inhibitory, synaptic transmission (Figure 2-5) by recruiting postsynaptic AMPA receptors (Um et al., 2016). Third, *Lrrtm3* KO mice shows increased excitatory release probability (Figure 6). Lastly, synaptic plasticity such as AMPA/NMDA ratio and LTP is not affected by the presence or the absence of LRRTM3 (Figure 7).

Limitations and contradictions of this study

In my first finding, it is contradictory because neurons that have higher RMP usually show more action potentials by same current injection in current-clamp mode. However, hippocampal DG granule cells from Lrrtm3 KO mice shows lower firing rates, but higher RMP (Figure 1a and 1c). To overcome this contradiction, more experiments, such as to check the expression patterns of channels involved in generating action potentials and modulating resting membrane potential, are needed.

In my second observation, the reason why the frequency of sEPSC is not changed but the frequency of mEPSC is increased in *Lrrtm3* KO mice is not clear (Figure 2a and 3a), but one possibility is that tetrodotoxin (TTX)-sensitive component of excitatory synaptic transmission is markedly inactive whereas TTX-resistant component is hyperactive.

These physiological results are also not matched well with previous synaptic structural studies (Um et al., 2016). Um et al reported that vGluT1, an excitatory presynaptic marker, and spine numbers observed by electron microscope were reduced in hippocampal DG areas from *Lrrtm3* KO mice, but the frequency of mEPSCs are increased (Figure 3a). I suppose these changes are a kind of homeostatic changes for compensation of pre- and postsynaptic and neuronal changes in *Lrrtm3* KO mice. This idea is supported by my third finding - presynaptic release probability (Pr) in *Lrrtm3* KO mice (Figure 6).

I stimulated lateral perforant path (LPP)-DG synapses that usually show paired-pulse facilitation (PPF), but my results were mainly paired-pulse depression (PPD), one of main characteristics in medial perforant path (MPP)-DG synapses (Figure 6a). The reason why I obtained these results was the composition of external solution. External solution A contains 4mM Ca^{2+} ions and it may induce more neurotransmitter releases. When I experimented with External Solution B containing normal external Ca^{2+} concentration (2.5 mM), PPF was recorded in LPP-DG synapses (Figure 6b).

The correlation between LRRTMs and synaptic plasticity such as LTP is unclear yet. Soler-Llavina et al reported that LTP was blocked by double knockdown (DKD) of LRRTM1 and LRRTM2 in hippocampal CA1 areas (DKD at postnatal day 0 (P0) or at P21 and recorded at 2 weeks or 5 weeks). And, LTP was recovered by rescue of LRRTM2 (Soler-Llavina et al., 2013). It means that LTP is induced when only one of LRRTMs is exist at postsynaptic membranes. *Lrrtm3* KO mice have normal LTP in PP-DG synapses (Figure 7b) because both LRRTM3 and LRRTM4 are expressed in hippocampal DG areas and there exist LRRTM4 proteins in PP-DG synapses in *Lrrtm3* KO mice. I am predicting that LTP was blocked by *Lrrtm3* and *Lrrtm4* DKO or LRRTM4 KD in *Lrrtm3* KO mice.

Comparison of physiological properties of LRRTM proteins

The expression patterns of LRRTM3 and LRRTM4 are same in the hippocampus – both of them are enriched in DG areas. Their roles in excitatory synapse development are also similar – to promote synaptogenesis by interacting presynaptic ligands. However, synaptic function, especially in excitatory synaptic transmission, of these two proteins are different. *Lrrtm4* KO mice showed decreased frequency, but normal amplitude of mEPSC in hippocampal DG granule cells (Siddiqui et al., 2013). However, *Lrrtm3* KO mice showed increased frequency, but decreased amplitude of mEPSC in hippocampal DG granule cells (Figure 3a). PPR in *Lrrtm4* KO mice was not different (Siddiqui et al., 2013), but *Lrrtm3* KO mice had decreased PPR (Figure 6a and 6b). Taken together, *Lrrtm4* KO mice generally shows reduced synapse number and excitatory synaptic transmission, but excitatory synapses in *Lrrtm3* KO mice homeostatically compensate with increased Pr and structural and functional postsynaptic defects (table 4). The molecular mechanism of these differences is unclear, but one possibility is the differences of presynaptic ligands; LRRTM3 binds with neurexins, but LRRTM4 binds not only with neurexins but also with PTPσ and GPCs (Jo et al., 2015; Um et al., 2016).

Further studies

Spatiotemporal expression pattern of LRRTM3 is changed. The expression level of LRRTM3 is increased during the development, and LRRTM3 is expressed not only in the hippocampal DG areas, but also in other brain regions such as cerebellum, striatum or medial prefrontal cortex (Um et al., 2016). In this study, however, I tested the synaptic function only in hippocampal PP-DG synapses at

juvenile stages. Therefore, it is necessary to study the detailed synaptic function in other circuits and other developmental stages.

In this study, I revealed the role of LRRTM3 only one aspect - loss-of-function of LRRTM3. It is necessary to investigate whether the physiological changes are recovered by overexpression of *Lrrtm3* via viral gene delivery in specific brain regions at specific neurodevelopmental stages in *Lrrtm3* KO mice. Especially, it was revealed that there are two types of splicing variants of LRRTM3 – LRRTM3S (short) and LRRTM3L (long), and these two proteins show different function. For example, both of them have strong synaptogentic effect, but they show different spatiotemporal expression patterns in the brain, and have different interaction ability with PSD-95; only LRRTM3S binds directly with PSD-95. It results differences in surface expression of GluA1 under the induction of chemical LTP (Um *et al*., 2016). Therefore, it is necessary to confirm the differences between LRRTM3S and LRRTM3L by overexpressing one of them in *Lrrtm3* KO mice.

Table 4. Comparison of physiological properties of LRRTM proteins.

LRRTM proteins			LRRTM3	LRRTM4		LRRTM1	LRRTM2
In vivo study	Animal models		*Lrrtm3* KO mice	*Lrrtm4* KO mice	*Lrrtm4* KD	*Lrrtm1* KO mice	*Lrrtm2* KD
Electrophysiology	Excitability		↓				
	mEPSC	Amp	↓	↔	↓		↓
		Freq	↑	↓	↔		↔
	sEPSC	Amp	↓				
		Freq	↔				
	eEPSC	I-O	↓	↓			
		PPR	↓	↔			↔
		STP	↓				
		A/N ratio	↔				↓
		LTP	↔				
	mIPSC	Amp	↔	↔			
		Freq	↔	↔			
Structure	IF	vGluT1	↓	↓		↑	
		GAD67 or GAD65	↔	↔			
		Basson				↔	
		GFP			↓		
	EM	Spine number	↓				
		PSD length	↔				
		PSD thickness	↔				

		Synapse density				↓	
		mean SV distance				↑	
	Golgi staining	Spine density	↓	↓		↔	
		Spine length				↑	
Studied brain areas			HP PP-DG synapses	HP PP-DG synapses	L2/3 neurons in SSCx	HP CA1 areas	HP PP-DG synapses
In vitro study	Presynaptic ligands		Neurexins (SS4-)	HSPGs	HSPGs / PTPs	Neurexins (SS4-)	Neurexins (SS4-)
	Roles		Excitatory synapse development / *function*				
References			Um *et al*., *Cell Rep* (2016).	Siddiqui *et al*., *Neuron* (2013).	de Wit *et al*., *Neuron* (2013); Ko *et al*., *Proc Natl Acad Sci USA* (2015).	Linhoff *et al*., *Neuron* (2009); Siddiqui *et al*., *J Neurosci* (2010); Takashima *et al*., *PLoS ONE* (2011).	Ko *et al*., *Neuron* (2009); de Wit *et al*., *Neuron* (2009); Siddiqui *et al*., *J Neurosci* (2010).

References

1. Betancur, C., Sakurai, T., Buxbaum, J.D. (2009) The emerging role of synaptic cell-adhesion pathways in the pathogenesis of autism spectrum disorders. Trends Neurosci. 32(7):402-12.

2. Budreck, E.C., Scheiffele, P. (2007) Neuroligin-3 is a neuronal adhesion protein at GABAergic and glutamatergic synapses. Eur J Neurosci. 26(7):1738-48.

3. Choi, T.Y., Jung, S., Nah, J., Ko, H.Y., Jo, S.H., Chung, G., Park, K., Jung, Y.K., Choi, S.Y. (2015) Low levels of methyl β-cyclodextrin disrupt GluA1-dependent synaptic potentiation but not synaptic depression. J Neurochem. 132(3):276-85.

4. Clem, R.L., Huganir, R.L. (2010) Calcium-permeable AMPA receptor dynamics mediate fear memory erasure. Science. 330(6007):1108-12.

5. Dalva, M.B., McClelland, A.C., Kayser, M.S. (2007) Cell adhesion molecules: signalling functions at the synapse. Nat Rev Neurosci. 8(3):206-20.

6. de Wit, J., Ghosh, A. (2014) Control of neural circuit formation by leucine-rich repeat proteins. Trends Neurosci. 37(10):539-50.

7. de Wit, J., Ghosh, A. (2016) Specification of synaptic connectivity by cell surface interactions, Nat Rev Neurosci. 17:22-39.

8. de Wit, J., Hong, W., Luo, L., Ghosh, A. (2011) Role of leucine-rich repeat proteins in the development and function of neural circuits. Annu Rev Cell Dev Biol. 27:697-729.

9. de Wit, J., Sylwestrak, E., O'Sullivan, M.L., Otto, S., Tiglio, K., Savas, J.N., Yates, J.R. 3rd., Comoletti, D., Taylor, P., Ghosh, A. (2009) LRRTM2 interacts with Neurexin1 and regulates excitatory synapse formation. Neuron. 64(6):799-806.

10. Hebb, D. (1949) The organization of behavior.

11. Jo, S., Yarishkin, O., Hwang, Y.J., Chun, Y.E., Park, M., Woo, D.H., Bae, J.Y., Kim, T., Lee, J., Chun, H., Park, H.J., Lee, da Y., Hong, J., Kim, H.Y., Oh, S.J., Park, S.J., Lee, H., Yoon, B.E., Kim, Y., Jeong, Y., et al., (2014) GABA from reactive astrocytes impairs memory in mouse models of Alzheimer's disease. Nat Med. 20(8):886-96.

12. Ko, J. (2012) The leucine-rich repeat superfamily of synaptic adhesion molecules: LRRTMs and Slitrks. Mol Cells. 34(4):335-40.

13. Ko, J., Kim, E. (2007) Leucine-rich repeat proteins of synapses. J Neurosci Res. 85(13):2824-32.

14. Ko, J.S., Pramanik, G., Um, J.W., Shim, J.S., Lee, D., Kim, K.H., Chung, G.Y., Condomitti, G., Kim, H.M., Kim, H., de Wit, J., Park, K.S., Tabuchi, K., Ko, J. (2015) PTPσ functions as a presynaptic receptor for the glypican-4/LRRTM4 complex and is essential for excitatory synaptic transmission. Proc Natl Acad Sci U S A. 112(6):1874-9.

15. Laakso, T., Muggalla, P., Kysenius, K., Laurén, J., Paatero, A., Huttunen, H.J., Airaksinen, M.S. (2012) LRRTM3 is dispensable for amyloid-β production in mice. J Alzheimers Dis. 31(4):759-64.

16. Laurén, J., Airaksinen, M.S., Saarma, M., Timmusk, T. (2003) A novel gene family encoding leucine-rich repeat transmembrane proteins differentially expressed in the nervous system. Genomics. 81(4):411-21.

17. Lincoln, S., Allen, M., Cox, C.L., Walker, L.P., Malphrus, K., Qui, Y. (2013) LRRTM3 interacts with APP and BASE1 and has variants associating with late-onset Alzheimer's disease (LOAD). PLoS ONE. 8(6):e64164.

18. Linhoff, M.W., Laurén, J., Cassidy, R.M., Dobie, F.A., Takahashi, H., Nygaard, H.B., Airaksinen, M.S., Strittmatter, S.M., Craig, A.M. (2009) An unbiased expression screen for synaptogenic proteins identifies the LRRTM protein family as synaptic organizers. Neuron. 61(5):734-49.

19. Majercak, J., Ray, W.J., Espeseth, A., Simon, A., Shi, X.P., Wolffe, C., Getty, K., Marine, S., Stec, E., Ferrer, M., Strulovici, B., Bartz, S., Gates, A., Xu, M., Huang, Q., Ma, L., Shughrue, P., Burchard, J., Colussi, D., Pietrak, B., et al., (2006) LRRTM3 promotes processing of amyloid-precursor protein by BACE1 and is a positional candidate gene for late-onset Alzheimer's disease. Proc Natl Acad Sci U S A. 103(47):17967-72.

20. Michaelson, J.J., Shi, Y., Gujral, M., Zheng, H., Malhotra, D., Jin, X., Jian, M., Liu, G., Greer, D., Bhandari, A., Wu, W., Corominas, R., Peoples, A., Koren, A., Gore, A., Kang, S., Lin, G.N., Estabillo, J., Gadomski, T., Singh, B., et al., (2012) Whole-genome sequencing in autism identifies hot spots for de novo germline mutation. Cell. 151(7):1431-42.

21. Seo, J., Giusti-Rodríguez, P., Zhou, Y., Rudenko, A., Cho, S., Ota, K.T., Park, C., Patzke, H., Madabhushi, R., Pan, L., Mungenast, A.E., Guan, J.S., Delalle, I., Tsai, L.H. (2014) Activity-dependent p25 generation regulates synaptic plasticity and Aβ-induced cognitive impairment. Cell. 157(2):486-98.

22. Shanks, N.F., Savas, J.N., Maruo, T., Cais, O., Hirao, A., Oe, S., Ghosh, A., Noda, Y., Greger, I.H., Yates, J.R. 3rd., Nakagawa, T. (2012) Differences in AMPA and kainate receptor interactomes facilitate identification of AMPA receptor auxiliary subunit GSG1L. Cell Rep. 1(6):590-8.

23. Siddiqui, T.J., Pancaroglu, R., Kang, Y., Rooyakkers, A., Craig. A.M. (2010) LRRTMs and neuroligins bind neurexins with a differential code to cooperate in glutamate synapse development. J Neurosci. 30(22):7495-506.

24. Siddiqui, T.J., Tari, P.K., Connor, S.A., Zhang, P., Dobie, F.A., She, K., Kawabe, H., Wang, Y.T., Brose, N., Craig, A.M. (2013) An LRRTM4-HSPG complex mediates excitatory synapse development on dentate gyrus granule cells. Neuron. 79(4):680-95.

25. Sousa, I., Clark, T.G., Holt, R., Pagnamenta, A.T., Mulder, E.J., Minderaa, R.B., Bailey, A.J., Battaglia, A., Klauck, S.M., Poustka, F., Monaco, A.P.; International Molecular Genetic Study of Autism Consortium (IMGSAC). (2010) Polymorphisms in leucine-rich repeat genes are associated with autism spectrum disorder susceptibility in populations of European ancestry. Mol Autism. 1(1):7.

26. Südhof, T.C. (2008) Neuroligins and neurexins link synaptic function to cognitive disease. Nature. 455(7215):903-11.

27. Takashima, N., Odaka, Y.S., Sakoori, K., Akagi, T., Hashikawa, T., Morimura, N., Yamada, K., Aruga, J. (2011) Impaired cognitive function and altered hippocampal synapse morphology in mice lacking Lrrtm1, a gene associated with schizophrenia. PLoS One. 6(7):e22716.

28. Um, J.W., Choi, T.Y., Kang, H., Cho, Y.S., Choii, G., Uvarov, P., Park, D., Jeong, D., Jeon, S., Lee, D., Kim, H., Lee, S.H., Bae, Y.C., Choi, S.Y., Airaksinen, M.S., Ko, J. (2016) LRRTM3 Regulates Excitatory Synapse Development through Alternative Splicing and Neurexin Binding. Cell Rep. 14(4):808-22.

29. Varoqueaux, F., Jamain, S., Brose, N. (2004) Neuroligin 2 is exclusively localized to inhibitory synapses. Eur J Cell Biol. 83(9):449-56.

30. Voikar, V., Kulesskaya, N., Laakso, T., Lauren, J., Strittmatter, S.M., Airaksinen, M.S. (2013) LRRTM1-deficient mice show a rare phenotype of

avoiding small enclosures--a tentative mouse model for claustrophobia-like behaviour. Behav Brain Res. 238:69-78.

31. Wang, Y., Wu, J., Rowan, M.J., Anwyl, R. (1997) Conditions for the induction of long-term potentiation and long-term depression by conjunctive pairing in the dentate gyrus in vitro. J Neurophysiol. 78(5):2569-73.

Chapter II.

Cereblon (*CRBN*), a human intellectual disability-related gene, maintains synaptic and cognitive function by modulating BK channels.

Abstract

Intellectual disability is one of the most common cognitive disorders; however, its molecular mechanisms remain poorly understood. Recent studies have revealed a series of synaptic proteins as factors related to this disease. Mutations in the *cereblon* (*CRBN*) gene cause intellectual disability in humans, but the detailed mechanisms of CRBN in the synapse are mostly unclear yet. Here we studied the role of CRBN in synaptic function using *Crbn* knockout (KO) mice. Various types of long-term synaptic plasticity, a cellular and molecular mechanism of learning and memory, such as long-tern potentiation (LTP) and long-term depression (LTD) in hippocampal Schaffer-collateral (SC)-CA1 synapses from *Crbn* KO mice are intact. However, presynaptic excitatory, but not inhibitory, neurotransmitter release was impaired in *Crbn* KO mice, mostly due to altered activity of the BK channel, a large-conductance Ca^{2+}-activated K^{+} channel. Strong teratogen which binds and inhibits CRBN also reduced neurotransmitter release, and BK channel blocker recovers thalidomide-induced synaptic- and cognitive-deficits. These results provide a potential explanation for the possible involvement of BK channel abnormality in intellectual disability, as well as in the presynaptic and cognitive impairments caused by *CRBN* mutations.

Introduction

Human intellectual disability, also widely known as mental retardation, is a neuropsychiatric disease characterized by intelligence quotient (IQ) scores lower than 70 and cognitive impairments such as decreases in language development and memory and problem-solving skills (Greenspan & Woods, 2014). It has been reported that intellectual disability is thought to be caused by many different genetic etiological factors. Among them, a nonsense mutation (1274C→T) in the *CRBN* gene, located on chromosome 3 (3p26.3) exon 11, is thought to cause mild intellectual disability in human (Higgins et al., 2004; Higgins et al., 2008). Deletion or microduplication of 3p26.3 including CRBN also results in cognitive and behavioral impairment (Dijkhuizen et al., 2006; Papuc et al., 2015). However, the cellular and molecular mechanisms of cognitive impairment caused by *CRBN* mutations remain unclear.

Recently the molecular and cellular function of CRBN was investigated. CRBN forms a $CRL4^{CRBN}$ E3 ubiquitin ligase complex with DNA-binding protein 1 (DDB1), cullin-4A (CUL4A), and regulator of cullins 1 (ROC1) as a substrate receptor (Fischer et al., 2014; Liu et al., 2014; Ito et al., 2010). CRBN is also known as a target of thalidomide, a strong teratogen. After binding to CRBN, thalidomide inhibits $CRL4^{CRBN}$ E3 ubiquitin ligase function (Chang & Stewart, 2011; Fischer et al., 2014; Ito et al., 2010; Ito et al., 2011; Liu et al., 2015). Because thalidomide results in abnormal limb formation (Ito et al., 2010), CRBN mutations have been suggested to cause cognitive impairment through abnormal neurodevelopment. However, this hypothesis has not been tested yet. To address these questions, I studied the cellular and molecular mechanism of CRBN-related intellectual disability using *Crbn* knockout (KO) mice.

Crbn mRNAs are widely existed in the postmitotic period in most parts of the rodent brain, including the hippocampus, cerebral cortex, and cerebellum (Aizawa et al., 2011; Higgins et al., 2010). I was interested in whether CRBN mutations induces abnormal brain development or structural malformation of the brain. *Crbn* KO mice, a loss-of-function animal model for *Crbn*, had normal brain development, but impaired cognitive function which was previously reported by another group (Rajadhyaksha et al., 2011). Research into synaptopathy and channelopathy has determined the molecular mechanisms of cognitive disorders and identified genes and factors associated with neuropsychiatric diseases such as fragile X mental retardation and autism spectrum disorder (Pavlowsky et al., 2012; Vaillend et al., 2008). I applied this approach to the *Crbn* KO mice and found that *Crbn* KO mice had reduced neurotransmitter release only in excitatory synapses because of increased activity of the BK channel, a large-conductance Ca^{2+}-activated K^{+} channel and BK channel blocker recovered impaired Pr in *Crbn* KO mice. I also confirmed that thalidomide acting like a CRBN inhibitor mimics synaptic and behavioral deficits observed in *Crbn* KO mice and BK channel blocker rescues thalidomide-induced synaptic and behavioral problems.

Materials and Methods

Animals

All mice were housed in an animal facility with a specific pathogen-free barrier under controlled environmental conditions (temperature, 22 ± 1℃; humidity, 55%; and a 12h/12h light/dark cycle, lights on at 07:00). Mice were allowed access to food and water *ad libitum*. Wild-type (WT) and *Crbn* KO mice of the C57BL/6 background were used (Lee et al., 2013). All experiments were approved by the Institutional Animal Care and Use Committee (IACUC) at Seoul National University.

Immunohistochemistry

Mice were anesthetized with urethane (1000 mg/kg), transcardially perfused with phosphate-buffered saline (PBS) and then a fixative solution (4% paraformaldehyde (PFA) in PBS). The isolated brains were kept in the fixative solution for overnight and then cryoprotected in 30% sucrose (in PBS) for 24h at 4°C. Coronal brain sections (50 μm) were collected at -20°C with cryostat (CM3050, Leica). Sections were washed with PBS and incubated in blocking solution (0.3% Triton X-100 and 5% goat serum in PBS) for 1h at RT under gentle agitation, and incubated for 24h at 4°C with primary antibody (see table 1) diluted in PBS. Sections were washed 5 times (10 min each time) in PBS, treated with second antibody (see table 1) at 4°C overnight, and washed 5 times (10 min each time) in PBS. Sections were then mounted on superfront slides and covered with DAPI containing mounting media

(H-1200, Vectorlabs). Images were acquired using a confocal microscope (LSM700, Carl Zeiss).

Western blotting

Hippocampal slices from 3- to 5-week-old WT and *Crbn* KO mice or treated with vehicle or thalidomide (100 μM, purchased from Tocris) and/or MG132 (10μM, purchased from Sigma-Aldrich) when the slices were incubated in an incubator, prepared using the same method of slice preparation as for the electrophysiological experiments, were homogenized in ice-cold lysis buffer (T-PER tissue protein extraction reagent, Thermo Scientific, 78510) combined with a protease inhibitor cocktail (Sigma, P8340). Homogenates were centrifuged at 13,000 rpm for 30 min at 4^{o}C and supernatants were stored at -80^{o}C. Protein concentrations were measured using the BCA Protein Assay Kit (Thermo Scientific, 23225). Equal amounts (30 μg) of protein were loaded into the lanes of a SDS polyacrylamide gel (10%). Separated proteins were then transferred onto PVDF membranes, blocked with 5% skim milk in TBST for 1 h at room temperature, and incubated overnight with primary antibodies (see table 1) for immunoblotting. Membranes were washed with TBST and then incubated with horseradish peroxidase (HRP)-conjugated secondary antibodies (see table 1) for 1 h. HRP was detected using SuperSignal West Pico Chemiluminescent substrate (Thermo Scientific, 34080) and a Bio-Image Analyzer (Bio-Rad ChemiDoc MP). Membranes were stripped with Restore Western Blot Stripping Buffer (Thermo Scientific, 21059) and reprobed for β-actin.

Drug preparation and in vivo injection for behavioral test

Thalidomide or paxilline (Tocris) was dissolved to a 25 mM or 10 mM

concentration in dimethylsulfoxide (DMSO, Sigma-Aldrich) and then diluted 1:10 or 1:2,000 in saline (the concentration of DMSO was 10% or 0.05%, v/v). Thalidomide and/or paxilline were injected at 30 mg/kg or 3 μg/kg body weight, i.p. 10% DMSO was used for vehicle treatment.

Behavioral test

Passive avoidance test: The passive avoidance test was performed using 8-9 week-old C57BL/6 male mice (DBL, Eumseung, Korea). The observer was blinded to the pharmacological treatment of the animal. The passive avoidance apparatus consisted of a light and dark chamber separated by a guillotine door. The floor of the dark chamber was made of stainless-steel grids. During habituation, mice were allowed to freely explore the box for 5 min with the door open, and were then returned to their home cage. For conditioning, after 24 h, the mice were placed into the light chamber and the sliding door was closed when both hindlimbs of the mice had entered into the dark chamber. Then, an electric foot shock (0.25 mA, 2 s) was delivered via the floor grids. Ten seconds later, the mice were returned to their home cage. Tests were carried out 24 h after conditioning, and the latency time required for mice to enter the dark chamber was measured with a 300-second cut-off.

Electrophysiology

Slice preparation: Using 3- to 5-week-old (both sexes) or 10- to 12-week-old (male) WT and *Crbn* KO mice, transverse hippocampal slices (300 μm for whole-cell recordings or 400 μm for extracellular field potential recordings) were prepared as described previously (Choi et al., 2015; Seo et al., 2014). After decapitation, brains

were rapidly removed and placed in ice-cold, oxygenated (95% O_2 and 5% CO_2), dissection buffer (see table 2). Slices were transferred to a holding chamber in an incubator containing oxygenated (95% O_2 and 5% CO_2) artificial cerebrospinal fluid (ACSF, see table 2) at 28–30°C for at least 1 h before recording. Experiments with thalidomide treatment were performed using hippocampal slices incubated in ACSF containing thalidomide (100 μM) at least 3 h.

Extracellular field potential recordings: After recovery, slices were transferred to a submerged recording chamber where they were continuously perfused with oxygenated ACSF (28–30°C) at a flow rate of 2 ml/min. Extracellular field excitatory postsynaptic potential (fEPSP) was evoked by Schaffer-collateral (SC) stimulation (0.2-ms current pulses) using a concentric bipolar electrode. Synaptic responses were recorded with ACSF-filled microelectrodes (1 to 3 MΩ) and were quantified as the initial slope of fEPSP in CA1 regions. Recordings were performed using an AM-1800 microelectrode amplifier (A-M systems, Sequim, WA), a PG 4000A stimulator (Cygnus Technology, Delaware Water Gap, PA), and a SIU-90 isolated current source (Cygnus Technology). Baseline responses were collected at 0.07 Hz with a stimulation intensity that yielded a 40–60% maximal response. NMDAR-dependent LTP was induced by high-frequency stimulation (HFS, 100 Hz for 1 s) or four episodes of theta burst stimulation (TBS) at 10-s intervals. TBS consisted of 10 stimulus trains delivered at 5 Hz; each train consisted of four pulses at 100 Hz. NMDAR-dependent LTD was induced by low-frequency stimulation (LFS; 900 pulses at 1 Hz for 900 s). L-LTP was induced by 4 trains of HFS separated by 5-min intervals. Group I mGluR-dependent LTD was induced by 10 min bath-application of 100 μM (R,S)-3,5-DHPG (Tocris). Data from slices with stable

recordings (<5% change over the baseline period) were included in the analysis. All data are presented as mean ± standard error of mean (SEM) normalized to the preconditioning baseline (at least 20 min of stable responses). The experimenters were blind to mouse genotypes. IGOR software (Wavemetrics, Lake Oswego, OR) was used for digitizing and analyzing the responses.

Whole-cell recordings: After recovery, slices were transferred to a submerged recording chamber where they were continuously perfused with ACSF gassed with 95% O_2 / 5% CO_2 at a flow rate of 2 ml/min. Slices were equilibrated for 5 min prior to the recordings and all of the experiments were performed at room temperature. All recordings were performed in hippocampal CA1 or CA3 pyramidal neurons or dentate gyrus (DG) granule cells identified by their size and morphology. Recordings were obtained using a Multiclamp 700B amplifier (Molecular Devices) under visual control with differential interference contrast illumination in an upright microscope (BX51WI; Olympus). Patch pipettes (4-6 MΩ) were filled with various internal solutions for the purposes of experiments (see table 3). The external solutions were modified by adding some inhibitors or blockers for experimental purposes (see table 4). Evoked synaptic responses were elicited by SC stimulation (0.2-ms current pulses) using a concentric bipolar electrode placed 200-300 μm in front of the postsynaptic pyramidal cell. All eEPSC and eIPSC recordings were conducted in an external solution containing elevated divalent cations (4 mM Ca^{2+} and Mg^{2+}) to reduce network excitability and prevent polysynaptic responses upon stimulation (Clem & Huganir, 2010) or reducing the concentration of KCl in ACSF to 2.5 mM. Only cells with an access resistance <20 MΩ and an input resistance >100 MΩ were studied. The cells were discarded if the input or the access resistance changed more than 20%. Data were acquired and analyzed using pClamp 10.6 (Molecular Devices). Signals were filtered at 2 kHz

and digitized at 10 kHz with Digidata 1440A (Axon Instruments).

Statistical analysis

Data analyses and graphical display were performed with SigmaPlot (Version 11.0, Systat Software, Germany). All displayed values represent the mean ± standard error of mean (SEM). Significant differences between groups were determined using unpaired or paired Student′s t-test, and multiple comparisons were performed using two-way ANOVA.

Antibodies

Table 1. List of antibodies used in this study.

No.	Antibody name	Catalog No.	Clone (if monoclonal)	Manufacturer	Dilution
Primary antibody for immunohistochemistry					
1	Anti-NeuN	MAB377	A60	Millipore	1:1000
Secondary antibody for immunohistochemistry					
2	Goat anti-mouse IgG-R	sc-2092		Santa Cruz Biotechnology	1:1000
Primary antibodies for Western blotting					
3	Anti-GluA1	ab31232		abcam	1:500
4	Anti-GluA2	MAB397	6C4	Millipore	1:500
5	Anti-GluN1	PA3-102		Thermo Scientific	1:1000
6	Anti-GluN2A	sc-1468	c-17	Santa Cruz Biotechnology	1:1000
7	Anti-GluN2B	sc-1469	c-20	Santa Cruz Biotechnology	1:1000
8	Anti-synapsin1	AB1543		Millipore	1:1000
9	Anti-synaptophysin	sc-9116	H-93	Santa Cruz Biotechnology	1:1000
10	Anti-vGluT1	MAB5502	3C10.2	Millipore	1:500
11	Anti-GAD67	MAB5406	1G10.2	Millipore	1:5000
12	Anti-vGAT	AB5062P		Millipore	1:500
13	Anti-PSD95	MA1-046	7E3-1B8	Thermo Scientific	1:2000

14	Anti-gephyrin	sc-6411	R-20	Santa Cruz Biotechnology	1:1000
15	Anti-CRBN	HAP045910		Siama-Aldrich	1:2000
16	Anti-BK_{Ca}	611248		BD Bioscience	1:1000
17	Anti-β-actin	sc-47778	C4	Santa Cruz Biotechnology	1:1000
Secondary antibodies for Western blotting (HRP; horseradish peroxidase-conjugated)					
18	HRP-conjugated anti-mouse IgG	ab6728		abcam	1:10000
19	HRP-conjugated anti-rabbit IgG	ab6802		abcam	1:10000
20	HRP-conjugated anti-goat IgG	805-035-180		Jacson Laboratory	1:10000

Table 2. Composition of dissection buffer and ACSF.

(in mM)	Dissection buffer	Normal ACSF
NaCl		124
KCl	5	5
NaH_2PO_4	1.23	1.23
$NaHCO_3$	26	26
Glucose	10	10
Sucrose	212.7	
$MgCl_2$	10	1.5
$CaCl_2$	0.5	2.5
Applications	Slice preparation	Slice recovery, fEPSP experiments (Fig 3a, 3d, Fig 8), measuring neuronal intrinsic properties (Fig 9, Fig 12), sEPSC and sIPSC recordings (Fig 5m-o, Fig 6, Fig 13c)

Table 3. Composition of internal solutions using in this study.

(in M)	Cs-based Internal Solution-1	Cs-based Internal Solution-2	K-based Internal Solution-1	K-based Internal Solution-2
Cs-$MeSO_4$	130			
CsCl		130		
K-gluconate			135	145
EGTA	0.5	1.1		0.2
TEA-Cl	5			
NaCl	8	10	8	5
$MgCl_2$		2		1
$CaCl_2$		0.1		
HEPES	10	10	10	10
QX-314	1			
ATP-Mg	4	2	2	2
GTP-Na	0.4		0.2	0.1
Phosphocreatine-Na_2	10			
Spermine	0.1			
Commom requirements	pH 7.4			
	280-290 mOsm			
Applications	mEPSC recordings (Fig 5a-5f), eEPSC & eIPSC recordings (Fig 3b, 3c, 3e-3h, Fig 7, Fig 10b-10c, Fig 13b)	mIPSC recordings (Fig 5g-5l)	Calcium-activated potassium current recordings (Fig 10a, Fig 13a)	Measuring neuronal intrinsic properties (Fig 9, Fig 12) sEPSC and sIPSC recordings (Fig 5m-5o, Fig 6, Fig 13c)

Table 4. Composition of external solutions using in this study.

(in mM)	Modified ACSF-1	Modified ACSF-2	Modified ACSF-3	Modified ACSF-4	Modified ACSF-5	Modified ACSF-6
NaCl	124	125	125	125	125	125
KCl	5	5	5	5	5	2.5
NaH_2PO_4	1.23	1.23	1.23	1.23	1.23	1.23
$NaHCO_3$	26	26	26	26	26	26
Glucose	10	10	10	10	10	10
$MgCl_2$	1.5	4	1.5	1.5	1.5	1.5
$CaCl_2$	2.5	4	2.5	2.5	2.5	2.5
Picrotoxin	0.1	0.1				0.1
Tetrodotoxin (TTX)	0.001		0.001		0.001	
DL-AP5	0.05		0.05	0.05		
CNQX			0.02	0.02		
Applications	mEPSC recordings (Fig 5a-5f)	eEPSC recordings (Fig 3b,3e,3g, Fig 10b-10c, Fig 13b), *Fig 4 without picotoxin	mIPSC recordings (Fig 4g-5l)	eIPSC recordings (Fig 3c,3f,3h)	Calcium-activated potassium current recordings (Fig 10a, Fig 13a)	eEPSC recordings (Fig 7)

Results

Crbn KO mice have cognitive impairments.

It was previously reported *CRBN*-mutated human intellectual disability patients have cognitive impairments (Dijkhuizen et al., 2006; Higgins et al., 2004; Papuc et al., 2015) and *Crbn*-deficiencient animals also show memory impairments similarly observed in human patients (Rajadhyaksha et al, 2011). I and my collaborator also tested whether *Crbn* KO mice used in this study also have cognitive problems (Lee et al., 2013), and we obtained reproducible data similar with the results previously reported (data not shown). It means that *Crbn* KO mice used in this study also have cognitive impairment similarly observed in *CRBN*-mutated human intellectual disability patients. Therefore, I used this animal as an animal model of *CRBN* mutation-induced intellectual disability in this study.

Crbn KO mice show normal brain or synaptic architecture.

Because CRBN is inhibited by thalidomide, a strong teratogenic compound, and it causes limb malformation (Ito et al., 2010), I and my collaborators tested whether the cognitive impairments by *Crbn* deficiency in mice were caused by structural malformation or developmental problems in the brain. When NeuN-stained brain sections of WT and Crbn KO mice were examined, however, no appreciable anatomical abnormalities were detected in adult (12 weeks) mice (Figure 1). My collaborator also checked brain structural changes in early stage, postnatal day 2 (P2), and synaptic ultrastructures, because morphological changes in synaptic structure generally affect the cognitive function of mammalian brains (Kasai et al.,

2010; Sala & Segal, 2014) in *Crbn* KO mice. However, there were no significant differences in brain architecture at P2 and spine morphologies between WT and *Crbn* KO neurons (data not shown). Therefore, memory impairment observed in *Crbn* KO mice is not caused by the change of the brain gross morphology and synaptic ultrastructure.

Crbn KO mice exhibit abnormal expression patterns of some synaptic proteins.

Next, I compared the expression levels of several synaptic proteins in hippocampal tissues from WT or *Crbn* KO mice. Expression levels of most synaptic proteins, including glutamate receptor subunits (GluA1, GluA2, GluN1, GluN2A, and GluN2B), excitatory (PSD95) and inhibitory postsynaptic proteins (gephyrin), and excitatory (synaptophysin, vGluT1) and inhibitory presynaptic proteins (GAD67) were identical between WT and *Crbn* KO mice (Figure 2). I found that *Crbn* KO mice showed increased synapsin I expression, and decreased vGlut1 expression (Figure 2), but the physiological relevance and mechanism of these changes were not clear.

Crbn KO mice have decreased excitatory neurotransmitter release.

The absence of *Crbn* gene induces cognitive impairment but it does not affect brain gross and synaptic ultrastructural morphological changes. Next I tested whether synaptic function such as synaptic transmission and plasticity is altered in *Crbn* KO mice. CRBN is expressed in all brain areas, but highly enriched in the hippocampus that is important brain areas for learning and memory. I therefore tested electrophysiological experiments in this brain region. Input-output relationship measured by extracellular field potential recordings in Schaffer-

collateral (SC)-CA1 synapses in the hippocampus was slightly but significantly decreased in *Crbn* KO mice (Figure 3a). I next checked how the basal synaptic transmission is reduced in Crbn KO mice; is excitatory synaptic transmission decreased or is inhibitory synaptic transmission increased? To address this question, I measured evoked basal excitatory or inhibitory synaptic transmission in hippocampal SC-CA1 synapses (Figure 4). As a result, basal excitatory, but not inhibitory, synaptic transmission was significantly reduced in *Crbn* KO mice (Figure 4a-4c). It means that the balance between excitatory vs. inhibitory synaptic transmission (E/I balance) is altered in *Crbn* KO mice (Figure 4d). I also measured miniature excitatory or inhibitory postsynaptic currents (mEPSCs or mIPSCs), but the amplitudes and the frequency of mEPSCs (Figure 5a-5f) and mIPSCs (Figure 5g-5l) are not different between WT and *Crbn* KO mice (Figure 5). Only the decay time of mEPSC is increased in *Crbn* KO mice (Figure 5j). Spontaneous IPSCs (sIPSCs), basal synaptic transmission recorded without blocking neuronal activity, were also similar between two groups (Figure 5m-5o). These results indicate that decreased excitatory synaptic transmission is not caused by postsynaptic alteration because the amplitude of mEPSC and the expression levels of several subunits of glutamate receptors are not changed in *Crbn* KO mice. I thus checked presynaptic release probability (Pr) by recording paired-pulse ratio in hippocampal SC-CA1 synapses. As a result, *Crbn* KO mice showed an increased paired-pulse ratio (PPR) by extracellular field potential recordings (Figure 3d). For further analysis, I tested excitatory or inhibitory in PPR in WT and *Crbn* KO mice. Figure 3e and 3f shows that *Crbn* KO mice have increased excitatory, but not inhibitory, PPR (Figure 3e and 3f). It means that release probability of excitatory, but not inhibitory, neurotransmission, is decreased in *Crbn* KO mice. I also confirmed the decreased Pr in excitatory synaptic transmission of *Crbn* KO mice using repetitive 20-Hz train stimulation. Crbn KO mice showed sustained responses to 20 pulses at 20 Hz

stimulation only in excitatory, but not in inhibitory, synaptic transmission (Figure 3g and 3h). These results suggest that *Crbn* KO mice have decreased excitatory Pr.

Learning and memory are mediated by the processing and the storage of information in various brain areas, especially in temporal lobes including the hippocampus. Hippocampus receives their inputs from entorhinal cortex via perforant path (PP) to dentate gyrus (DG), and DG projects their axons to CA3 pyramidal neurons through mossy fiber path. CA3 areas connect to CA1 pyramidal neurons via Schaffer-collateral (SC) synapses, the most popular neural circuits for the research of synaptic plasticity and learning and memory. These three types of synapses are called hippocampal trisynaptic pathway, and they involve various cognitive behaviors and have distinct properties. Therefore, I studied the synaptic function in hippocampal CA3 and DG areas of *Crbn* KO mice. Amplitude and frequency of spontaneous EPSC (sEPSC) in the CA3 pyramidal neurons and DG granule cells were not significantly different between WT and *Crbn* KO mice (Figure 6a and 6b). It means that *Crbn* KO mice have normal spontaneous or miniature excitatory synaptic transmission in hippocampal trisynaptic circuits. I also tested paired-pulse ratio (PPR) and responses to repetitive stimulation consisting of 20 pulses at 20 Hz in hippocampal PP-DG synapses. As a result, PPR was also increased in PP-DG synapses similarly observed in SC-CA1 synapses from *Crbn* KO mice (Figure 7a). Responses to 20 Hz-train stimulation were different between WT and *Crbn* KO mice (Figure 7b), but the patterns were different compared with the results observed in hippocampal SC-CA1 synapses (Figure 3g). These results indicate that *Crbn* KO mice have decreased excitatory Pr in another hippocampal synapses.

Crbn KO mice have normal long-term synaptic plasticity.

Because many animal models for neuropsychiatric diseases with learning and memory impairments have abnormal long-term synaptic plasticity, that is well known cellular or molecular mechanisms of learning and memory (Vaillend et al., 2008), I thus tested several kinds of long-term synaptic plasticity in the hippocampal SC - CA1 synapses; one the major center for the cognitive function, especially in the spatial memory, and the location where CRBN is highly expressed in. *Crbn* KO mice had normal induction of high-frequency stimulation (HFS) or theta-burst stimulation (TBS)-induced NMDA receptor-dependent LTP (HFS-LTP, Figure 8a; TBS-LTP, Figure 8b). CRBN negatively regulate AMP kinase (Lee et al., 2011; Lee et al., 2013; Lee et al., 2014), and Porter *et al* reported that AMP kinase affects protein synthesis-dependent late-phase LTP (L-LTP) (Potter et al., 2010). However, *Crbn* KO mice have normal L-LTP in hippocampal SC-CA1 synapses (Figure 8c). Because we and previous behavioral study found cognitive impairment in *Crbn* KO mice at young adult ages, I also checked LTP experiments using 10- to 12-week-old animals, but there were no differences between two groups (Figure 8d). NMDAR-dependent Long-term depression (LTD) induced by low-frequency-stimulation (LFS) (LFS-LTD, Figure 8e) and DHPG-induced group I mGluR-dependent LTD (DHPG-LTD; Figure 8f) were also not different between WT and Crbn KO mice. These results indicated that CRBN did not affect long-term synaptic plasticity, and memory impairment in *Crbn* KO mice is not caused by the problem of hippocampal long-term synaptic plasticity.

Lack of CRBN affects action potential duration and neuronal intrinsic properties.

Some animal models of intellectual disability have altered neuronal intrinsic properties (Contractor et al., 2015; Franzoni et al., 2015; Ozkan et al., 2014; Zhang

et al., 2014). I therefore tested whether *Crbn* deficiency altered neuronal firing rates or other kinds of intrinsic properties. As a result, the action potential duration was decreased (Figure 9b), although the firing rate of action potentials was normal in hippocampal CA1 pyramidal neurons from *Crbn* KO mice (Figure 9a). I also checked other intrinsic properties such as membrane capacitance (C_m), input resistance (R_{in}) or resting membrane potential (RMP). Figure 9c shows that *Crbn* KO neurons have higher C_m than WT neurons (Figure 9c), but R_{in} and RMP were similar in hippocampal CA1 pyramidal neurons from WT and *Crbn* KO mice (Figure 9d and 9e).

Crbn KO mice show increased BK channel activity.

I discovered two major physiological changes in *Crbn* KO mice; reduced excitatory Pr and shortened action potential duration. Thus, my next question is how the excitatory Pr and the action potential duration are affected by CRBN. CRBN negatively modulates surface expression and function of the BK channel, a large-conductance Ca^{2+}-activated K^+ channel (Liu et al., 2014; Jo et al., 2005), one of CRBN interacting proteins. An increase in BK channel activity is generally thought to shorten the action potential duration (Shao et al., 1999), and Pr is enhanced by the inhibition of BK channel activity (Hu et al., 2001; Raffaelli et al., 2004). Based on my results showing decreased action potential duration (Figure 9b), I hypothesized that the reduction of excitatory Pr in *Crbn* KO mice might be due to BK channel hyperactivity, and I tested this hypothesis by directly measuring BK channel activity in *Crbn* KO neurons. Applying depolarization from -50 mV to 0 mV with bath-application of TTX to block voltage-gated sodium channels induces outward tail currents, and these currents are calcium-activated potassium currents (Aoki & Baraban, 2001). *Crbn* KO mice showed two-fold higher calcium-activated

potassium currents, and paxilline, a pan-BK channel blocker, completely reduced these currents to similar level of WT (Figure 10a). It means that paxilline-sensitive K^+ (BK) currents are increased in *Crbn* KO neurons. In addition, paxilline eliminated the increase in excitatory PPR (Figure 10b) and excitatory short-term plasticity induced by 20-Hz train stimulation (Figure 10c). These results strongly support that *Crbn* KO mice have increased BK channel activity-mediated excitatory presynaptic release dysfunction.

Thalidomide increases CRBN expression in the hippocampus.

Thalidomide binds to CRBN, decreases ubiquitination their target proteins by inhibiting $CRL4^{CRBN}$ E3 ligase function and increases CRBN expression by inhibiting CRBN auto-ubiquitination (Ito et al., 2010; Liu et al., 2015; Xu et al., 2013). Thus, a thalidomide-mediated increase in CRBN expression is an indicator of ubiquitinational modulation by thalidomide. Thalidomide treatment with (statistically insignificant) or without (statistically significant) MG132, a potent and selective protease inhibitor, increased CRBN protein expression in hippocampal tissues (Figure 11a and 11b); however, it did not affect GluA1 expression (Figure 11a and 11c), which is consistent with the unaltered GluA1 and GluA2 expression in *Crbn* KO mice (Figure 2). I next checked whether the expression of α subunit of BK channel is regulated by the treatment of thalidomide. However, thalidomide did not affect the expression levels of this channel (Figure 11a and 11e). I also studied whether thalidomide affects these specific two proteins that the expression levels are altered – synapsin 1, which is increased, and vGAT, which is decreased, in *Crbn* KO mice (Figure 2). However, these the expression levels of two proteins were not affected by the treatment of thalidomide (Figure 11a, 11f and 11g). These results

indicate that thalidomide inhibits a part of CRBN-related biochemical events, but did not reproduce every changes observed in *Crbn* KO mice.

Thalidomide mimics BK channel hyperactivation-induced excitatory Pr reduction observed in Crbn KO mice.

Next, I tested whether thalidomide treatment to the normal animals induces neuronal, synaptic and behavioral changes observed in *Crbn* KO mice. To address this question, I first treated thalidomide on hippocampal slices during incubation period after slice preparation (100 μM, at least 3h). Neuronal excitability was not altered, but action potential duration was partially reduced by thalidomide treatment similarly observed in *Crbn* KO mice (Figure 12a and 12b). However, the pattern of change in neuronal intrinsic properties are different between *Crbn* KO neurons and thalidomide-treated neurons; CA1 pyramidal neurons from *Crbn* KO mice showed increased Cm (Figure 9c), but R_{in} was enhanced in thalidomide-treated neurons (Figure 12d). Cm and RMP are not affected by the treatment of thalidomide (Figure 12c and 12e).

Hippocampal slices with thalidomide treatment from WT mice also showed slightly increased Ca^{2+}-activated K^+ currents and decreased excitatory Pr; these changes were rescued by paxilline (Figure 13a and 13b). Amplitude and frequency of sEPSC are not different in CA1 pyramidal neurons from between vehicle- or thalidomide-treated hippocampal slices (Figure 13c). However, the distribution of the interevent intervals (IEIs) were increased; it means that the frequency of sEPSC, an indicator of excitatory Pr, was slightly, but not significantly, decreased by thalidomide (Figure 13c). It means that thalidomide mildly mimicked the neuronal and synaptic phenotypes seen in *Crbn* KO mice.

Thalidomide causes memory impairment and BK channel blocker recovers this change.

Recently, there were some reports that multiple myeloma patients who were prescribed IMiDs such as thalidomide or lenalidomide showed cognitive problems (Patel et al., 2015; Rollin-Sillaire et al., 2013). Because thalidomide binds and inhibits CRBN protein, and the absence or loss-of-function of *CRBN* induces cognitive impairment, I hypothesized that thalidomide induces memory deficits by inhibiting CRBN and then hyperactivating BK channels. To verify this hypothesis, I treated thalidomide and tested passive avoidance memory in normal animals. As a result, I finally confirmed that thalidomide induced cognitive dysfunction in WT mice (Figure 14). Treatment of the BK channel blocker paxilline with thalidomide inhibited cognitive impairment induced by thalidomide (Figure 14). Therefore, I concluded that the absence of CRBN or inhibition of CRBN activity by thalidomide causes synaptic and behavioral changes via upregulation of BK channel activity.

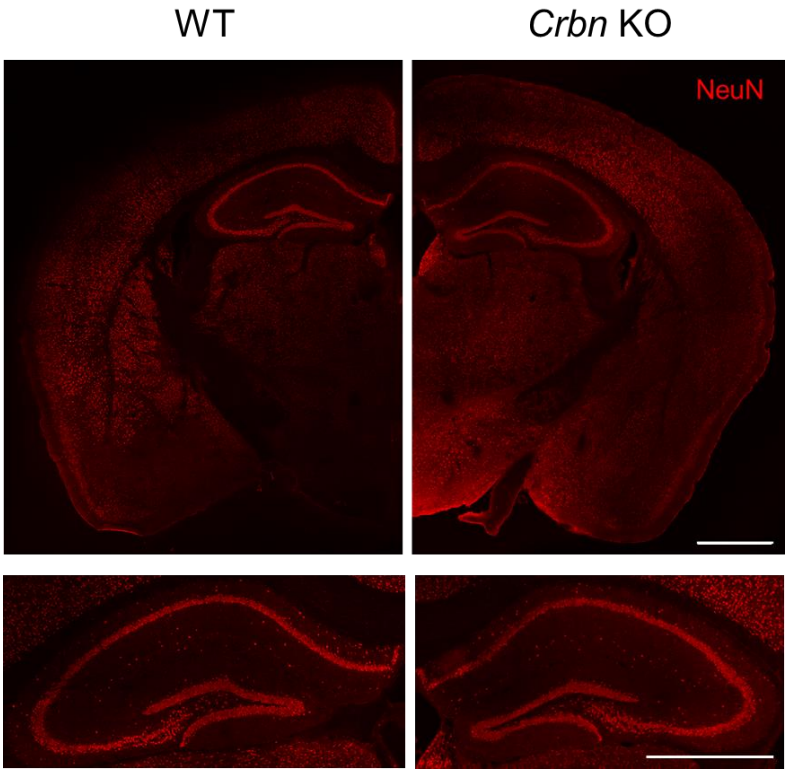

Figure 1. *Crbn* KO mice have normal brain architecture.

Normal brain gross morphology of Crbn KO whole brain (top) and hippocampus (bottom) at at 12-week-ole age, as determined by staining for the neuronal marker NeuN in coronal section. Scale bar = 1.0 mm.

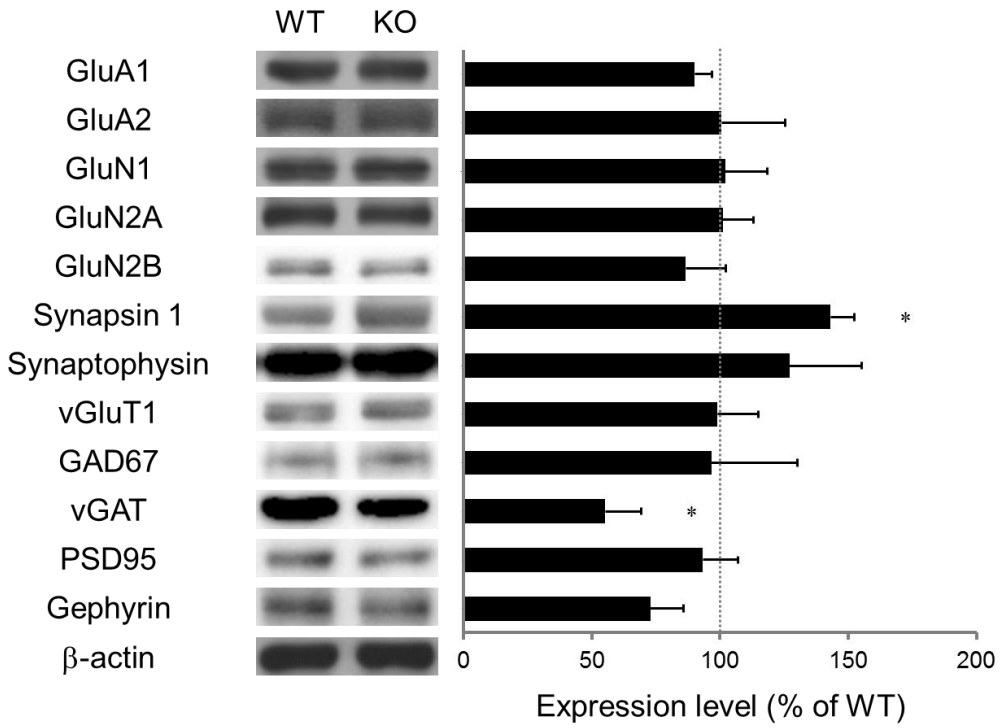

Figure 2. Analysis of the expression patterns of synaptic proteins in *Crbn* KO mice.

Synapsin1, an excitatory presynaptic protein, is increased, and vGAT, an inhibitory presynaptic protein, is decreased in *Crbn* KO mice. Hippocampal homogenates from 3- to 5-week-old WT and *Crbn* KO mice are immunoblotted to evaluate the levels of several synaptic proteins. All protein signals are normalized relative to β-actin levels before comparisons between genotypes were made. Bar graphs represent means ± SEM (*$p < 0.05$, Student's t-test; WT, n = 4 mice; and KO, n = 5).

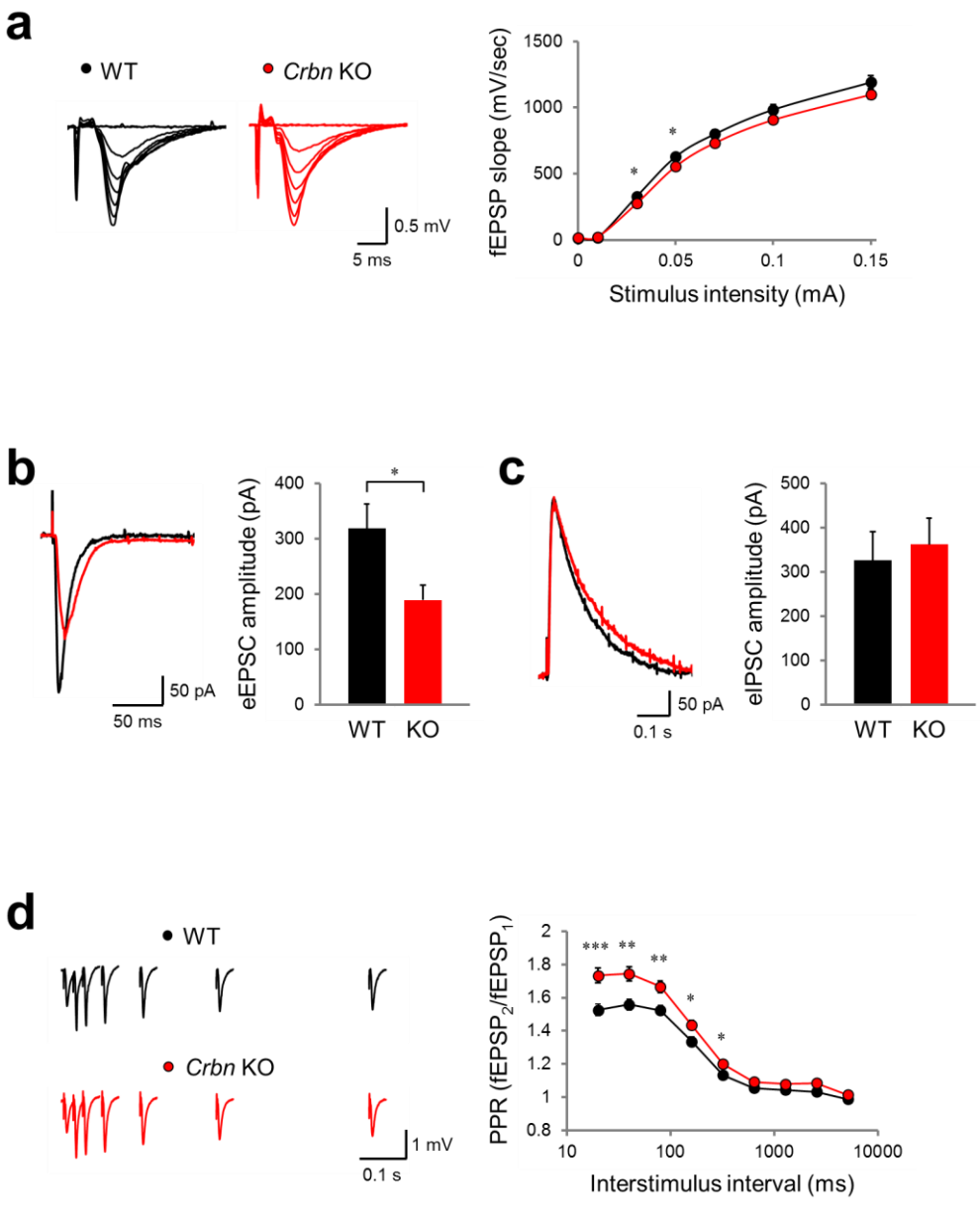
a
WT
Crbn KO
0.5 mV
5 ms
fEPSP slope (mV/sec)
1500
1000
500
0
0
0.05
0.1
0.15
Stimulus intensity (mA)
b
50 pA
50 ms
eEPSC amplitude (pA)
400
300
200
100
0
WT
KO
c
50 pA
0.1 s
eIPSC amplitude (pA)
500
400
300
200
100
0
WT
KO
d
WT
Crbn KO
1 mV
0.1 s
PPR (fEPSP2/fEPSP1)
2
1.8
1.6
1.4
1.2
1
0.8
10
100
1000
10000
Interstimulus interval (ms)

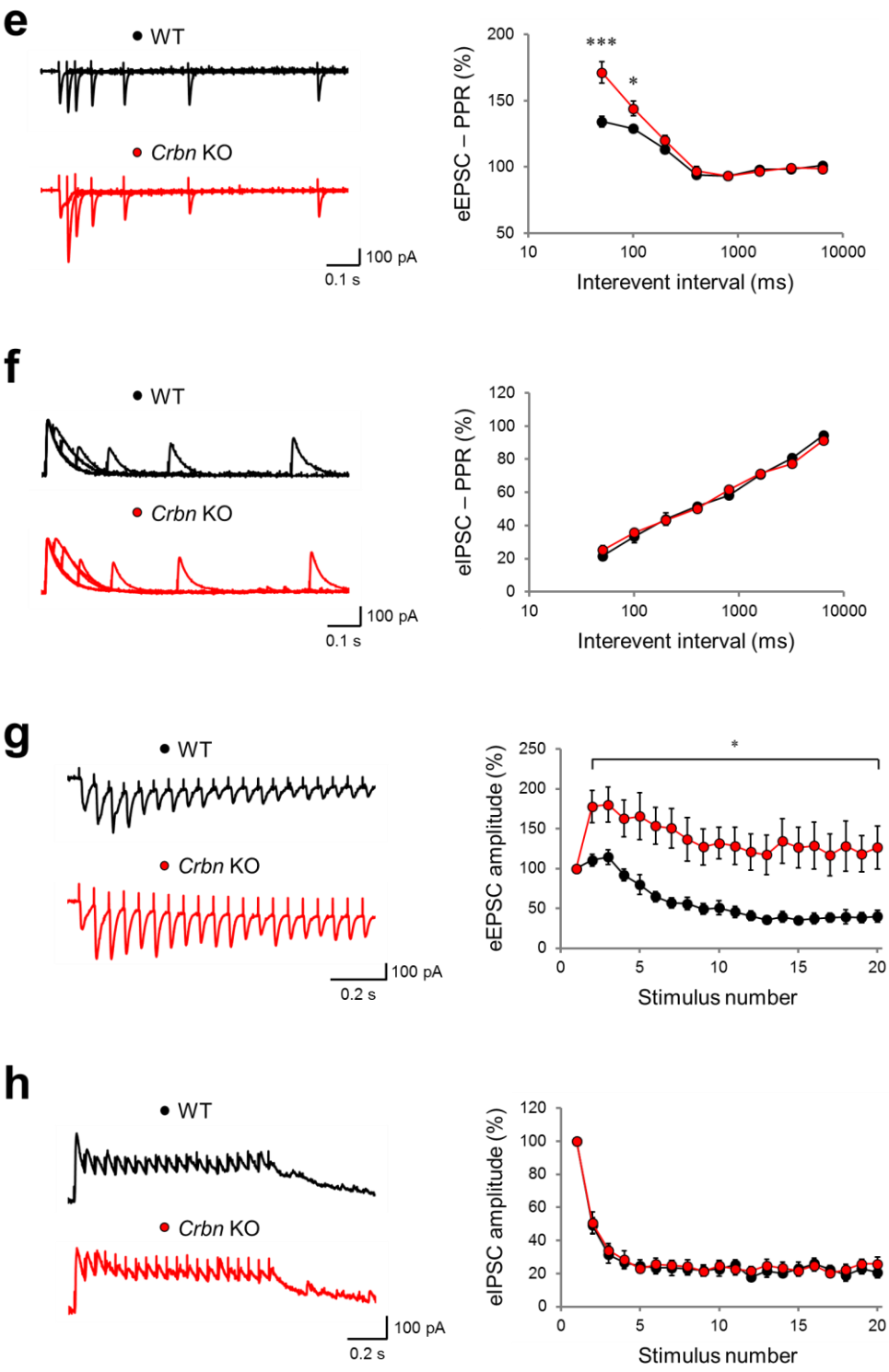
e
WT
Crbn KO
100 pA
0.1 s
***
*
eEPSC – PPR (%)
200
150
100
50
10
100
1000
10000
Interevent interval (ms)
f
WT
Crbn KO
100 pA
0.1 s
eIPSC – PPR (%)
120
100
80
60
40
20
0
10
100
1000
10000
Interevent interval (ms)
g
WT
Crbn KO
100 pA
0.2 s
*
eEPSC amplitude (%)
250
200
150
100
50
0
0
5
10
15
20
Stimulus number
h
WT
Crbn KO
100 pA
0.2 s
eIPSC amplitude (%)
120
100
80
60
40
20
0
0
5
10
15
20
Stimulus number

Figure 3. Excitatory, but not inbitory, presynaptic neurotransmitter release is reduced in hippocampal SC-CA1 synapses of *Crbn* KO mice.

(a) Basal synaptic transmission is reduced in *Crbn* KO mice by low stimulus intensities (0.03 and 0.05 mA; half-maximum), but not by higher stimulus intensities. Representative traces (left) and summary graphs of the input-output (I-O) relationship by extracellular field potential recordings in hippocampal SC-CA1 synapses from WT (black) or *Crbn* KO mice (red). The I-O results are obtained by plotting the slopes of fEPSP against stimulus intensities. Individual points represent means ± SEM (*$p < 0.05$, Student's t-test; WT, n = 43 slices from 8 mice; and KO, n = 47, 8).

(b-c) The amplitude of evoked excitatory postsynaptic currents (eEPSCs), but not of evoked inhibitory postsynaptic currents (eIPSCs), is decreased in *Crbn* KO mice. Representative traces (left) and quantitative comparison (right) of the amplitude of eEPSC (b) or eIPSC (c) by half-maximal stimulus intensity in hippocampal SC-CA1 synapses from WT (black) or *Crbn* KO mice (red). Bar graphs represent means ± SEM (*$p < 0.05$, Student's t-test; WT_{EPSC}, n = 13 cells from 2 mice; KO_{EPSC}, n = 15, 3; WT_{IPSC}, n = 12, 3; and KO_{IPSC}, n = 13, 3).

(d) *Crbn* KO mice show increased paired-pulse ratio (PPR) compared with WT. Representative traces (left) or summary graphs (right) of the PPR by extracellular field potential recordings in hippocampal SC-CA1 synapses from WT (black) or *Crbn* KO mice (red). PPRs are plotted against interstimulus intervals. Individual points represent means ± SEM (*$p < 0.05$, **$p < 0.01$ and ***$p < 0.001$, Student's t-test; WT, n = 25 slices from 8 mice; and KO, n = 28, 8).

(e-f) *Crbn* KO mice show increased paired-pulse ratio (PPR) in excitatory (eEPSC-PPR), but not inhibitory (eIPSC-PPR), synaptic transmission in hippocampal SC-CA1 synapses. Representative traces (left) and summary graphs (right). eEPSC-

PPR (e) or eIPSC-PPR (f) is plotted against interstimuli intervals. Individual points represent means ± SEM (*p < 0.05 and ***p < 0.001, Student's t-test; WT_{EPSC}, n = 13 cells from 2 mice; KO_{EPSC}, n = 15, 3; WT_{IPSC}, n = 12, 2; and KO_{IPSC}, n = 12, 2).

(g-h) Short-term synaptic plasticity induced by repetitive stimulation consisting of 20 pulses at 20 Hz stimulation is enhanced in excitatory, but not inhibitory, synaptic transmission in hippocampal SC-CA1 synapses from *Crbn* KO mice. Representative traces (left) and summary graphs (right). Relative amplitudes of eEPSCs (g) or eIPSC (h) are plotted against stimulus number. Individual points represent means ± SEM (*p < 0.05, Student's t-test; WT_{EPSC}, n = 8 cells from 2 mice; KO_{EPSC}, n = 8, 2; WT_{IPSC}, n = 13, 2; and KO_{IPSC}, n = 12, 2).

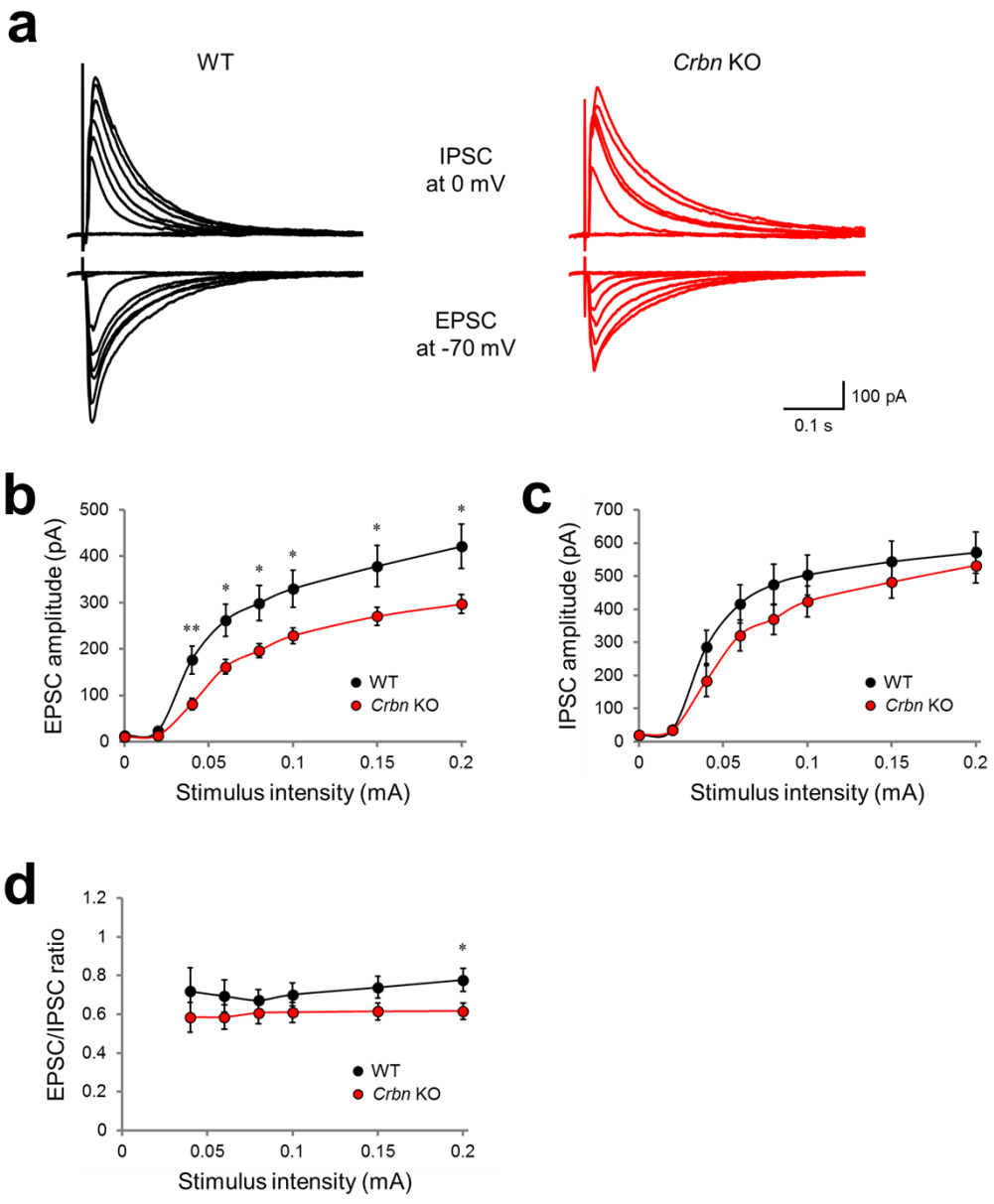
a
WT
Crbn KO
IPSC
at 0 mV
EPSC
at -70 mV
100 pA
0.1 s
b
EPSC amplitude (pA)
Stimulus intensity (mA)
WT
Crbn KO
c
IPSC amplitude (pA)
Stimulus intensity (mA)
WT
Crbn KO
d
EPSC/IPSC ratio
Stimulus intensity (mA)
WT
Crbn KO

Figure 4. E/I balance is decreased in hippocampal SC-CA1 synapses of *Crbn* KO mice.

(a) Representative traces of the input-output (I-O) relationship recorded by whole-cell patch clamp recordings in hippocampal SC-CA1 synapses from WT (left, black) or *Crbn* KO mice (right, red). eEPSCs were recorded holding at -70 mV and eIPSCs were monitored at 0 mV in the same cells.

(b-c) The amplitude of evoked excitatory postsynaptic currents (eEPSCs) (b), but not of evoked inhibitory postsynaptic currents (eIPSCs) (c), is decreased in *Crbn* KO mice. I/O curves are obtained by plotting the amplitudes of eEPSC (b) or eIPSC (c) against stimulus intensities. Individual points represent means ± SEM (**$p < 0.01$ and *$p < 0.05$, Student's t-test; WT, n = 21 cells from 3 mice; KO, n = 20, 3).

(d) EPSC/IPSC ratio was decreased in *Crbn* KO mice. Summary graph was plotted by EPSC/IPSC ratio calculated by dividing each EPSC amplitudes with each IPSC amplitudes against stimulus intensities. Individual points represent means ± SEM (*$p < 0.05$, Student's t-test).

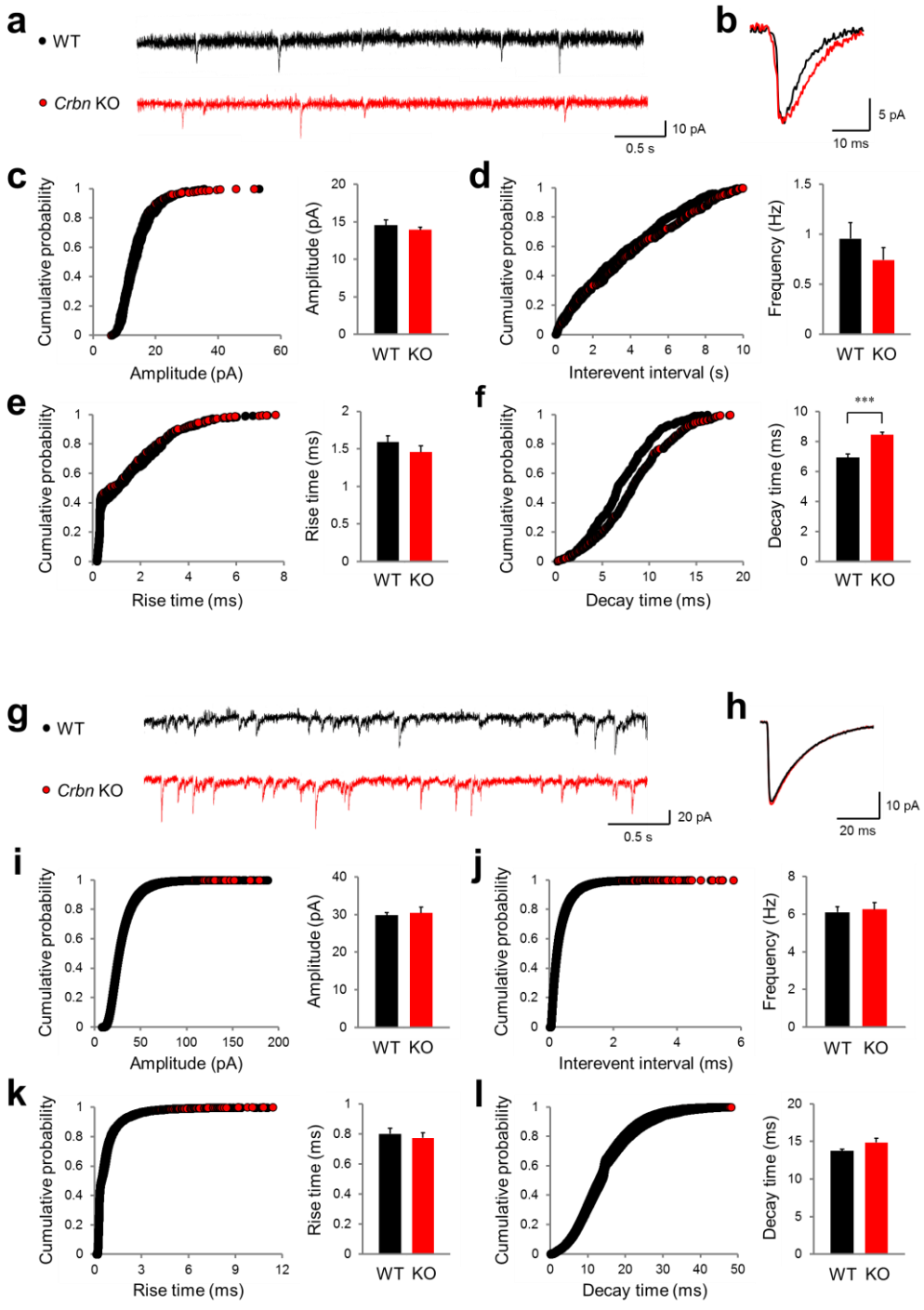
a
WT
Crbn KO
10 pA
0.5 s
b
5 pA
10 ms
c
Cumulative probability
Amplitude (pA)
Amplitude (pA)
WT KO
d
Cumulative probability
Interevent interval (s)
Frequency (Hz)
WT KO
e
Cumulative probability
Rise time (ms)
Rise time (ms)
WT KO
f
Cumulative probability
Decay time (ms)
***
Decay time (ms)
WT KO
g
WT
Crbn KO
20 pA
0.5 s
h
10 pA
20 ms
i
Cumulative probability
Amplitude (pA)
Amplitude (pA)
WT KO
j
Cumulative probability
Interevent interval (ms)
Frequency (Hz)
WT KO
k
Cumulative probability
Rise time (ms)
Rise time (ms)
WT KO
l
Cumulative probability
Decay time (ms)
Decay time (ms)
WT KO

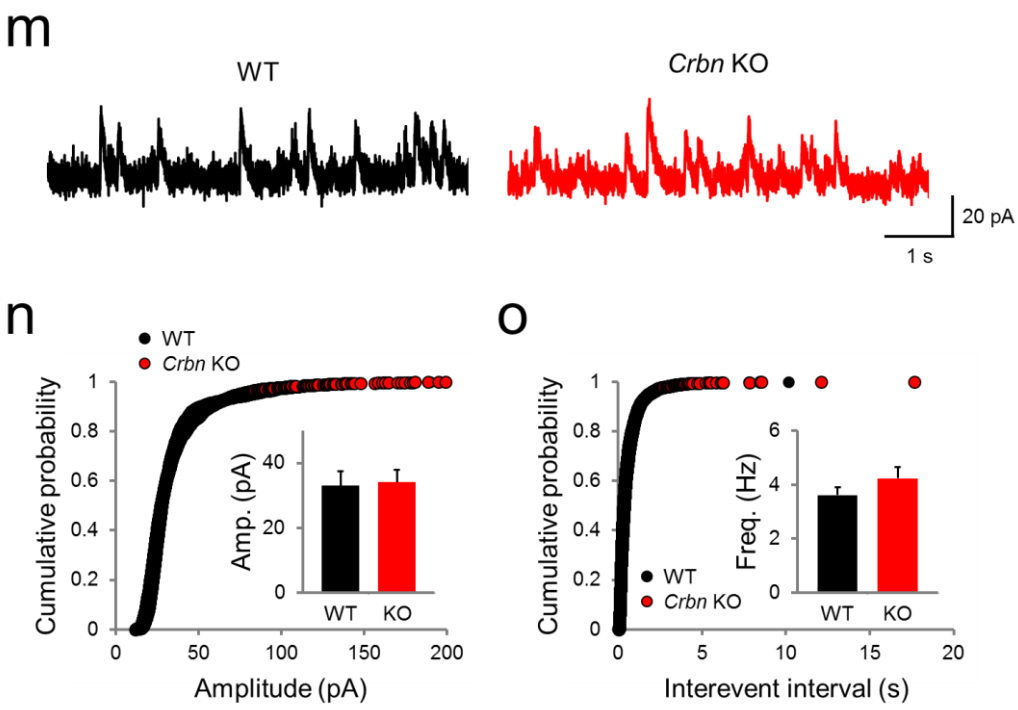
m
WT
Crbn KO
20 pA
1 s
n
WT
Crbn KO
Cumulative probability
Amplitude (pA)
Amp. (pA)
WT
KO
o
Cumulative probability
Interevent interval (s)
Freq. (Hz)
WT
Crbn KO
WT
KO

Figure 5. *Crbn* deficiency increases decay time without affecting the amplitude, frequency, or rise time of mEPSCs, and does not affect mIPSCs and sIPSCs.

(a-b) Representative traces (a) and averaged single event (b) of mEPSC in hippocampal CA1 pyramidal neurons of WT (black) or *Crbn* KO mice (red).

(c-f) The decay time (f), but not the amplitude (c), the frequency (d), or the rise time (e), of mEPSC is increased in the hippocampal CA1 pyramidal neurons from *Crbn* KO mice. Cumulative plots (left) and quantitative comparison with bar graphs (right). Bar graphs represent means ± SEM. (*** $p < 0.001$, Student's t-test; WT, n = 19 cells from 4 mice; and KO, n = 20, 5).

(g-h) Representative traces (a) and averaged single event (b) of mIPSC in hippocampal CA1 pyramidal neurons of WT (black) or *Crbn* KO mice (red).

(i-l) The amplitude (i), the frequency (j), the rise time (k), and the rise time (l) of mIPSC are similar between WT and *Crbn* KO mice. Cumulative plots (left) and quantitative comparison with bar graphs (right). Bar graphs represent means ± SEM. (WT, n = 27 cells from 3 mice; and KO, n = 22, 3).

(m) Representative traces of sIPSC in hippocampal CA1 pyramidal neurons of WT (left, black) or *Crbn* KO mice (right, red).

(n-o) Amplitudes (n) and frequencies (o) of sIPSCs are not significantly different in hippocampal CA1 pyramidal neurons from WT and *Crbn* KO mice. Cumulative plots of amplitudes (n) and frequencies (o). The inset compares the average of amplitude or frequency of sIPSCs. Bar graphs represent means ± SEM (WT, n = 10 cells from 3 mice; and KO, n = 12, 3).

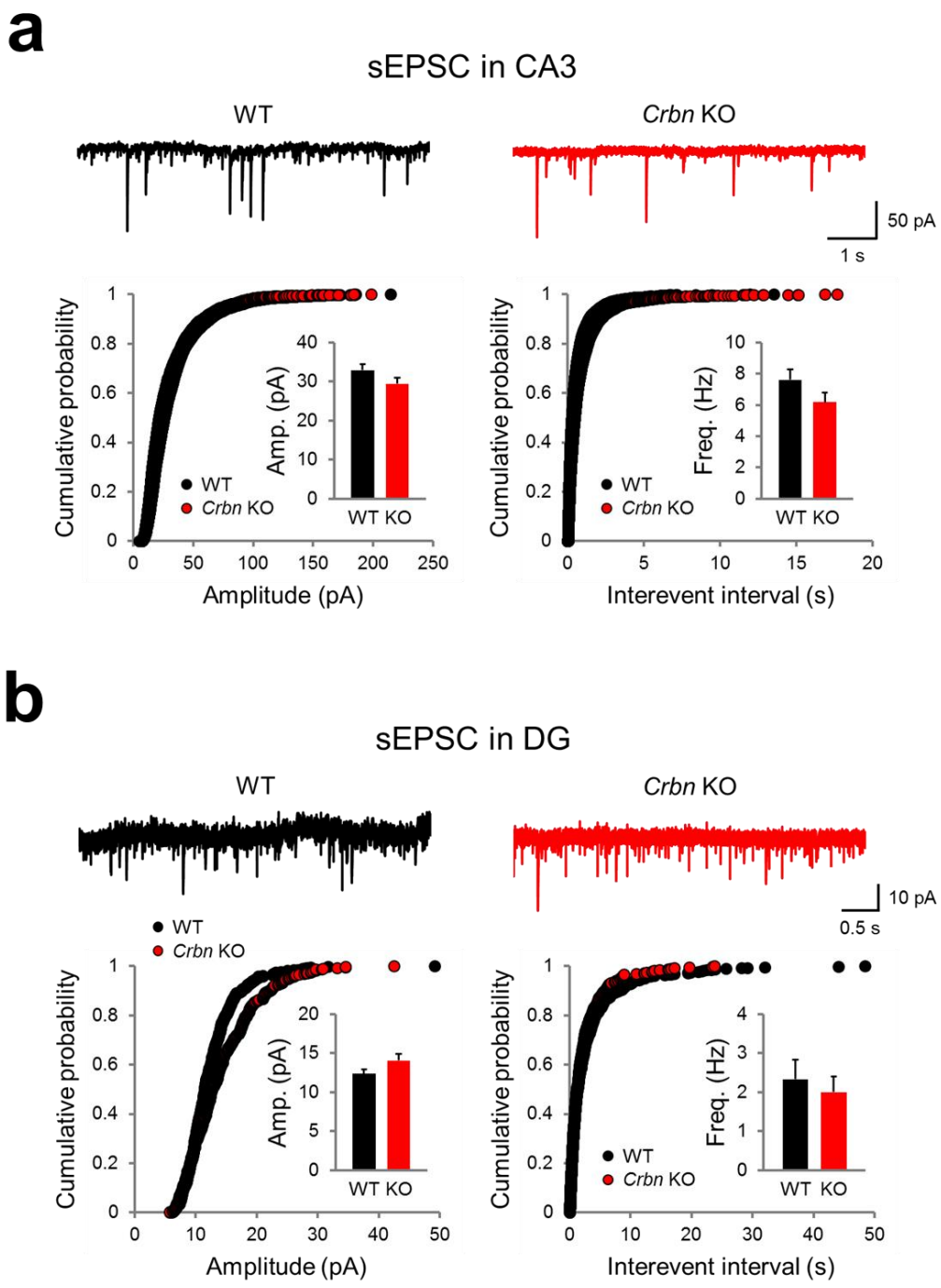
a
sEPSC in CA3
WT
Crbn KO
50 pA
1 s
Cumulative probability
Amplitude (pA)
Amp. (pA)
WT KO
WT
Crbn KO
Interevent interval (s)
Freq. (Hz)
b
sEPSC in DG
10 pA
0.5 s

Figure 6. *Crbn* KO mice have similar sEPSCs in CA3 pyramidal neurons and DG granule cells.

(a-b) Representative traces (top) and cumulative plots (bottom) of sEPSCs in CA3 pyramidal neurons (a) or DG granule cells (b) of WT (black) or *Crbn* KO mice (red). Amplitudes (left) and frequencies (rifht) of sEPSCs are not significantly different in hippocampal CA3 pyramidal neurons or DG granule cells from WT and *Crbn* KO mice. The inset compares the average of amplitude or frequency of sEPSCs. Bar graphs represent means ± SEM (WT_{CA3}, n = 35 cells from 3 mice; KO_{CA3}, n = 40, 3; WT_{DG}, n = 10, 2; and KO_{DG}, n = 9, 1).

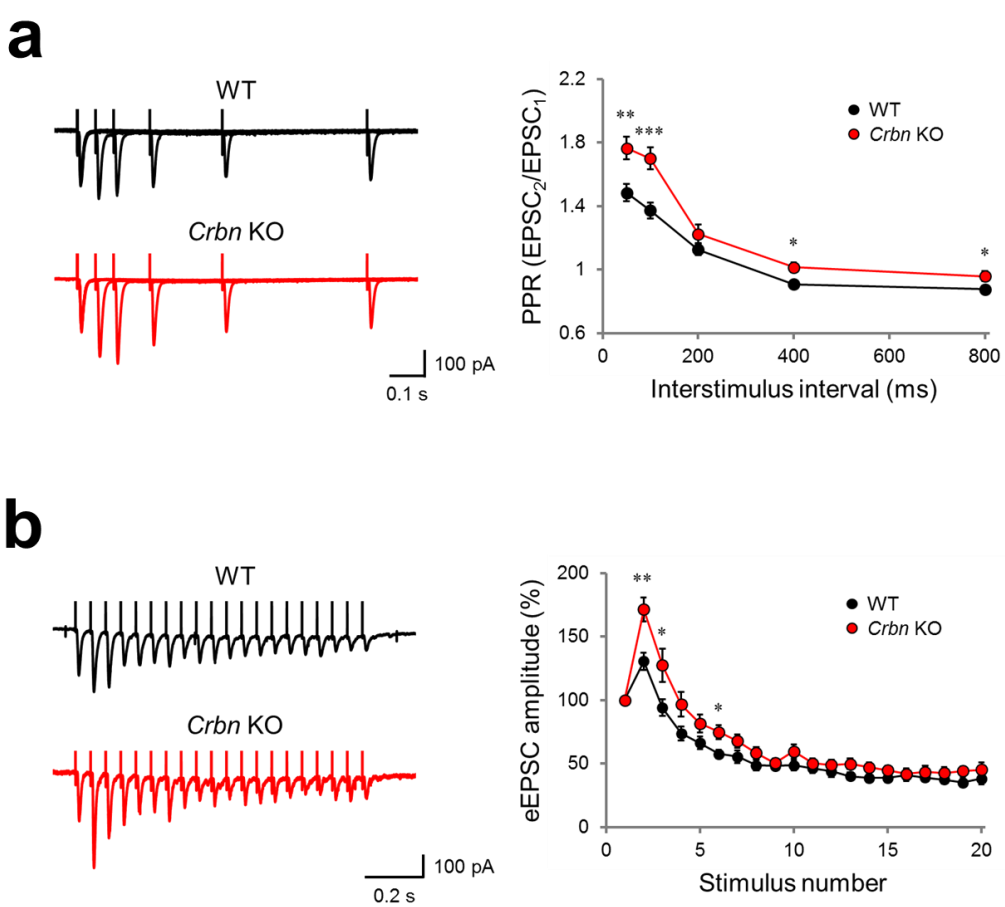
a
WT
Crbn KO
100 pA
0.1 s
PPR (EPSC2/EPSC1)
2.2
1.8
1.4
1
0.6
0
200
400
600
800
Interstimulus interval (ms)
WT
Crbn KO
**
***
*
*
b
WT
Crbn KO
100 pA
0.2 s
eEPSC amplitude (%)
200
150
100
50
0
0
5
10
15
20
Stimulus number
WT
Crbn KO
**
*
*

Figure 7. Excitatory Pr is decreased in PP-DG synapses of *Crbn* KO mice.

(a) *Crbn* KO mice show increased excitatory PPR in hippocampal PP-DG synapses. Representative traces (left) and summary graphs (right). PPR is plotted against interstimuli intervals. Individual points represent means ± SEM (*$p < 0.05$, **$p < 0.01$ and ***$p < 0.001$, Student's t-test; WT, n = 16 cells from 2 mice; and KO, n = 21, 2).

(b) Short-term synaptic plasticity induced by repetitive stimulation consisting of 20 pulses at 20 Hz stimulation is enhanced in excitatory synaptic transmission in hippocampal PP-DG synapses from *Crbn* KO mice. Representative traces (left) and summary graphs (right). Relative amplitudes of eEPSCs are plotted against stimulus number. Individual points represent means ± SEM (*$p < 0.05$ and **$p < 0.01$, Student's t-test; WT, n = 14 cells from 2 mice; and KO, n = 18, 2).

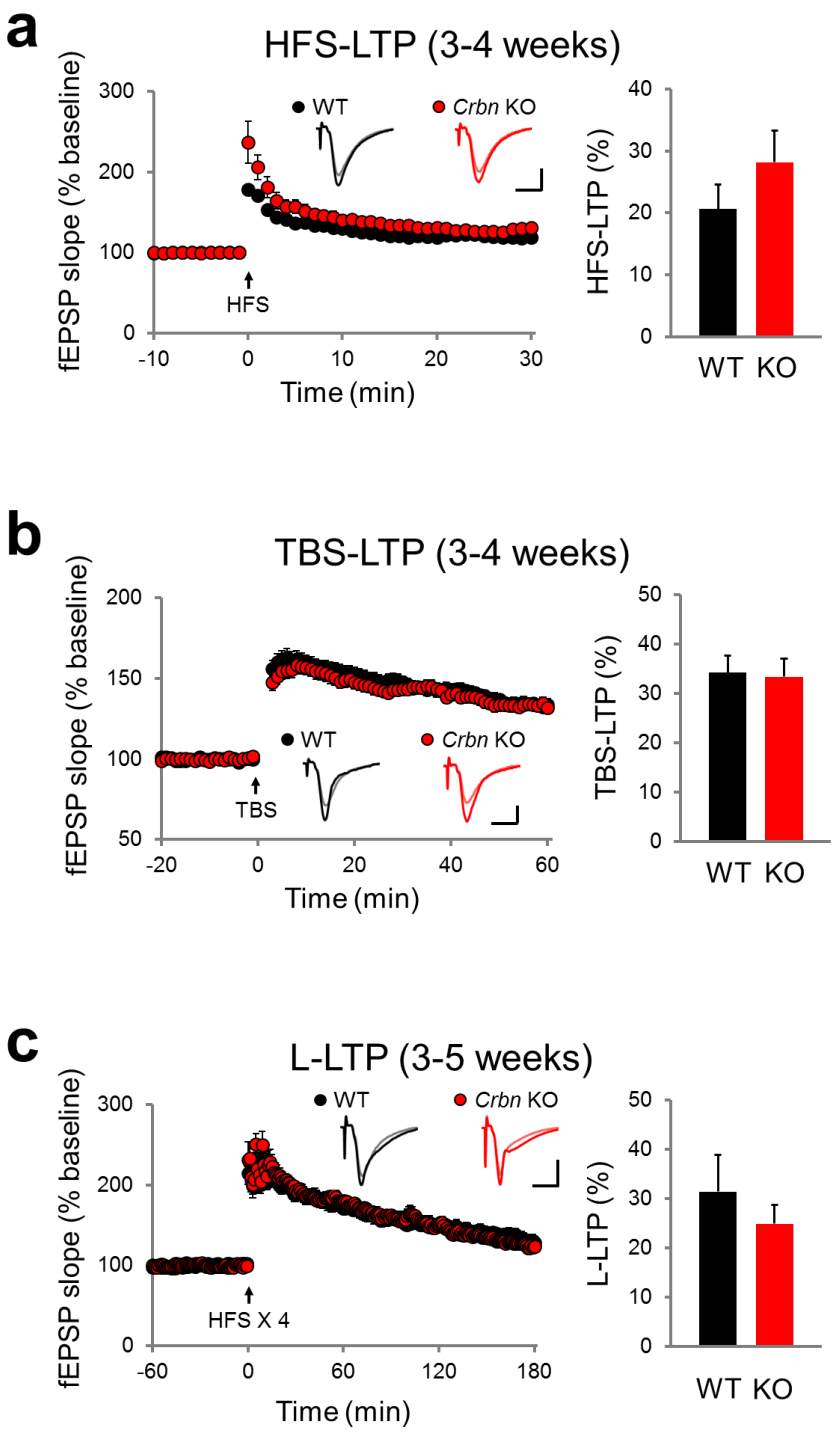
a
HFS-LTP (3-4 weeks)
fEPSP slope (% baseline)
300
200
100
0
WT
Crbn KO
HFS
-10
0
10
20
30
Time (min)
HFS-LTP (%)
40
30
20
10
0
WT KO
b
TBS-LTP (3-4 weeks)
fEPSP slope (% baseline)
200
150
100
50
WT
Crbn KO
TBS
-20
0
20
40
60
Time (min)
TBS-LTP (%)
50
40
30
20
10
0
WT KO
c
L-LTP (3-5 weeks)
fEPSP slope (% baseline)
300
200
100
0
WT
Crbn KO
HFS X 4
-60
0
60
120
180
Time (min)
L-LTP (%)
50
40
30
20
10
0
WT KO

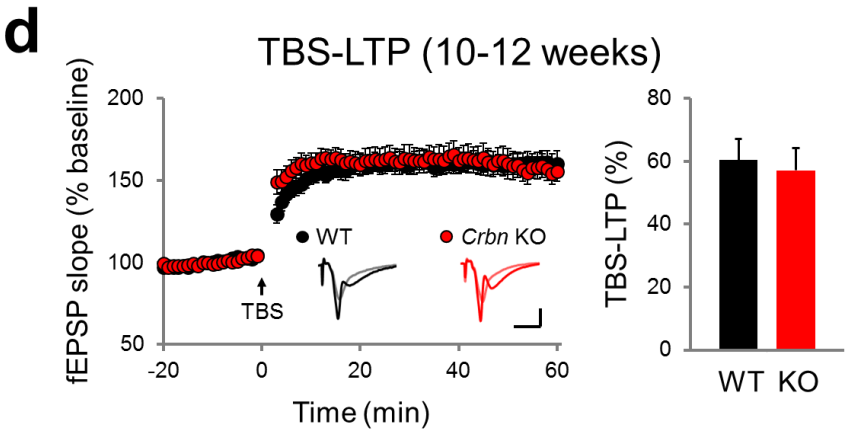
d
TBS-LTP (10-12 weeks)
fEPSP slope (% baseline)
200
150
100
50
-20
0
20
40
60
Time (min)
WT
Crbn KO
TBS
TBS-LTP (%)
80
60
40
20
0
WT KO

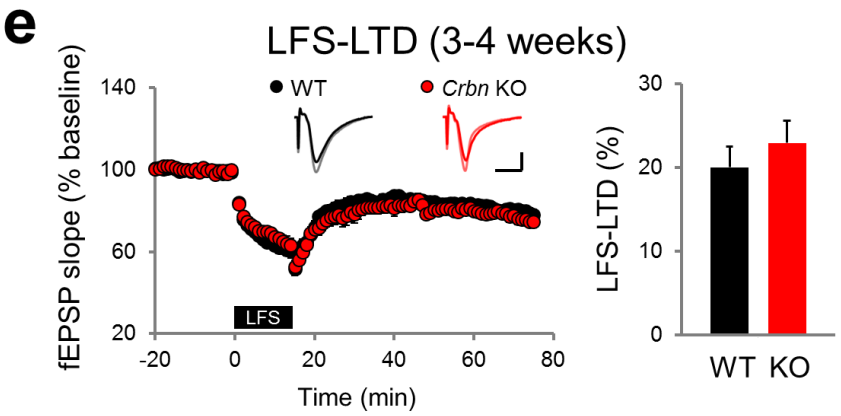
e
LFS-LTD (3-4 weeks)
fEPSP slope (% baseline)
140
100
60
20
-20
0
20
40
60
80
Time (min)
WT
Crbn KO
LFS
LFS-LTD (%)
30
20
10
0
WT KO

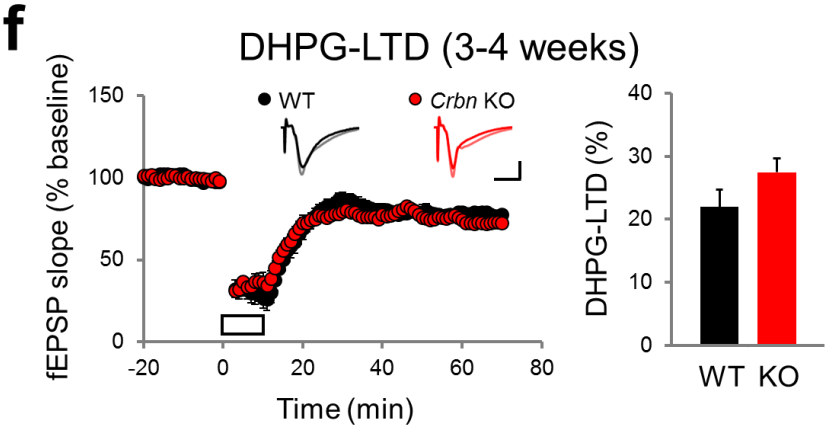
f
DHPG-LTD (3-4 weeks)
fEPSP slope (% baseline)
150
100
50
0
-20
0
20
40
60
80
Time (min)
WT
Crbn KO
DHPG-LTD (%)
40
30
20
10
0
WT KO

Figure 8. *Crbn* KO mice exhibit normal long-term synaptic plasticity in hippocampal SC-CA1 synapses.

(a-b) No differences in HFS- (a, HFS-LTP) or TBS-induced (b, TBS-LTP) NMDA receptor-dependent long-term potentiation (LTP) in hippocampal SC-CA1 synapses from 3- to 4-week-old WT and *Crbn* KO mice. Summary graphs (left) and quantitative comparisons with bar graphs (right). The magnitudes of LTP are calculated by comparing the average slopes of fEPSPs recorded during the last 5 (a) or 10 (b) min with those recorded before stimulation. Insets are representative traces; gray (WT) and pink (KO) mean 1 min before and black (WT) and red (KO) mean 30 min (a) or 1 h (b) after conditioning stimulation. Individual points and bar graphs represents mean ± SEM ($WT_{HFS\text{-}LTP}$, n = 8 slices from 3 mice; $KO_{HFS\text{-}LTP}$, n = 8, 2; $WT_{TBS\text{-}LTP}$, n = 27, 7; and $KO_{TBS\text{-}LTP}$, n = 28, 8).

(c) No differences in protein synthesis-dependent late-phase LTP (L-LTP) induced by four repeated HFS (HFS X 4) with 5-min intervals between WT and *Crbn* KO mice. The magnitudes of L-LTP are calculated by comparing the average slopes of fEPSPs recorded during the last 10 min with those recorded before stimulation. Insets are representative traces; gray (WT) and pink (KO) mean 1 min before and black (WT) and red (KO) mean or 3 h after conditioning stimulation. Individual points and bar graphs represents mean ± SEM ($WT_{L\text{-}LTP}$, n = 11 slices from 7 mice; and $KO_{L\text{-}LTP}$, n = 9, 6).

(d) No differences are observed in NMDA receptor-dependent LTP induced by TBS from 10- to 12-week-old WT and *Crbn* KO mice. The magnitudes of TBS-LTP from adult brain slices are calculated with last 10 min responses. Insets are representative traces; gray (WT) and pink (KO) mean 1 min before and black (WT) and red (KO)

mean 1 h after conditioning stimulation. Individual points and bar graphs represent mean ± SEM ($WT_{TBS\text{-}LTP}$, n = 13 slices from 8 mice; and $KO_{TBS\text{-}LTP}$, n = 10, 5).

(e-f) No differences in NMDA receptor-dependent LTD induced by LFS (e, LFS-LTD) or group I mGluR-dependent DHPG-induced LTD (f, DHPG-LTD). Summary graphs (left) and quantitative comparisons with bar graphs (right). The magnitudes of LTD are calculated by comparing the average slopes of fEPSPs recorded during the last 10 min with those recorded before stimulation. The insets are representative traces; gray (WT) and pink (KO) mean 1 min before and black (WT) and red (KO) mean 1 h after conditioning stimulation. Individual points and bar graphs represent mean ± SEM ($WT_{LFS\text{-}LTD}$, n = 13 slices from 3 mice; $KO_{LFS\text{-}LTD}$, n = 8, 4; $WT_{DHPG\text{-}LTD}$, n = 7, 3; and $KO_{DHPG\text{-}LTD}$, n = 6, 2).

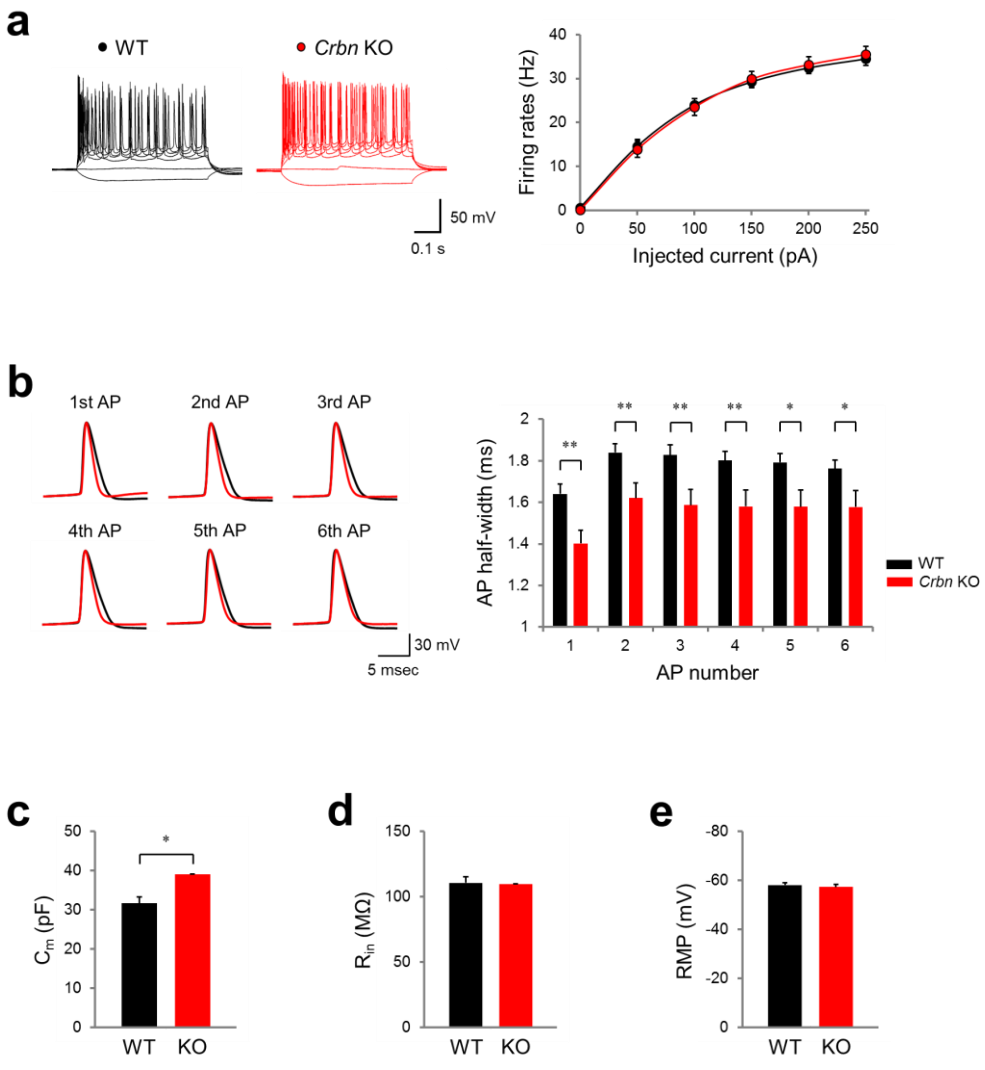
a
WT
Crbn KO
50 mV
0.1 s
Firing rates (Hz)
Injected current (pA)
b
1st AP
2nd AP
3rd AP
4th AP
5th AP
6th AP
30 mV
5 msec
AP half-width (ms)
AP number
WT
Crbn KO
c
Cm (pF)
WT KO
d
Rin (MΩ)
WT KO
e
RMP (mV)
WT KO

Figure 9. *Crbn* KO mice have reduced action potential duration and increased whole-cell capacitance, but other intrinsic properties are not altered.

(a) *Crbn* KO mice have normal neuronal excitability in hippocampal CA1 pyramidal neurons. Representative traces (left) and summary graphs (right) of neuronal excitability measured as firing rates in response to step depolarizing currents (500 ms duration) under current-clamp mode in hippocampal CA1 pyramidal neurons from WT (black) or *Crbn* KO mice (red). Individual points represent mean ± SEM (WT, n = 22 cells from 5 mice; and KO, n = 20, 3).

(b) Hippocampal CA1 pyramidal neurons from *Crbn* KO mice show reduced action potential (AP) half-width. Representative traces (left) and bar graphs (right). Bar graphs represent means ± SEM (*$p < 0.05$ and ** $p < 0.01$, Student's t-test; WT, n = 15 cells from 4 mice; and KO, n = 15, 3).

(c-e) Hippocampal CA1 pyramidal neurons from *Crbn* KO mice exhibit a higher whole-cell membrane capacitance (Cm) than WT (c). Input resistance (R_{in}) (d) and resting membrane potential (RMP) (e) are not statistically different between WT and *Crbn* KO mice. Bar graphs represent means ± SEM (*$p < 0.05$, Student's t-test; WT, n = 22 cells from 5 mice; and KO, n = 20, 3).

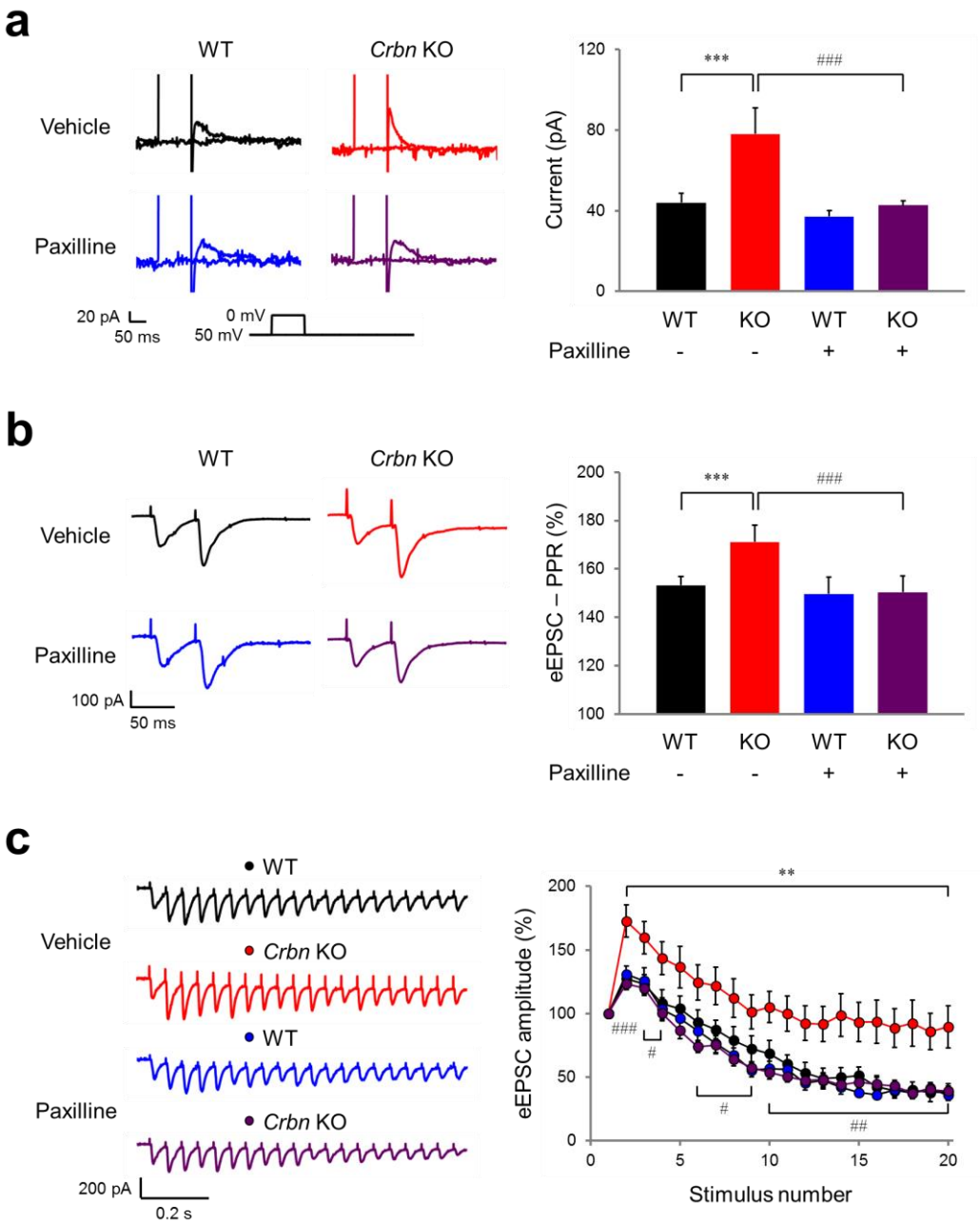
a
WT
Crbn KO
Vehicle
Paxilline
20 pA
50 ms
0 mV
50 mV
Current (pA)
120
80
40
0
***
###
WT
KO
WT
KO
Paxilline
-
-
+
+
b
WT
Crbn KO
Vehicle
Paxilline
100 pA
50 ms
eEPSC – PPR (%)
200
180
160
140
120
100
***
###
WT
KO
WT
KO
Paxilline
-
-
+
+
c
WT
Crbn KO
WT
Crbn KO
Vehicle
Paxilline
200 pA
0.2 s
eEPSC amplitude (%)
200
150
100
50
0
**
###
#
#
##
0
5
10
15
20
Stimulus number

Figure 10. Reduced excitatory presynaptic function in *Crbn* KO mice is rescued by BK channel blocker.

(a) Increased Ca^{2+}-activated K^+ currents in hippocampal CA1 pyramidal neurons from *Crbn* KO mice are selectively abolished by paxilline (a pan-BK channel blocker, 10 μM). Representative traces (left) and summary graphs (right) of Ca^{2+}-activated K^+ currents. Bar graphs represent mean ± SEM (***p < 0.001 compared to WT without paxilline and $^{###}$ p <0.001 compared to KO without vehicle, two-way ANOVA with Horm-Sidak's post hoc analysis; $WT_{Vehicle}$, n = 29 cells from 3 mice; $KO_{Vehicle}$, n = 17, 3; $WT_{Paxilline}$, n = 29, 3; and $KO_{Paxilline}$, n = 29, 3).

(b) Paxilline (10 μM) negates the increased excitatory PPR (50 ms of interstimulus interval) at *Crbn* KO SC-CA1 synapses. Representative traces (left) and summary graphs (right) of PPR. Bar graphs represent mean ± SEM (***p < 0.001 compared to WT without paxilline and $^{###}$ p <0.001 compared to KO without vehicle, two-way ANOVA with Horm-Sidak's post hoc analysis; $WT_{Vehicle}$, n = 15 cells from 3 mice; $KO_{Vehicle}$, n = 16, 3; $WT_{Paxilline}$, n = 14, 3; and $KO_{Paxilline}$, n = 16, 3).

(c) Altered short-term plasticity induced by repetitive stimulation (20 pulses at 20 Hz) in *Crbn* KO mice is rescued by paxilline (10 μM) at *Crbn* KO SC-CA1 synapses. Representative traces (left) and summary graphs (right). Individual points represents mean ± SEM (**p < 0.01 and ***p < 0.001 compared to WT without paxilline, $^{#}$p < 0.05, $^{##}$p < 0.01 and $^{###}$p < 0.001 compared to KO without vehicle, two-way ANOVA with Horm-Sidak's post hoc analysis; $WT_{Vehicle}$, n = 20 cells from 5 mice; $KO_{Vehicle}$, n = 16, 6; $WT_{Paxilline}$, n = 13, 3; and $KO_{Paxilline}$, n = 11, 3).

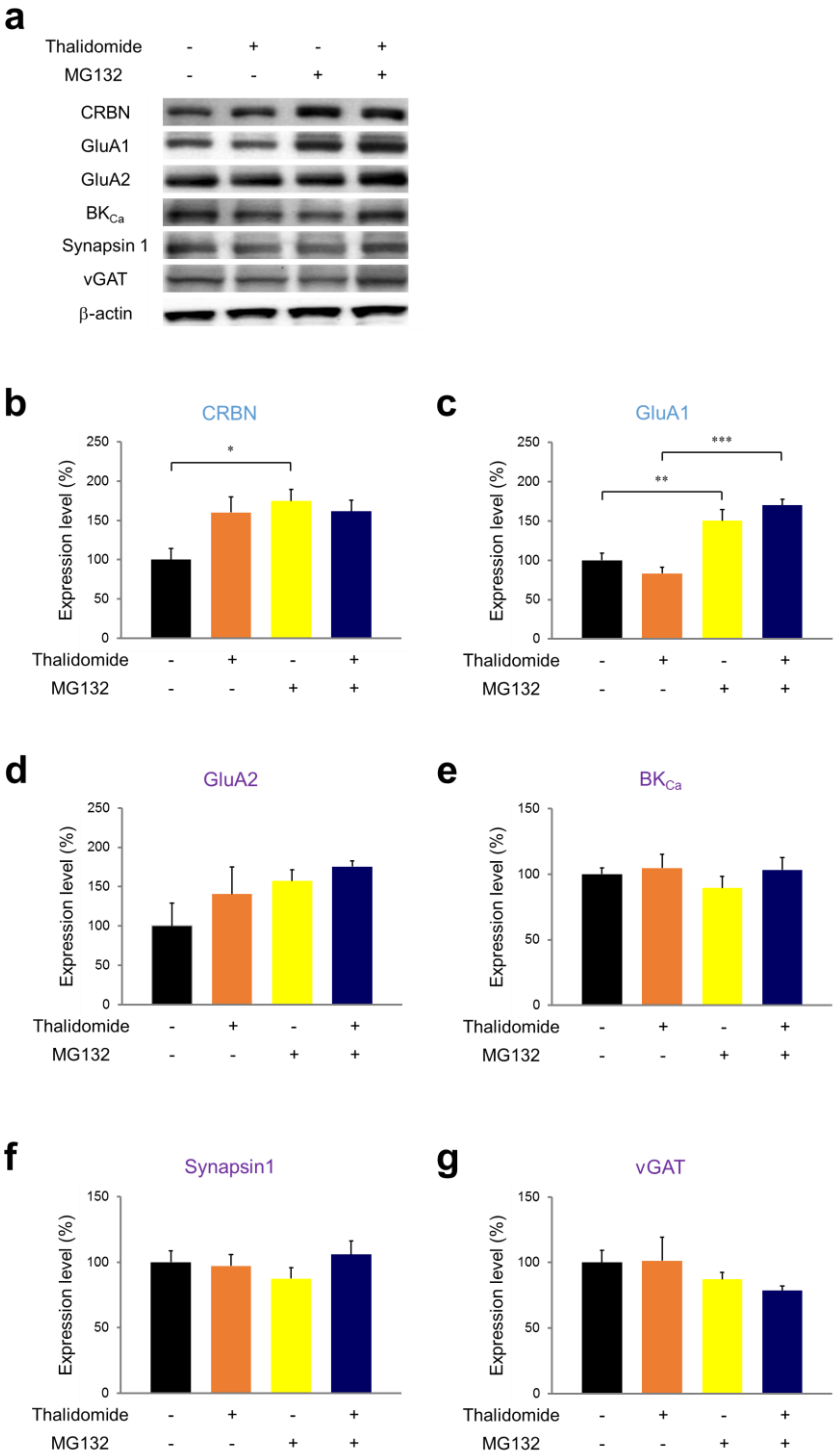
a
Thalidomide - + - +
MG132 - - + +
CRBN
GluA1
GluA2
BKCa
Synapsin 1
vGAT
β-actin
b
CRBN
c
GluA1
d
GluA2
e
BKCa
f
Synapsin1
g
vGAT
Expression level (%)
Thalidomide
MG132
*
**
***

Figure 11. Analysis of the expression patterns of CRBN, a subunit of BK channel and synaptic proteins after thalidomide treatment.

(a) Hippocampal slices from 3- to 4-week-old WT mice are treated with vehicle or thalidomide (100 μM) and/or MG132 (10 μM) for 3h, and then homogenized for immunoblotting to evaluate the expression levels of several proteins. All protein signals are normalized relative to β-actin levels.

(b) The expression level of CRBN protein is increased by thalidomide (but statistically insignificant, $p = 0.059$), MG132, or thalidomide and MG132. Bar graphs represent means ± SEM (*$p < 0.05$ compared to the treatment of MG132, two-way ANOVA with Horm-Sidak's post hoc analysis; WT, n = 4 mice; and KO, n = 4).

(c) Thalidomide does not change the expression level of GluA1 subunit, but MG132 alone or thalidomide and MG132 increases it. Bar graphs represent means ± SEM (**$p < 0.01$ compared to the treatment of MG132 and ***$p < 0.001$ compared to the treatment of thalidomide and MG132, two-way ANOVA with Horm-Sidak's post hoc analysis; WT, n = 4 mice; and KO, n = 4).

(d-g) The expression levels of GluA2 subunit, α subunit of BK channel, synapsin 1, and vGAT are not affected by the treatment of thalidomide and/or MG132. Bar graphs represent means ± SEM (WT, n = 4 mice; and KO, n = 4).

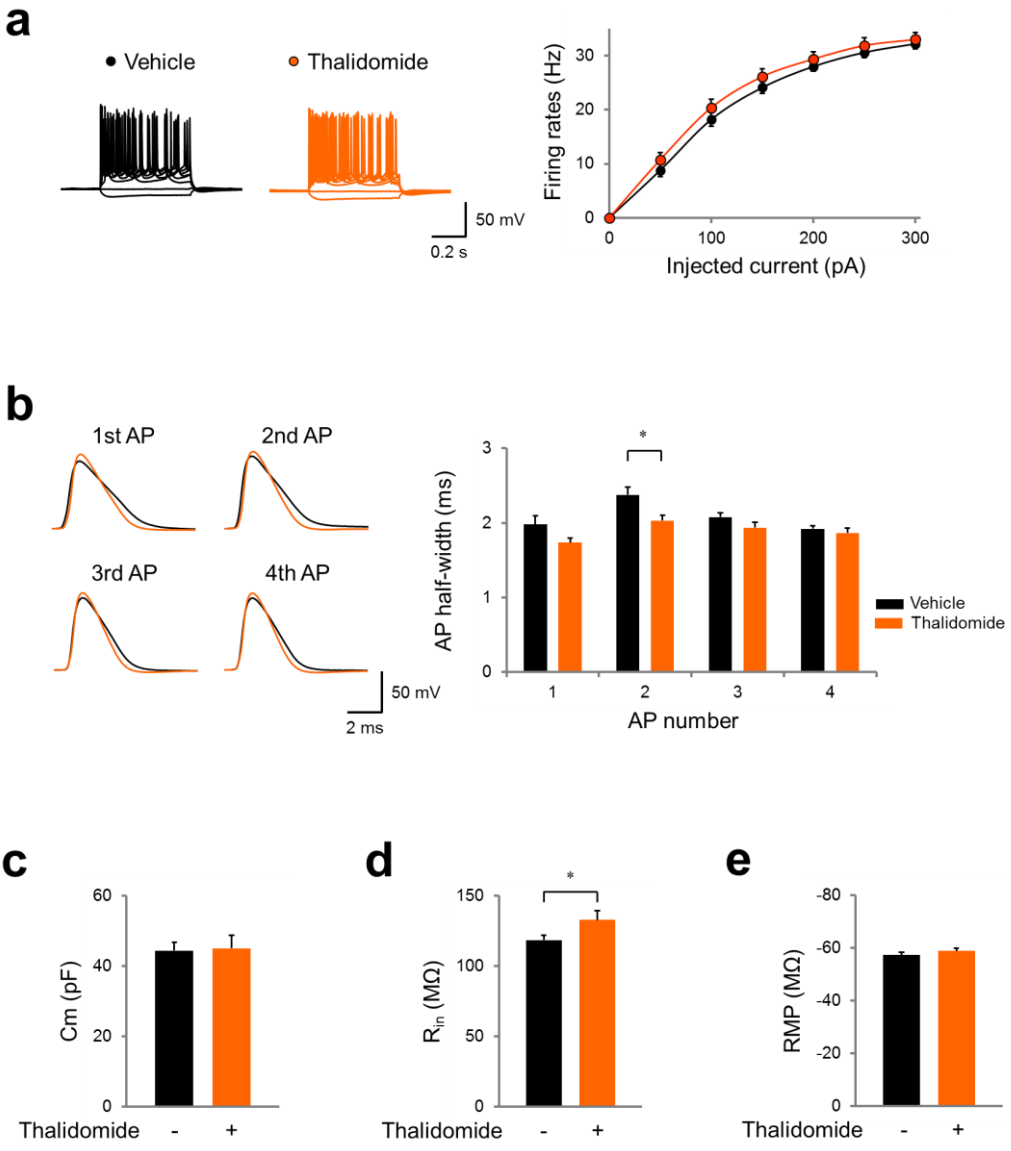
a
Vehicle
Thalidomide
50 mV
0.2 s
Firing rates (Hz)
Injected current (pA)
b
1st AP
2nd AP
3rd AP
4th AP
50 mV
2 ms
AP half-width (ms)
AP number
Vehicle
Thalidomide
c
Cm (pF)
Thalidomide - +
d
R_{in} (MΩ)
Thalidomide - +
e
RMP (MΩ)
Thalidomide - +

Figure 12. Thalidomide modulates neuronal intrinsic properties.

(a) Thalidomide incubation did not affect the neuronal excitability in hippocampal CA1 pyramidal neurons. Representative traces (left) and summary graphs (right) of neuronal excitability measured as firing rates in response to step depolarizing currents (500 ms duration) under current-clamp mode in hippocampal CA1 pyramidal neurons of vehicle-treated (black) or thalidomide-treated brain slices (orange). Individual points represent mean ± SEM (vehicle, n = 20 cells from 6 mice; and KO, n = 16, 4).

(b) Thalidomide-treated hippocampal CA1 pyramidal neurons show decreased action potential duration. Representative traces (left) and bar graphs (right). Bar graphs represent means ± SEM (*$p < 0.05$, Student's t-test; vehicle, n = 12 cells from 6 mice; and KO, n = 15, 5).

(c-e) Hippocampal CA1 pyramidal neurons from thalidomide-treated brain slices exhibit a higher input resistance (R_{in}) than control WT (d), but membrane capacitance (Cm) (c) and resting membrane potential (RMP) (e) are not statistically different between vehicle- and thalidomide-treated groups. Bar graphs represent means ± SEM (*$p < 0.05$, Student's t-test; vehicle, n = 20 cells from 6 mice; and thalidomice, n = 16, 4).

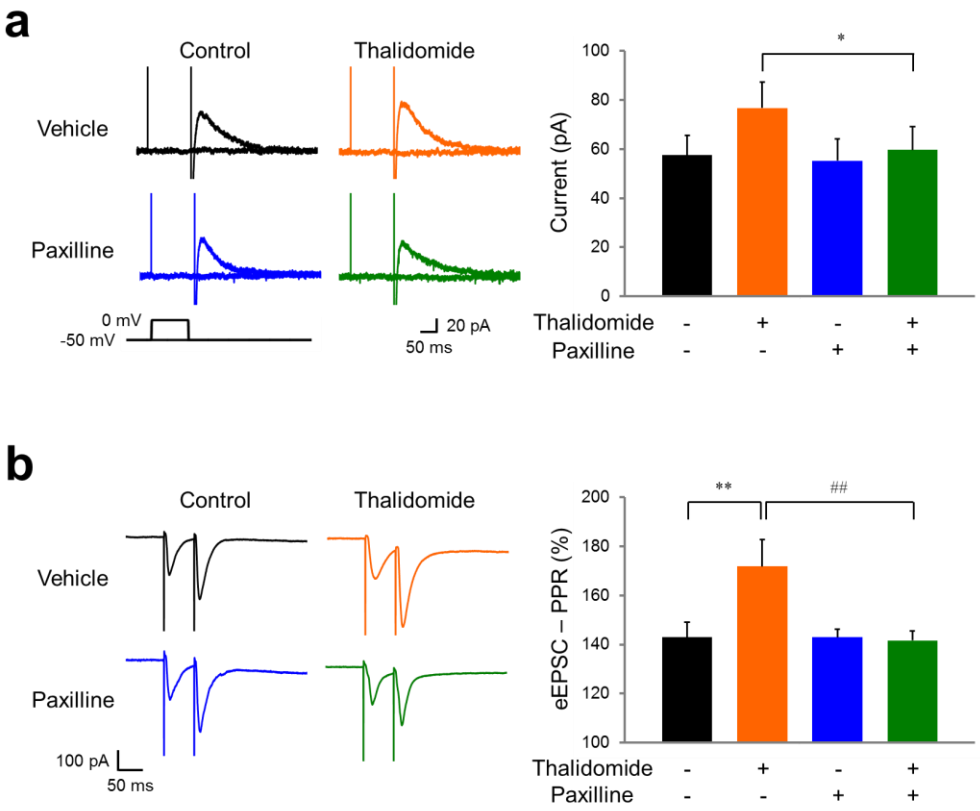
a
Control
Thalidomide
Vehicle
Paxilline
0 mV
-50 mV
20 pA
50 ms
Current (pA)
100
80
60
40
20
0
*
Thalidomide - + - +
Paxilline - - + +
b
Control
Thalidomide
Vehicle
Paxilline
100 pA
50 ms
eEPSC – PPR (%)
200
180
160
140
120
100
**
##
Thalidomide - + - +
Paxilline - - + +
c
Vehicle
Thalidomide
10 pA
1 s
Vehicle
Thalidomide
Cumulative probability
Amplitude (pA)
Amp. (pA)
Thalidomide - +
Interevent inverval (s)
Freq. (Hz)
Thalidomide - +

Figure 13. Thalidomide treatment mimics the synaptic phenotypes of *Crb*n KO mice.

(a) Thalidomide (100 μM) slightly increases Ca^{2+}-activated K^{+}-currents and this enhancement is selectively inhibited by BK channel blocker paxilline (10 mM) in the hippocampal CA1 pyramidal neurons. Representative traces (left) and summary graphs (right) of Ca^{2+}-activated K^{+}-currents. Bar graphs represent mean ± SEM (*p < 0.05, paired Student's t-test; vehicle ± paxilline, n = 13 cells from 2 mice; and thalidomide ± paxilline, n = 15, 2).

(b) Paxilline (10 μM) recovers the enhanced excitatory PPR (50 ms of interstimulus interval) in thalidomide-treated hippocampal SC-CA1 synapses. Representative traces (left) and summary graphs (right) of PPR. Bar graphs represent mean ± SEM (**p < 0.01 compared to vehicle without paxilline and $^{\#\#}$ p <0.01 compared to thalidomide without paxilline, two-way ANOVA with Horm-Sidak's post hoc analysis; vehicle only, n = 22 cells from 5 mice; thalidomide, n = 19, 6; paxilline, n = 29, 4; and thalidomide + paxilline, n = 20, 3).

(c) sEPSCs are not changed by thalidomide treatment. Representative traces (top) or cumulative plots (bottom) of sEPSC in hippocampal CA1 pyramidal neurons of vehicle-treated (black) or thalidomide-treated brain slices (orange). The inset compares the average of amplitude or frequency of sEPSCs. Bar graphs represent means ± SEM (vehicle, n = 19 cells from 7 mice; and thalidomide, n = 11, 4).

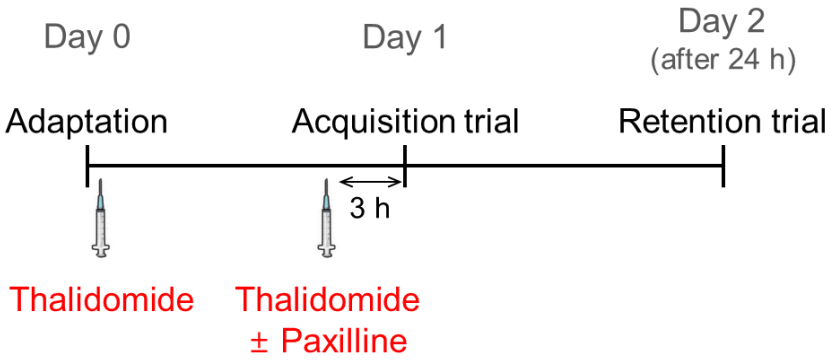
Day 0
Day 1
Day 2
(after 24 h)
Adaptation
Acquisition trial
Retention trial
3 h
Thalidomide
Thalidomide
± Paxilline

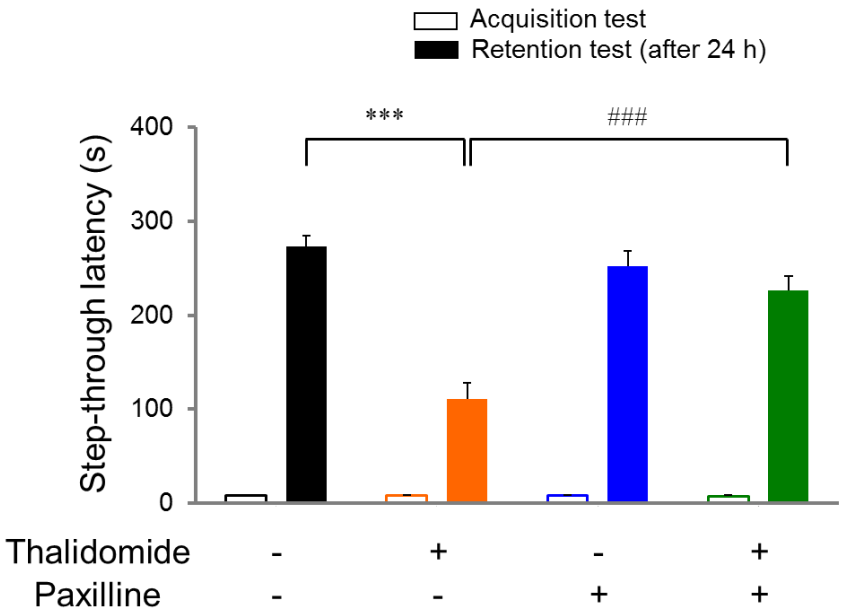
Acquisition test
Retention test (after 24 h)
***
###
Step-through latency (s)
400
300
200
100
0
Thalidomide - + - +
Paxilline - - + +

Figure 14. Thalidomide induces in passive avoidance memory impairment, and BK channel blocker recovers it.

Thalidomide-treated mice (30 mg/kg, i.p.) spent significantly more time in the dark chamber on day 2 of the passive avoidance test, and paxillin treatment (3 μg/kg, i.p.) negate the changes. Experimental procedures (top) and summary praphs (bottom). Bar graphs represent mean ± SEM (***$p < 0.001$ compared to vehicle without paxilline and $^{###}$ $p < 0.001$ compared to thalidomide without paxilline, two-way ANOVA with Horm-Sidak's post hoc analysis; vehicle only, n = 20 mice; thalidomide, n = 19; paxilline, n = 19; and thalidomide + paxilline, n = 20).

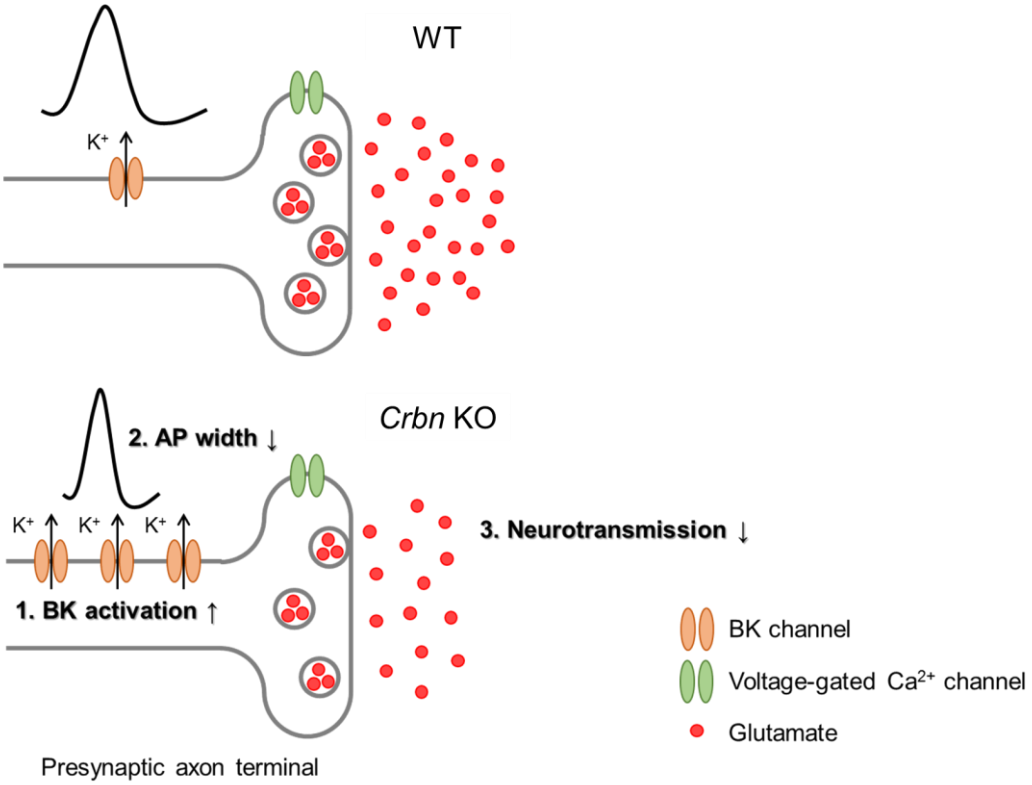

Figure 15. Schematic model of reduced excitatory presynaptic function in *Crbn* KO mice.

CRBN negatively modulates the surface expression of BK channels. BK channels are overexpressed on the presynaptic membrane, and therefore the hyperactivation of BK channels reduces the duration of action potential and decreases presynaptic glutamate release in *Crbn* KO mice. These are the core mechanisms of cognitive impairment in *Crbn* KO mice.

Discussion

Summary of this study

In this study, I found four key findings about synaptic and cognitive function of CRBN. First, *Crbn* KO mice shows cognitive impairment, but have normal brain gross and synaptic ultrastructual morphology (data not shown). Second, excitatory, but not inhibitory, presynaptic neurotransmitter release is decreased in the hippocampal SC-CA1 synapses (Figure 3 and 4) and PP-DG synapses (Figure 7) of *Crbn* KO mice. Third, enhancement of Pr is caused by hyperactivation of BK channel (Figure 10). All of these results were summarized in Figure 15. Lastly, thalidomide mimics synaptic and behavioral phenotypes observed in *Crbn* KO mice and BK channel blocker paxilline recovers them (Figure 12-14).

Limitations of this study and related further studies

However, there are some unsolved remaining points in present study. First of all, I could not explain how the expression levels of synapsin 1 and vGAT were changed in *Crbn* KO mice (Figure 2). One possibility is that the expression of these proteins are regulated by $CRL4^{CRBN}$ E3 ubiquitin ligase complex. To address this question, I will test ubiquitination levels of these proteins. Next, amplitude, frequency and rise time are not different, but only decay time of mEPSC is increased in *Crbn* KO mice (Figure 4j). It suggests that *Crbn* KO mice have different AMPA receptor composition. Although total expression level of GluA1 or GluA2 subunit is not altered in *Crbn* KO mice, it is possible to change the synaptic composition of AMPA receptors. Subunit composition of AMPA receptors is very important for the synaptic development and function, especially containing or lacking GluA2

subunit because this subunit determines the permeability of calcium ions of AMPA receptors (Cull-Candy et al., 2006; Issac et al., 2007; Man, 2011). Thus it is necessary to check the expression level of AMPA receptor subunits on the synaptic membrane, or calcium-permeability of AMPA receptors by measuring current-voltage relationship of this channels. Lastly, I have to test whether BK channel blocker recovers cognitive impairments in *Crbn* KO mice.

Although CRBN-mediated modulation of BK channel activity is suggested to affect cognitive function, no direct evidence is available at the synaptic or behavioral level. This study to reveal the synaptic function of CRBN in *ex vivo* brain slices from a *Crbn* KO animal model provides findings that have not been available for primary cultured neurons in previously reported studies on CRBN function (Ito et al., 2010; Jo et al., 2005; Liu et al., 2014). This study provides evidence of synaptic dysfunction in *Crbn* KO mice because hyperactivation of the BK channel promoted a decrease in action potential duration and presynaptic glutamate release.

Neuropsychiatric disorders related to BK channelopathy : Fmr1 & Crbn mutation

The role of K^+ channels in synaptic and cognitive functions has garnered wide interest (D'Adamo et al., 2013; Lee & Jan, 2012). Ca^{2+}-activated K^+ channels are typical K^+ channels that modulate the regulation and maintenance of synaptic function (Hu et al., 2001; Raffaelli et al., 2004; Wang, 2008; Wang et al., 2014). In particular, a decrease in BK channel activity, which has been studied for decades, mostly in relation to epilepsy, has recently been suggested to cause cognitive impairment. For instance, patients with *FMR1* missense mutations and *Fmr1* KO animals show decreased BK channel activity and increases in both action potential

duration and presynaptic neurotransmitter release (Deng et al., 2013; Deng & Klyachko, 2016; Myrick et al., 2015). In contrast, I found that *Crbn* KO mice exhibited increased BK channel activity and a subsequent decrease in excitatory Pr. Thus, results from this study strongly suggested that the maintenance of balanced BK channel activity was critical for synaptic and cognitive function. The importance of balanced synaptic protein activity is well studied in NMDA receptor-interacting proteins. For instance, impaired cognitive function is caused by both hyperactivity (e.g., bipolar disorder) and hypoactivity (e.g., schizophrenia) of the NMDA receptor (Lakhan et al., 2013). Thus, my study is meaningful for suggesting that not only the hypofunction such as fragile X intellectual disability, but also the hyperfunction of BK channel induced by *CRBN* mutation is an etiological factor in intellectual disability.

Neuropsychiatric disorders related to misregulation of ubiquitination

I propose that CRBN modulates synaptic and cognitive function by maintaining balanced BK channel activity. Since previous studies report that CRBN binds to the C-terminus of the α subunit of BK channel and inhibits surface expression of this channel (Jo et al., 2005), interaction has been reported between $CRL4^{CRBN}$ and the BK channel that promotes ubiquitination of the BK channel and blocks membrane exposure via ER retention of the BK channel (Liu et al., 2014). Thus, I tested whether the synaptic and cognitive impairments in *Crbn* KO mice were dependent upon $CRL4^{CRBN}$-mediated ubiquitination activity. To address my hypothesis, I used thalidomide, which inhibits $CRL4^{CRBN}$ E3 ubiquitin ligase $CRL4^{CRBN}$. I confirmed thalidomide-mediated inhibition of ubiquitination by monitoring how thalidomide increased CRBN expression in hippocampal slices. In addition, I found that thalidomide-treated wild type mice showed phenotypes similar to *Crbn* KO mice;

these effects were rescued by a BK channel inhibitor paxilline. These results indicate that abnormal BK channel activity and abnormal modulation of ubiquitination contributed to the etiology of CRBN mutation-related intellectual disability. These results suggest that BK channel inhibitor could be effective in mitigating the reported side effect of cognitive impairment of thalidomide and its analogs lenalidomide and pomalidomide, which are widely prescribed for multiple myeloma (Patel et al., 2015; Rollin-Sillaire et al., 2013).

Taken together, results of this study reveal that *Crbn* KO mice with cognitive deficits shows normal synaptic morphology and plasticity, but presynaptic dysfunction in glutamate release mediated by increased BK channel activity. These effects were mimicked by treating wild type animals with thalidomide. A large body of recent work suggests that cognitive impairment is caused by ubiquitination dysfunctions (Adorno et al., 2013; Haddad et al., 2013), synaptopathy (Bhakar et al., 2012; Wallace et al., 2012), and channelopathy (Guglielmi et al., 2015). Thus, my study using a *Crbn* KO mice that display all of these dysfunctions should contribute to future investigations of intellectual disability.

References

1. Adorno, M., Sikandar, S., Mitra, S.S., Kuo, A., Nicolis Di Robilant, B., Haro-Acosta, V., Ouadah, Y., Quarta, M., Rodriguez, J., Qian, D., Reddy, V.M., Cheshier, S., Garner, C.C., Clarke, M.F. (2013) Usp16 contributes to somatic stem-cell defects in Down's syndrome. Nature. 501(7467):380-4.

2. Aizawa, M., Abe, Y., Ito, T., Handa, H., Nawa, H. (2011) mRNA distribution of the thalidomide binding protein cereblon in adult mouse brain. Neurosci Res. 69(4):343-7.

3. Aoki, T., Baraban, S.C. (2001) Properties of a calcium-activated K($^{+}$) current on interneurons in the developing rat hippocampus. J Neurophysiol. 83(6):3453-61.

4. Bhakar, A.L., Dölen, G., Bear, M.F. (2012) The pathophysiology of fragile X (and what it teaches us about synapses). Annu Rev Neurosci. 35:417-43.

5. Chang, X.B., Stewart, A.K. (2011) What is the functional role of the thalidomide binding protein cereblon? Int J Biochem Mol Biol. 2(3):287-94.

6. Choi, T.Y., Jung, S., Nah, J., Ko, H.Y., Jo, S.H., Chung, G., Park, K., Jung, Y.K., Choi, S.Y. (2015) Low levels of methyl β-cyclodextrin disrupt GluA1-dependent synaptic potentiation but not synaptic depression. J Neurochem. 132(3):276-85.

7. Clem, R.L., Huganir, R.L. (2010) Calcium-permeable AMPA receptor dynamics mediate fear memory erasure. Science. 330(6007):1108-12.

8. Contractor, A., Klyachko, V.A., Portera-Cailliau, C. (2015) Altered Neuronal and Circuit Excitability in Fragile X Syndrome. Neuron. 87(4):699-715.

9. Cull-Candy, S., Kelly, L., Farrant, M. (2006) Regulation of Ca2+-permeable AMPA receptors: synaptic plasticity and beyond. Curr Opin Neurobiol. 16(3):288-97.

10. D'Adamo, M.C., Catacuzzeno, L., Di Giovanni, G., Franciolini, F., Pessia, M. (2013) K(+) channelepsy: progress in the neurobiology of potassium channels and epilepsy. Front Cell Neurosci. 7:134. doi: 10.3389/fncel.2013.00134.

11. Deng, P.Y., Klyachko, V.A. (2016) Genetic upregulation of BK channel activity normalizes multiple synaptic and circuit defects in a mouse model of fragile X syndrome. J Physiol. 594(1):83-97.

12. Deng, P.Y., Rotman, Z., Blundon, J.A., Cho, Y., Cui, J., Cavalli, V., Zakharenko, S.S., Klyachko, V.A. (2013) FMRP regulates neurotransmitter release and synaptic information transmission by modulating action potential duration via BK channels. Neuron. 77(4):696-711.

13. Dijkhuizen, T., van Essen, T., van der Vlies, P., Verheij, J.B., Sikkema-Raddatz, B., van der Veen, A.Y., Gerssen-Schoorl, K.B., Buys, C.H., Kok, K. (2006) FISH and array-CGH analysis of a complex chromosome 3 aberration suggests that loss of CNTN4 and CRBN contributes to mental retardation in 3pter deletions. Am J Med Genet A. 140(22):2482-7.

14. Fischer, E.S., Böhm, K., Lydeard, J.R., Yang, H., Stadler, M.B., Cavadini, S., Nagel, J., Serluca, F.3, Acker, V., Lingaraju, G.M, Tichkule, R.B., Schebesta, M., Forrester, W.C., Schirle, M., Hassiepen, U., Ottl, J., Hild, M., Beckwith, R.E., Harper, J.W., Jenkins, J.L., Thomä, N.H1. (2014) Structure of the DDB1-CRBN E3 ubiquitin ligase in complex with thalidomide. Nature. 512(7512):49-53.

15. Franzoni, E., Booker, S.A., Parthasarathy, S., Rehfeld, F., Grosser, S., Srivatsa, S., Fuchs, H.R., Tarabykin, V., Vida, I., Wulczyn, F.G. (2015) miR-128 regulates neuronal migration, outgrowth and intrinsic excitability via the intellectual disability gene Phf6. Elife. 4. doi: 10.7554/eLife.04263.

16. Guglielmi, L., Servettini, I., Caramia, M., Catacuzzeno, L., Franciolini, F., D'Adamo, M.C., Pessia, M. (2015) Update on the implication of potassium channels in autism: K(+) channelautism spectrum disorder. Front Cell Neurosci. 9:34. doi: 10.3389/fncel.2015.00034.

17. Greenspan, S., Woods, G.W. (2014) Intellectual disability as a disorder of reasoning and judgement: the gradual move away from intelligence quotient-ceilings. Curr Opin Psychiatry. 27(2):110-6.

18. Haddad, D.M., Vilain, S., Vos, M., Esposito, G., Matta, S., Kalscheuer, V.M., Craessaerts, K., Leyssen, M., Nascimento, R.M., Vianna-Morgante, A.M., De Strooper, B., Van Esch, H., Morais, V.A., Verstreken, P. (2013) Mutations in the intellectual disability gene Ube2a cause neuronal dysfunction and impair parkin-dependent mitophagy. Mol Cell. 50(6):831-43.

19. Higgins, J.J., Hao, J., Kosofsky, B.E., Rajadhyaksha, A.M. (2008) Dysregulation of large-conductance Ca^{2+}-activated K^{+} channel expression in nonsyndromal mental retardation due to a cereblon p.R419X mutation. Neurogenetics. 9(3):219-23.

20. Higgins, J.J., Pucilowska, J., Lombardi, R.Q., Rooney, J.P. (2004) A mutation in a novel ATP-dependent Lon protease gene in a kindred with mild mental retardation. Neurology. 2004 63(10):1927-31.

21. Higgins, J.J., Tal, A.L., Sun, X., Hauck, S.C., Hao, J., Kosofosky, B.E., Rajadhyaksha, A.M. (2010) Temporal and spatial mouse brain expression of

cereblon, an ionic channel regulator involved in human intelligence. J Neurogenet. 24(1):18-26.

22. Hu, H., Shao, L.R., Chavoshy, S., Gu, N., Trieb, M., Behrens, R., Laake, P., Pongs, O., Knaus, H.G., Ottersen, O.P., Storm, J.F. (2001) Presynaptic Ca^{2+}-activated K^{+} channels in glutamatergic hippocampal terminals and their role in spike repolarization and regulation of transmitter release. J Neurosci. 21(24):9585-97.

23. Isaac, J.T., Ashby, M.C., McBain, C.J. (2007) The role of the GluR2 subunit in AMPA receptor function and synaptic plasticity. Neuron. 54(6):859-71.

24. Ito, T., Ando, H., Handa, H. (2011) Teratogenic effects of thalidomide: molecular mechanisms. Cell Mol Life Sci. 68(9):1569-79.

25. Ito, T., Ando, H., Suzuki, T., Ogura, T., Hotta, K., Imamura, Y., Yamaguchi, Y., Handa, H. (2010) Identification of a primary target of thalidomide teratogenicity. Science. 327(5971):1345-50.

26. Kasai, H., Fukuda, M., Watanabe, S., Hayashi-Takagi, A., Noguchi, J. (2010) Structural dynamics of dendritic spines in memory and cognition. Trends Neurosci. 33(3):121-9.Lee, K.M., Jo, S., Kim, H., Lee, J., Park, C.S. (2011) Functional modulation of AMP-activated protein kinase by cereblon. Biochim Biophys Acta. 1813(3):448-55.

27. Jo, S., Lee, K.H., Song, S., Jung, Y.K., Park, C.S. (2005) Identification and functional characterization of cereblon as a binding protein for large-conductance calcium-activated potassium channel in rat brain. J Neurochem. 94(5):1212-24.

28. Lakhan, S.E., Caro, M., Hadzimichalis, N. (2013) NMDA Receptor Activity in Neuropsychiatric Disorders. Front Psychiatry. 4:52. doi: 10.3389/fpsyt.2013.00052.

29. Lee, H.Y., Jan, L.Y. (2012) Fragile X syndrome: mechanistic insights and therapeutic avenues regarding the role of potassium channels. Curr Opin Neurobiol. 22(5):887-94.

30. Lee, K.M., Jo, S., Kim, H., Lee, J., Park, C.S. (2011) Functional modulation of AMP-activated protein kinase by cereblon. Biochim Biophys Acta. 1813(3):448-55.

31. Lee, K.M., Yang, S.J., Choi, J.H., Park, C.S. (2014) Functional effects of a pathogenic mutation in Cereblon (CRBN) on the regulation of protein synthesis via the AMPK-mTOR cascade. J Biol Chem. 289(34):23343-52.

32. Lee, K.M., Yang, S.J., Kim, Y.D., Choi, Y.D., Nam, J.H., Choi, C.S., Choi, H.S., Park, C.S. (2013) Disruption of the cereblon gene enhances hepatic AMPK activity and prevents high-fat diet-induced obesity and insulin resistance in mice. Diabetes. 62(6):1855-64.

33. Liu, Y., Huang, X., He, X., Zhou, Y., Jiang, X., Chen-Kiang, S., Jaffrey, S.R., Xu, G. (2015) A novel effect of thalidomide and its analogs: suppression of cereblon ubiquitination enhances ubiquitin ligase function. FASEB J. 29(12):4829-39.

34. Liu, J., Ye, J., Zou, X., Xu, Z., Feng, Y., Zou, X., Chen, Z., Li, Y., Cang, Y. (2014) CRL4A(CRBN) E3 ubiquitin ligase restricts BK channel activity and prevents epileptogenesis. Nat Commun. 5:3924.

35. Man, H.Y. (2011) GluA2-lacking, calcium-permeable AMPA receptors--inducers of plasticity? Curr Opin Neurobiol. 21(2):291-8.

36. Myrick, L.K., Deng, P.Y., Hashimoto, H., Oh, Y.M., Cho, Y., Poidevin, M.J., Suhl, J.A., Visootsak, J., Cavalli, V., Jin, P., Cheng, X., Warren, S.T., Klyachko, V.A. (2015) Independent role for presynaptic FMRP revealed by an FMR1 missense mutation associated with intellectual disability and seizures. Proc Natl Acad Sci U S A. 112(4):949-56.

37. Ozkan, E.D., Creson, T.K., Kramár, E.A., Rojas, C., Seese, R.R., Babyan, A.H., Shi, Y., Lucero, R., Xu, X., Noebels, J.L., Miller, C.A., Lynch, G., Rumbaugh, G. (2014) Reduced cognition in Syngap1 mutants is caused by isolated damage within developing forebrain excitatory neurons. Neuron. 82(6):1317-33.

38. Papuc, S.M., Hackmann, K., Andrieux, J., Vincent-Delorme, C., Budişteanu, M., Arghir, A., Schrock, E., Ţuţulan-Cuniţă, A.C., Di Donato, N. (2015) Microduplications of 3p26.3p26.2 containing CRBN gene in patients with intellectual disability and behavior abnormalities. Eur J Med Genet. 58(5):319-23.

39. Patel, U.H., Mir, M.A., Sivik, J.K., Raheja, D., Pandey, M.K., Talamo, G. (2015) Central neurotoxicity of immunomodulatory drugs in multiple myeloma. Hematol Rep. 7(1):5704.

40. Pavlowsky, A., Chelly, J., Billuart, P. (2012) Emerging major synaptic signaling pathways involved in intellectual disability. Mol Psychiatry. 17(7):682-93.

41. Potter, W.B., O'Riordan, K.J., Barnett, D., Osting, S.M., Wagoner, M., Burger, C., Roopra, A. (2010) Metabolic regulation of neuronal plasticity by the energy sensor AMPK. PLoS One. 5(2):e8996.

42. Raffaelli, G., Saviane, C., Mohajerani, M.H., Pedarzani, P., Cherubini, E. (2004) BK potassium channels control transmitter release at CA3-CA3 synapses in the rat hippocampus. J Physiol. 557(Pt 1):147-57.

43. Rajadhyaksha, A.M., Ra, S., Kishinevsky, S., Lee, A.S., Romanienko, P., DuBoff, M., Yang, C., Zupan, B., Byrne, M., Daruwalla, Z.R., Mark, W., Kosofsky, B.E., Toth, M., Higgins, J.J. (2011) Behavioral characterization of cereblon forebrain-specific conditional null mice: a model for human non-syndromic intellectual disability. Behav Brain Res. 226(2):428-34.

44. Rollin-Sillaire, A., Delbeuck, X., Pollet, M., Mackowiak, M.A., Lenfant, P., Noel, M.P., Facon, T., Leleu, X., Pasquier, F., Le Rhun, E. (2013) Memory loss during lenalidomide treatment: a report on two cases. BMC Pharmacol Toxicol. 14:41.

45. Sala, C., Segal, M. (2014) Dendritic spines: the locus of structural and functional plasticity. Physiol Rev. 94(1):141-88.

46. Seo, J., Giusti-Rodríguez, P., Zhou, Y., Rudenko, A., Cho, S., Ota, K.T., Park, C., Patzke, H., Madabhushi, R., Pan, L., Mungenast, A.E., Guan, J.S., Delalle, I., Tsai, L.H. (2014) Activity-dependent p25 generation regulates synaptic plasticity and Aβ-induced cognitive impairment. Cell. 157(2):486-98.

47. Shao, L.R., Halvorsrud, R., Borg-Graham, L., Storm, J.F. (1999) The role of BK-type Ca^{2+}-dependent K^{+} channels in spike broadening during repetitive firing in rat hippocampal pyramidal cells. J Physiol. 521 Pt 1:135-46.

48. Vaillend, C., Poirier, R., Laroche, S. (2008) Genes, plasticity and mental retardation. Behav Brain Res. 192(1):88-105.

49. Wallace, M.L., Burette, A.C., Weinberg, R.J., Philpot, B.D. (2012) Maternal loss of Ube3a produces an excitatory/inhibitory imbalance through neuron type-specific synaptic defects. Neuron. 74(5):793-800.

50. Wang, B., Jaffe, D.B., Brenner, R. (2014) Current understanding of iberiotoxin-resistant BK channels in the nervous system. Front Physiol. 5:382. doi: 10.3389/fphys.2014.00382.

51. Wang, Z.W. (2008) Regulation of synaptic transmission by presynaptic CaMKII and BK channels. Mol Neurobiol. 38(2):153-66.

52. Xu, G., Jiang, X., Jaffrey, S.R. (2013) A mental retardation-linked nonsense mutation in cereblon is rescued by proteasome inhibition. J Biol Chem. 288(41):29573-85.

53. Zhang, W., Peterson, M., Beyer, B., Frankel, W.N., Zhang, Z.W. (2014) Loss of MeCP2 from forebrain excitatory neurons leads to cortical hyperexcitation and seizures. J Neurosci. 34(7):2754-63.

국문초록

신경정신질환 관련 유전자 *Cereblon* 및 *Lrrtm3*의 시냅스 및 행동학적 기능 연구

최 태 용

서울대학교 대학원

협동과정 뇌과학 전공

우리 몸에서 가장 복잡한 기관인 뇌는 우리의 모든 행동을 조절하며 이러한 신경계는 수많은 신경세포로 구성되어있다. 그리고 이러한 신경세포는 서로 연결되어 있으며 신호를 주고받으면서 기능하게 되는데, 이렇게 신호를 주고받는 공간을 시냅스(synapse)라고 한다. 신경세포 및 시냅스 주변에는 수많은 단백질들이 발현하고 있으며 이들은 각각 신경세포와 시냅스의 발달에 따른 구조 형성 및 신경계의 주요 기능 중 하나인 시냅스를 통한 신경세포의 신호 전달에 중요한 기능을 하고 있다. 만약 이러한 단백질이 잘못되었을 경우 신경계는 제대로 기능을 할 수 없게 되며, 이는 결국 다양한 뇌 질환을 야기하게 된다. 이처럼 시냅스의 기능 이상에 의해 야기되는 질환을 시냅스질환(synaptopathy)라고 한다. 이러한 시냅스질환을 극복하기

위해서는 질병을 야기하는 돌연변이 된 유전자가 만드는 단백질이 시냅스 및 신경세포에서 원래는 어떠한 기능을 하는지를 이해해야 하고, 더불어 이 돌연변이가 기능을 어떻게 변화시키는지 알아야 할 것이다. 이러한 이해는 뇌에 대한 우리의 이해를 넓혀줄 뿐만 아니라, 장차 다양한 신경정신질환의 효과적인 치료법을 도출하는데 기여할 것이다.

시냅스는 신경세포의 특수화된 구조로 전시냅스세포와 후시냅스세포가 연결되어 정상적인 기능을 수행하기 위해서는 접착제 역할을 하는 시냅스 접착 단백질(synaptic cell-adhesion molecule)들이 필요하다. LRRTMs(leucine-rich repeated transmembrane proteins)는 최근에 발견된 시냅스접착단백질로써 흥분성 후시냅스막에 발현하여 이의 발달과 기능에 기여한다는 것이 최근 들어 밝혀지고 있으며, 다양한 신경정신질환과 이들의 돌연변이 사이의 연관성이 보고되고 있다. LRRTMs은 LRRTM1-4의 네 종류가 있는데, 이 중에서 *LRRTM3*의 돌연변이와 알츠하이머성 치매, 자폐증과 같은 질병 사이의 연관성에 대한 임상학적 보고들이 여러 차례 소개된 반면, 이 단백질에 대한 분자 및 세포 수준의 이해는 부족하다. 이러한 중요성에 착안하여 1장에서는 *Lrrtm3* 유전자 손실 생쥐를 이용하여 신경세포 및 시냅스에서 LRRTM3의 기능을 확인하였다.

지적장애(intellectual disability) 역시 흔한 신경정신질환으로 최근의 많은 연구에서 시냅스질환으로 받아들여지고 있다. *Cereblon*(*CRBN*)은 IQ 50에서 70 사이의 경도 지적장애(mild intellectual disability)를 보이는 환자들에서 유전자 돌연변이가 보고된 이래로 *CRBN* 유전자 및 이를 포함한 유전체 영역의 다양한 변이에 의한 지적장애 및 발달장애가 보고되었다. CRBN은 다른 여러 단백질들과 함께 $CRL4^{CRBN}$ E3 ubiquitin ligase complex를 형성하며 여기서 CRBN은 ubiquitination 조절을 받을 단백질과 결합하여 이들을 E3 ubiquitin

ligase complex로 데려오는 substrate receptor 역할을 한다는 것이 최근에 밝혀졌다. CRBN과 결합하는 것으로 알려진 단백질들은 BK channel의 α subunit, AMP kinase의 α subunit 등이 있다. 하지만 CRBN이 어떻게 신경계의 기능을 조절하며 *CRBN*의 돌연변이가 어떻게 지적장애를 유발하는지에 대해서는 알려져 있지 않았다. 2장에서는 CRBN이 신경세포 및 시냅스에서 어떤 역할을 하는지 확인하기 위해 *Crbn* 유전자 결손 생쥐를 이용하여 다양한 동물행동학, 전기생리학, 생화학적인 실험 기법들을 통해 CRBN의 신경계 기능을 확인하였다.

신경정신질환의 원인 유전자들이 신경세포 및 시냅스에서 어떻게 작용하는지를 확인한 본 연구들은 이 유전자들의 돌연변이에 의한 신경정신질환들의 원인 기전을 이해하는데 필수적일 뿐만 아니라 향후 치료 기전을 확립하는데 주요하게 응용될 것으로 기대된다.

주요어 : 시냅스, 시냅스가소성, 시냅스질환, 신경정신질환,
Cereblon, LRRTM3

학 번 : 2013-30928